Dissertations, Master's Theses and Master's Reports

2021

EFFECTS OF MICROPOROUS STRUCTURE ON THE ENZYMATIC CONVERSION OF BIOMASS USING A MULTISCALE MODEL

Saketh Merugu
Michigan Technological University, smerugu@mtu.edu

EFFECTS OF MICROPOROUS STRUCTURE ON THE ENZYMATIC CONVERSION
OF BIOMASS USING A MULTISCALE MODEL

By

Saketh Merugu

A THESIS

Submitted in partial fulfillment of the requirements for the degree of

MASTER OF SCIENCE

In Chemical Engineering

MICHIGAN TECHNOLOGICAL UNIVERSITY

2021

This thesis has been approved in partial fulfillment of the requirements for the Degree of MASTER OF SCIENCE in Chemical Engineering.

Department of Chemical Engineering

Thesis Advisor: *Dr. David R. Shonnard*

Committee Member: *Dr. Rebecca G. Ong*

Committee Member: *Dr. Pradeep K. Agarwal*

Department Chair: *Dr. Pradeep K. Agarwal*

Table of Contents

List of Figures

iv

List of Tables

List of Abbreviations

EH − Enzymatic hydrolysis

DAP − Dilute acid pretreatment

BG − β-glucosidase enzyme

CE − Cellobiohydrolase and Endoglucanase enzymes

NMR cryoporometry− Nuclear magnetic resonance cryoporometry

AFEX − Ammonia fiber expansion

PDE − Partial differential equation

ODE – Ordinary differential equation

SGCS – Sieve ground corn stover

UGCS – Ultra ground corn stover

PWS – Pretreated wheat straw

OB – Organosolv bagasse

HB – Hydrothermal bagasse

Acknowledgments

Abstract

The generation of biofuels from lignocellulosic biomass involves innovative process technology that is being investigated worldwide. Enzymatic hydrolysis is a major step in the contemporary process of the generation of biofuels. Guided by pore size distribution measured using NMR cryoporometry, we developed pore-enzyme diffusion and adsorption models at the particle level coupled with a kinetic model for cellulose, cellobiose, and glucose production at flask level. By simulating these models in MATLAB, COMSOL, and Polymath software packages, we investigate the effects of various biomass particle-related parameters (particle dimensions, porosity, enzyme accessibility) on the characteristic time of enzyme diffusion and adsorption and enzymatic hydrolysis yield for lignocellulosic biomass. The multiscale model predictions for glucose concentration agree with the experimental kinetic data from the literature. The model was applied to predict the effect of changing microporous structures on the glucose yield from hydrolysis of dilute acid-pretreated hybrid poplar.

1 INTRODUCTION

The steady rise of the global population has exponentially increased the consumption of fossil fuels to support energy needs. The combustion of fossil fuels is the most significant contributor to greenhouse gas emissions, climate change, and air pollution (Perera, 2017). The increase in greenhouse gasses in the atmosphere is responsible for increasing temperatures globally, which a consensus of climate scientists predicts will result in extreme weather events and climate change. The continued use of fossil fuels is likely to increase global temperatures. According to the 2015 Paris agreement, governments across the globe pledged to voluntarily curb the use of fossil fuels and limit the global temperature rise to 1.5 °C (Paris agreement, 2015). To reduce global fossil fuel consumption, we need alternative renewable and clean energy sources to support the growing energy needs. One reliable alternative to conventional fuels is low-carbon fuels such as biofuels. The principal use of biofuels such as ethanol is as a blend in the transportation sector, where currently, in many countries across the globe, 10% of ethanol is blended with gasoline (IES, 2013). The global biofuel use decreased by 8.7% in 2020 due to the COVID19 pandemic but is projected to recover and increase in 2021 and 2022 as developing countries target to increase their blending rates (IES, 2015).

Biofuels are produced from biomass by enzymatic hydrolysis, a preliminary step that releases fermentable sugars, which we will discuss later in this study. There are several diverse types of biomass feedstocks for bioconversion, such as maize, sugarcane, molasses, wheat, grains, cassava, sugar beets, and products made from biomass such as rapeseed oil, soybean oil, palm oil as well as woody energy crops such as poplar, aspen, eucalyptus, willow, switch grass and corn stover. The majority of these biomass feedstocks are converted to liquid biofuels such as bioethanol and biodiesel. The production of bioethanol is projected to increase to 132 billion liters and biodiesel to 50 billion liters by 2030(IES, 2015). Because transportation biofuels are derived from agricultural biomass, these biofuels require large areas of land for cultivation. Food insecurity and unsustainable land usage are significant challenges to the production of biofuels. This triggers the need to rely on other biomass materials such as the lignocellulosic biomass (poplar, corn stover, etc.), which do not compete with food crops, leading to food insecurity.

The conventional conversion pathways shown in Figure 1 from biomass feedstock to biofuels involve two significant steps: deconstruction and fractionation and synthesis and upgrading. The first step is the deconstruction of biomass into its component chemicals using enzymes, chemicals, and heat. The primary deconstruction techniques can be divided into high and low-temperature deconstruction. Examples of high-temperature deconstruction techniques are pyrolysis, gasification, and hydrothermal liquefaction. The low-temperature deconstruction technique is pretreatment of biomass followed by enzymatic hydrolysis. After the deconstruction of biomass, based on the type of chemical components obtained, they undergo further separations and synthesis. In the case of hydrolysis deconstruction, the produced sugars are fermented using microorganisms to

bioethanol. The conversion of lignocellulosic materials using these processes is expensive, and to commercialize the production of biofuels from lignocellulosic biomass, we need to improve the efficiency of the process and optimize the biofuel yield. One key step to enhancing biomass conversion efficiency is understanding the effects of biomass particle size, adsorption capacity, porosity, and accessibility factor, which is possible by modeling the enzymatic hydrolysis.

| (1) Biomass | (2) Pretreatment | (3) Enzymatic hydrolysis | (4) Sugar fermentation | (5) Biofuel |
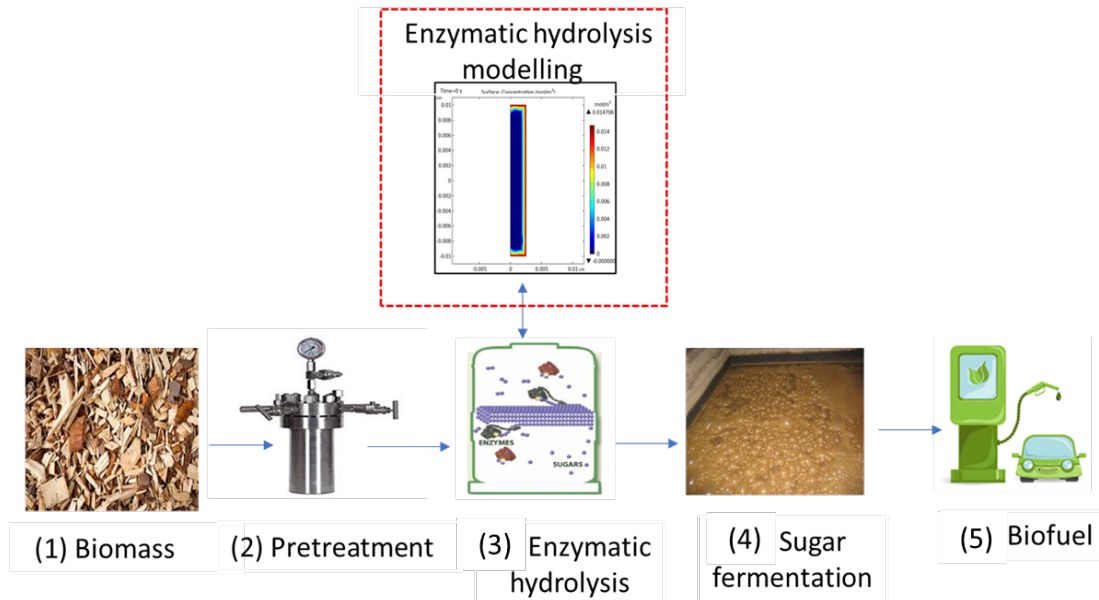
In this study, we focus on modeling the enzymatic hydrolysis of lignocellulosic biomass and observe the effects of particle size and pore volume on glucose yield using a multi-scale model of diffusion and adsorption of hydrolytic enzymes model at the particle level coupled with an enzymatic hydrolysis kinetic model at the flask level, which accounts for the conversion of cellulose to glucose. A bioconversion pathway incorporating the modeling of enzymatic hydrolysis for a better understanding of factors influencing glucose yield is shown in Figure 1. Understanding the two precursor components of EH of biomass, lignocellulosic biomass, and pretreatment is crucial for developing an effective EH model.

The plant cell wall of lignocellulosic biomass is made up of a matrix of cellulose, hemicellulose, lignin, extractives, and ash. The different types of lignocellulosic biomass have different compositions of lignocellulose components. The lignocellulose components vary in terms of chemical composition, chemical bonds, and physical and chemical properties. Cellulose has a molecular formula $(C_6H_{10}O_5)_n$; it is made up of β-D- glucose monomers linked together by β-1,4 glycosidic bonds, forming a linear β-1,4 glucan polymer with cellobiose as the repeating unit at different degrees of polymerization. Cellobiose is a disaccharide made up of two molecules of d-glucose linked by a β-1,4'

glycosidic bond. Glucose is a monosaccharide with the molecular formula $C_6H_{12}O_6$. The other significant component of the plant cell wall is hemicellulose. The hemicellulose is made of sugar polymers such as D-glucopyranose, D-xylopyranose, D-glucopyranosyluronic acid, D-galactopyranose, D-mannopyranose, and L-arabinofuranose. All the monosaccharides in a hemicellulose molecule have D-configuration except for arabinose. The third major component of the plant cell wall is the lignin; it is made up of aliphatic and aromatic structures; however, lignin by itself doesn't contain any carbohydrate monomers, and therefore it is not capable of producing glucose when hydrolyzed but is linked to hemicellulose which is capable of converting into xylose. The compositions of different biomass are listed in a later section of this thesis in Table 3.

Due to their complex structure, the presence of lignin and hemicellulose acts as a protective layer for the plant cell wall in nature, making it difficult for enzymes to hydrolyze the lignocellulosic material into monosaccharides and making the EH process time consuming and expensive. The pretreatment helps overcome the recalcitrance of lignocellulosic biomass by exposing the reactive cellulose fiber, altering the structural features, and increasing the porosity and pore sizes (Sasmsal., 2017). The pretreatment methods can be broadly classified into physical, physicochemical, chemical, and biological pretreatments (Kumar et al., 2009). The physical pretreatment can be further divided into mechanical comminution and pyrolysis. Examples for physiochemical pretreatments include steam explosion, Ammonia Fiber Expansion (AFEX), and CO_2 explosion. Examples of chemical pretreatment techniques are ozonolysis, dilute acid hydrolysis, alkaline hydrolysis, oxidative delignification, and the organosolv process (Zhang et al., 2021).

The pretreated biomass is then hydrolyzed using adsorbing enzymes (cellobiohydrolase and endoglucanase) and non-adsorbing (β-glucosidase) enzymes into fermentable sugars in a process called enzymatic hydrolysis. The six key steps of this process are (Zhang et al., 2021):

(1) mass transfer of enzymes from the bulk aqueous phase to the surface of the biomass particle,

(2) diffusion of the enzymes into the biomass particle,

(3) adsorption of the enzymes to cellulose and formation of enzyme-substrate complexes,

(4) hydrolysis of the cellulose,

(5) diffusion to the particle surface and mass transfer of the hydrolysis products from the surface of the cellulosic particles to the bulk aqueous phase, and

(6) hydrolysis of cellobiose to glucose in the aqueous phase.

The process variables of an enzymatic hydrolysis reaction are solids or substrate loading, enzyme loading, particle porosity, temperature, pH, and mixing rate. The next step after enzymatic hydrolysis is fermentation. The fermentation process involves the conversion of

sugars produced by enzymatic hydrolysis into ethanol using microorganisms such as bacteria, yeasts, and fungi.

In the coming sections of Chapter 2, based on studies by different researchers, the effects of microporous structure on EH and the effect of diffusion and adsorption on EH will be reviewed and discussed, followed by a literature review on EH modeling by various researchers and identification of research gaps. Based on this, the overall research objectives for this project will be presented in Chapter 3.

2 LITERATURE REVIEW

Enzymatic hydrolysis is a complex process with simultaneous molecular mass transfer and reaction kinetics, making it challenging to model. Since the last decade, many researchers have developed experimental methods to deepen the understanding of factors influencing the rate of hydrolysis and carried out several experiments to optimize the efficiency of conversion. Despite numerous experimental studies, progress has been limited since experimental studies rely on practical and macroscopic understanding. Numerous influencing factors affect the yield of enzymatic hydrolysis, such as pretreatment conditions, process variables of enzymatic hydrolysis, and substrate morphology makes experimental studies time-consuming and economically draining. Due to these complications, many researchers have turned to enzymatic hydrolysis modeling. Before discussing the different modeling efforts and development, first, a review of the various experimental studies conducted to study the effect of microstructure on enzyme adsorption and hydrolysis, and the impact of diffusion and adsorption of enzymes on hydrolysis will be presented to understand why it is essential to model these systems parameters.

2.1 Overview of the effect of microstructure on enzyme adsorption and hydrolysis

The role of distinct influencing parameters in the recalcitrance of lignocellulosic biomass hydrolysis was investigated by multiple researchers. Ji et al., (2018) studied the effect of particle size and found that adsorption was effective when the size of the particle was smaller and pore size was larger, with particle size showing a significant correlation with enzymatic hydrolysis yield. The study by Grethlein et al., (1985) concluded that only pores larger than 51°A were accessible to the enzymes and found that larger pores were mandatory for higher enzyme adsorption and improving hydrolysis rate. The study by Cho et al., (2020) on the specific surface area of a biomass particle found that the greater the accessible surface area, the greater the availability of active sites for enzyme binding, which significantly improved the hydrolysis rate. Liu et al., (2019) studied the effect of cellulose crystallinity and found that the amorphous cellulose had more interaction with enzymes compared to crystalline cellulose and the degradation rate of amorphous cellulose was thirty times greater than the crystalline cellulose. The correlation between cellulose and hydrolysis was also studied by Liu et al., (2019) and found that the hydrolysis rate increased with a decrease in the degree of polymerization.

2.2 Effect of diffusion and adsorption of enzymes on hydrolysis

The diffusion of enzymes is crucial to understanding the mechanism of enzymatic hydrolysis, and the rate-limiting effect of diffusion was proved to be significant for larger biomass particles by Chen et al., (2015). Supporting this, Luterbacher et al., (2012)

developed a pore diffusion model and studied the effects of diffusion on the enzymatic hydrolysis process using mass transfer and reaction kinetics and found that diffusion is not a critical rate-limiting step for small particles below 50 microns. Numerous studies were carried out to understand the effect of enzyme adsorption on enzymatic hydrolysis, such as Varnai et al., (2013) and Pakarinen et al., (2014), who indicated that there was no correlation between enzyme adsorbed and enzymatic hydrolysis yield. Contrary to Varnai et al., Gao et al., demonstrated that enzyme adsorption capacity and enzymatic hydrolysis yield have a weak connection (Gao et al., 2013). Another researcher, Zhang et al. showed that EH yield and adsorption capacity had a strong relationship using model-fitting methods (Zhang et al., 2017). Some studies explored the relationship between equilibrium adsorption capacity and adsorption rate constants using the Freundlich model (Fierro., 2008), and some studies used the Langmuir adsorption isotherm (Machado et al.,2015).

2.3 Overview of different models for cellulose hydrolysis

Enzymatic hydrolysis models can be broadly classified into three major types: non-mechanistic, semi-mechanistic, and mechanistic models, which can be divided further into functionally based models, and structurally based models, according to Zhang and Lynd (2004). A model developed using the correlation between the rate of hydrolysis and parameters such as enzyme loading, substrate morphology, and time of hydrolysis are classified as non-mechanistic models. According to Zhang et al., (2021), structural and functional-based models provide deeper insight and predictive capability compared to non-mechanistic models but are challenging to model due to the non-availability of model data required. Sousa Jr et al. (2011) reviewed non-mechanistic and semi-mechanistic models by several authors such as Kadam et al., (2004), Yi Zheng et al., (2009), Li et al., (2004), Carrillo et al.,(2005), and O'Dwyer et al. (2007); functional and structural based models by Zhang and Lynd (2004), and Levine et al., (2010) and multiple other studies and found that semi mechanistic models considering Langmuir adsorption isotherm and Michaelis Menten kinetics were applied more frequently. Kadam et al., (2004) developed a multi-reaction kinetic model for enzymatic hydrolysis of corn stover to predict cellulose hydrolysis trends. Similar to Kadam, Yi Zheng, Li, Carrillo conducted kinetic studies on EH of Lignocellulosic biomasses. Wang et al., (2004) developed a mechanistic kinetic model for EH of cotton fibers which could quantitatively estimate the synergism of cellulase components. Based on these reviews, Sousa Jr et al. (2011) found that functionally based models lead to a substantial number of parameters to fit the model's data to experimental data. The semi-mechanistic model developed by Kadam et al., (2004), for example, showed that the kinetic model is capable of predicting enzymatic hydrolysis yield. Zhang et al., (2016) developed a pore-surface diffusion model which can predict the adsorption kinetics but does not reflect on reaction kinetics. A diffusion and reaction model with spatial variations was developed by Luterbacher et al., (2012), which succeeded in predicting the enzymatic hydrolysis kinetics when pore size distribution data and initial substrate loading data were provided but did not seem to indicate the effect of evolving pore morphology and particle size on enzymatic hydrolysis yield. The study by Ankathi et

al., (2019) showed that the porosity and available pore volume change gradually as the enzymatic hydrolysis progresses. Incorporating the effect of pore morphology and particle sizes is crucial to successfully predict the enzymatic hydrolysis yield and determine which pretreatment has higher conversion efficiencies.

In a recent study by Rohrbach and Luterbacher (2021), they developed a multiscale model and predicted the glucose yields based on the change in enzyme concentrations at the cellulose surface area due to adsorption and desorption. Using their multiscale model, they studied the effect of particle size, enzyme loading, and biomass loading. Assuming a cylindrical biomass particle, their model predicted changes in porosity as a function of radial position and time as a result of hydrolysis by enzymes within the particles and then incorporated these predicted changes on the diffusion of enzymes, adsorption/desorption, and hydrolysis. However, they did not compare predicted changes in porosity to measured values because the study lacked sufficient experimental verification for porosity. The model developed by Rohrbach has some other limitations, such as it does not account for inaccessible pore volumes within the biomass particles. Although the model is able to predict glucose yields, the study did not show changes in cellulose concentration at different radial positions in the biomass particle and did not predict the characteristic times of enzyme diffusion and adsorption and their effects on the glucose yields.

Based on the literature review, the current research lacks a relationship between particle scale diffusion and adsorption and flask level kinetics which can predict the effect of pretreatment, the particle size of biomass, porosity, and available pore volume on enzymatic hydrolysis glucose yields. The main goal of this project is to develop a multiscale model that couples the mass transfer of enzymes at the biomass particle level with enzyme reaction kinetics that determines sugar concentrations in the bulk of the solution inside the flask. The model to be presented can predict enzymatic hydrolysis sugar production kinetics and use the multiscale model to study the effects of system parameters on glucose yields. In this modeling study, measured changes in porosity and accessibility factor are incorporated into the glucose yield predictions in scenario analyses. The model developed here predicts the characteristic time of diffusion and how different system parameters affect the characteristic times of diffusion.

3 THESIS OBJECTIVES

The main research objectives for this thesis project are listed below.

- Develop a multiscale model that couples the mass transfer of enzymes at the biomass particle level with reaction kinetics in the bulk of the solution inside the flask, which can predict enzymatic hydrolysis sugar production kinetics and yield.

- Study the effect of substrate characteristics such as particle size and different pretreatment times on enzymatic hydrolysis glucose yield.

- Study the effect of measured changes in the microporous structure such as accessibility factor $'\varphi'$ and porosity $'\epsilon'$ on the glucose yield.

- Develop a pore-enzyme diffusion model to predict the characteristic time of diffusion for non-adsorbing and adsorbing hydrolytic enzymes into biomass particles.

- Study the effect of substrate characteristics such as particle size and porosity on the characteristic time of diffusion of non-adsorbing enzymes.

- Study the effect of substrate characteristics such as particle size, porosity, adsorption capacity, and affinity constant on the characteristic time of diffusion of adsorbing enzymes.

Each of these research objectives will be addressed in the various sections of Chapter 4.

4 MECHANISTIC MODEL FOR ENZYMATIC HYDROLYSIS OF LIGNOCELLULOSIC BIOMASS

4.1 Effects of microporous structure on transient diffusion of non-adsorbing hydrolytic enzymes into biomass

The enzymatic hydrolysis (EH) of lignocellulosic biomass is a vital process in the conversion of woody biomass into advanced biofuels, such as cellulosic ethanol. EH involves a complex set of diffusion and enzyme-catalyzed reaction steps, which ultimately solubilize the cellulose fraction of woody biomass, producing glucose for fermentation. It is essential to understand the relative rates of diffusion compared to enzymatic hydrolysis reactions in order to optimize the parameters of the system for minimum process residence time and to maximize yields of sugars. In this section, the characteristic time for diffusion of non-adsorbing enzymes into woody biomass will be investigated.

The mechanistic model for transient diffusion of non-adsorbing hydrolytic enzymes into lignocellulosic biomass particles is formulated using Fick's law of diffusion. In this section of Chapter 4, only the diffusion of enzymes has been modeled to account for the non-adsorbing enzymes such as the β-glucosidase, which show no significant adsorption onto biomass particles (Machado et al.,2015). The diffusion and adsorption of the other hydrolytic enzymes are discussed in section 4.2. The lignocellulosic biomass particles are assumed to be cylindrical in this model since cylindrical geometry resembles the closest to real-life biomass particles. In this model, we consider that diffusion occurs only in the radial direction, considering that the aspect ratio of the particles is large (particle length to radius). Diffusion at the ends of the cylinder is neglected since the cylinder is exceedingly long. We also assume that the cell lumens inside a biomass particle are prefilled with water before adding the enzymes, based on which we can neglect the effect of bulk water movement on enzyme transport, making the biomass particle isotropic. The transient diffusion mechanism is described by a partial differential equation (PDE). In this model, the PDE is dependent upon biomass particle porosity and the ratio of available pore volume and total pore volume because enzymes are excluded from pores of size smaller than approximately 5 nm. The model parameters are mostly experimental values sourced from various literature, but, when necessary, parameters were estimated using appropriate equations. The model and its numerical solution were validated using an analytical solution to ensure the efficiency and accuracy of the model.

4.1.1 Model development

The diffusion of enzymes is influenced by the physiochemical properties such as particle size and porosity of the biomass particle (Zhang et al., 2021). The porosity 'ε' of a biomass particle can be calculated using the equation adapted from Zhang et al., (2016):

$$\epsilon = \frac{V_P}{V_P + \dfrac{1}{\rho_s}},$$
(1)

where V_P is the pore volume and ρ_s is the solid density of the particle (density of the wood itself, not accounting for the voids), calculated using an equation adapted from Zhang et al., (2016):

$$\rho_s = \frac{1}{M_c/\rho_c + M_h/\rho_h + M_l/\rho_l + M_o/\rho_o},$$
(2)

where M_c, M_h, M_l and M_o Stand for the mass percentages of cellulose (c), hemicellulose (h), lignin (l), and other components (o) on a dry weight basis, respectively. $\rho_c, \rho_h,$ and ρ_l Stand for the solid densities of cellulose, hemicellulose, and lignin on a dry weight basis, respectively. The molecular diffusivity of an enzyme in water (D_w) is a fundamental property of the substance and is affected by temperature and the properties of water. The effective diffusion coefficient of the enzyme within the biomass particle (D_p) is lower than D_w because of the tortuous path, dead-end path, and non-uniform pore widths that exist in biomass particles. D_p is calculated using equation 3, a correlation derived from Whitaker (1999):

$$D_p = D_w \left(\frac{\epsilon}{2-\epsilon}\right),$$
(3)

where D_w is the diffusion coefficient of enzymes in pure water with no porous media present, and ϵ is the porosity.

Because there is no bulk flow of fluid through the small pores in the biomass, the mass transfer in this system occurs through diffusion only, which can be given by equation 4, an adaptation from Whitaker (1999):

$$\epsilon \frac{\partial BG}{\partial t} = \varphi \frac{1}{r} \frac{\partial}{\partial r}\left(r D_p \frac{\partial BG}{\partial r}\right),$$
(4)

where BG is the concentration of non-adsorbing enzymes in the pore fluid of the particle at radial position r, φ is the ratio of pore volume accessible to the enzymes (V_{PA}) to the total pore volume (V_P), r is a radial position inside the particle, and D_p is the pore effective diffusion coefficient. In this derivation of the diffusion equation for non-adsorbing enzymes into biomass particles, accessibility factor φ is located prior to the diffusion term on the right-hand side of equation 4. This location is appropriate because if, for example, φ is zero, no pores are accessible to diffusing enzymes, and therefore no change in pore concentration can occur compared to the initial condition. Furthermore, the accessibility factor should not be part of the diffusion coefficient because effectivity diffusivity is only dependent on porosity, as shown by equation 3.

4.1.2 Boundary conditions

$r = 0, B = 0$

$r = R, B = C_{L_B}$
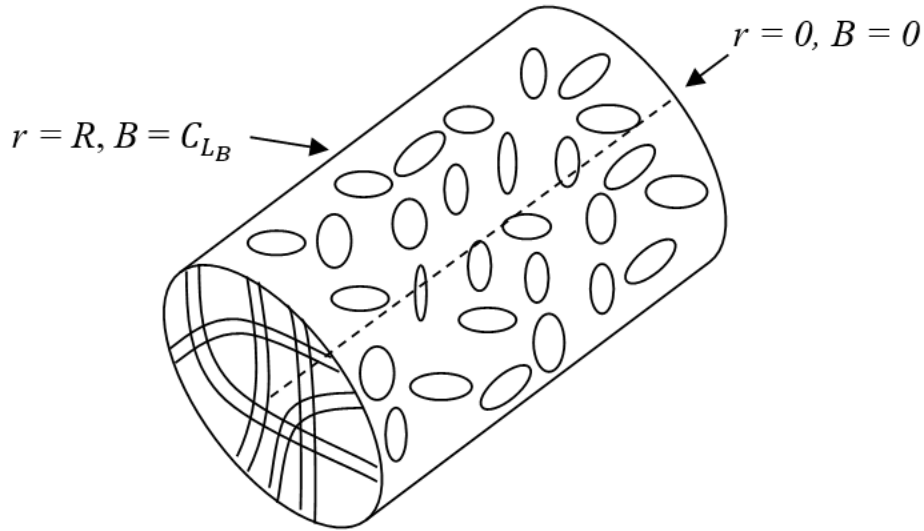
Figure 2. Schematic diagram of a typical porous cylindrical biomass particle with boundary conditions adapted from Zhang et al.,(2021).

The initial condition for the model is given by:

Boundary conditions for the model are given by:

$t > 0$

At $r = 0$

$$\frac{\partial BG}{\partial r} = 0 \tag{6}$$

At r= R

$$BG = [C_L]_{BG} \tag{7}$$

4.1.3 Material properties and list of parameters

For this study in section 4.1, Avicel PH-101 was chosen as the substrate due to sheer data availability, and β-glucosidase enzymes are used in this model. The data needed for this model are listed in Table 1.

Table 1. Material properties and a list of parameters used in the model.

Parameter	Description	Units	Value	Source
Biomass	-	-	Avicel PH101	[F]
Particle shape	-	-	Cylinder	[L]
Particle size	Diameter of particle	cm	0.005	[F]
ρ_S	Solid density	g/cm^3	1.52	[A]
M_c	Mass percentage of cellulose	%	100	[F]
ρ_c	Cellulose density	g/cm^3	1.52	[G]
V_{PA}	Pore volume accessible to the enzyme	cm^3/g	-	-
φ	Pore volume accessible to the enzyme/total pore volume	-	1	[D]
D_P	Pore diffusion coefficient	cm^2/sec	1×10^{-7}	[A]
ϵ	Porosity	-	0.3	[B]
V_P	Total pore volume	cm^3/g	0.282	[H]
B	The concentration of enzyme mixture inside the biomass in the pore fluid	mg/ml	-	-
BG	Concentration of non-adsorbing enzymes inside the biomass in the pore fluid	mg/ml	-	-
C_{L_B}	Concentration of enzyme mixture in the bulk solution	mg/ml	-	-
$C_{L_{BG}}$	Concentration of BG in the bulk solution	mg/ml	1	[D]
D_w	Diffusion coefficient of enzymes in pure water	cm^2/sec	5.67×10^{-7}	[L][E]
t	Enzyme diffusion time	sec	-	-

τ	Characteristic time	sec	-	-
r	Radial position inside the particle	cm	-	-
R	Radius of the particle	cm	0.0025	[F]

A- calculated using eq.2, B- calculated using eq.1, C- calculated using eq.3, D-Assumption, E- D_w ranges from 10^{-6} to 10^{-7} cm^2/sec and assumption, and the characteristic time in the above table is defined as the time needed for the enzyme concentration inside the particle at $r = 0$ to reach 99% of the enzyme concentration in the bulk solution, F- Machado et al.,(2015), G- Zhang et al., (2016), H- Tantasucharit., (1995), I- Yohana et al., (2020).

In this model, due to constant boundary conditions, the characteristic time of diffusion is not affected by the BG enzyme loading, so we assume '1' mg/ml as the bulk BG concentration to show results in such a way that it is easier for the reader to interpret. We also assumed that the φ is 1 due to a lack of data on evolving pore volume data for Avicel.

4.1.4 Method of Solution

The transient diffusion model is numerically solved using eq. 4, boundary conditions, and data from Table 1. The characteristic time is calculated using a custom-written program in MATLAB (MathWorks, Natick, MA, USA). The numerical solution is validated using the analytical solution in Crank (1956), assuming the same model parameters as in the numerical solution. The effect of porosity and pore size on the characteristic time is estimated by varying the porosity from 0.1 to 1 with intervals of 0.1 and varying the biomass particle radius from 0.0025 cm to 0.025 cm with intervals of 0.0025 cm.

4.1.5 Results and discussion

The concentration of β-glucosidase enzyme at different radial positions inside the cylindrical biomass particle was found by numerically solving eq. 4 using a parabolic partial differential equation solver (i.e., PDEPE function) available in MATLAB and using the model parameters listed in Table 1. The graph in Figure 3 shows the concentration of β-glucosidase enzyme as a function of time (sec.) at different radial positions inside the biomass particle. The concentration of BG at $r=R=0.0025$ cm remains constant at 1 mg/ml for all times because this is the boundary condition for the diffusion of the enzyme into the particle. For radial positions close to the particle surface (r near to R), the concentration of BG increases very rapidly with time, but then concentration increases much slower as time increases. For radial positions near the particle center (near to $r=0$), there is a delay of less than 1 sec before concentration begins to increase rapidly. Otherwise, the shapes of the concentration vs. time curves are similar for all radial positions.
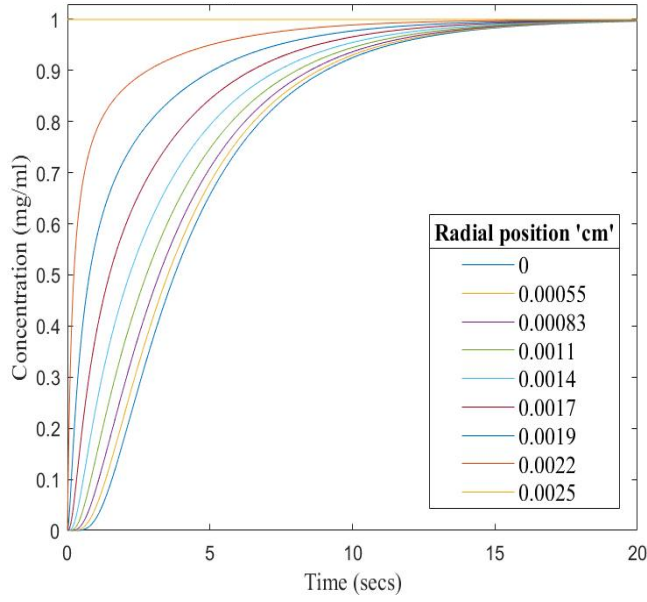
Figure 3. Concentration of β-glucosidase enzyme vs time (sec) at different radial positions inside the cylindrical Avicel PH-101 biomass particle.

The characteristic time $'\tau'_{numerical}$ For β-glucosidase to diffuse into the particle was found to be 16.65 secs. The concentration profile agrees with the specified initial and boundary conditions. The characteristic time $'\tau'_{analytical}$ found using the analytical solution is 16.254 sec, which is comparatively close to the numerical characteristic time. The enzyme concentrations at different radial positions and times found numerically are compared in Figure 4. Based on the comparison, we can conclude that the numerical solution obtained using MATLAB agrees with the analytical solution provided by Crank (1956) for the diffusion of non-adsorbing enzymes into a cylindrical particle.

14
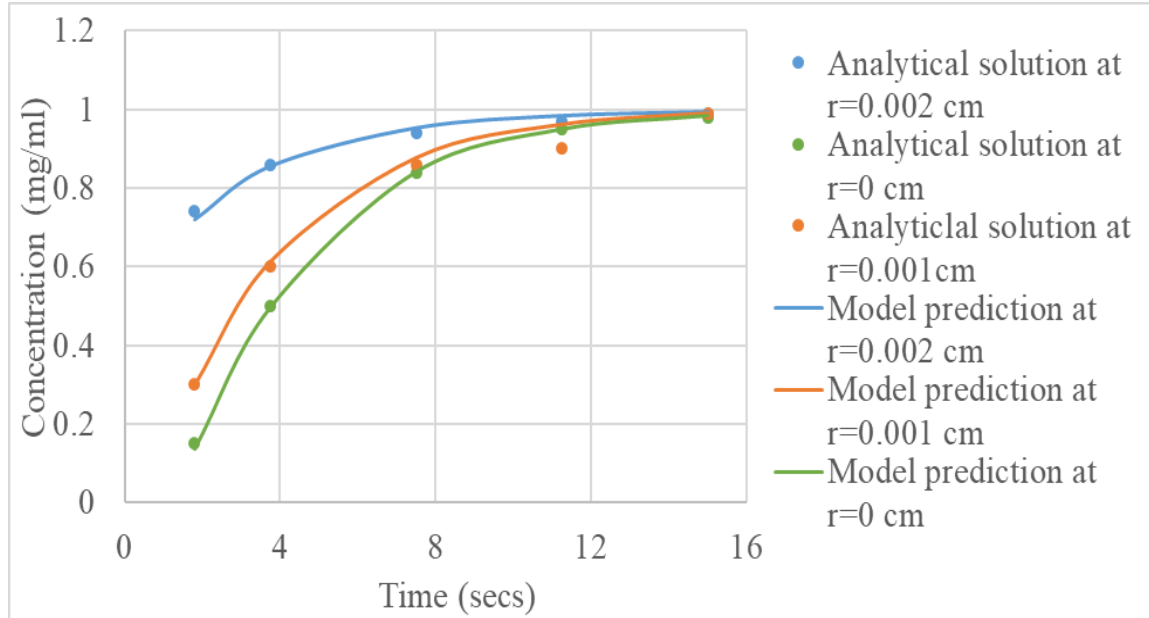
Figure 4. Comparison of characteristic times of diffusion of enzymes into Avicel PH-101 particle predicted by model and analytical solution found using Crank. J., (1956).

According to a few studies, cellulose accessibility to the interior of a biomass particle has a significant effect on the rates of enzymatic hydrolysis (Zhang et al., 2021, Arantes et al., 2011) because the efficiency of enzymatic hydrolysis depends on the surface area available for intimate contact between cellulose and enzymes. The major contributors to surface area for enzyme diffusion are particle size and porosity (Zhao et al., 2012). If the porosity is too small, enzymes will act mainly at the particle surface rather than inside the particle, which slows hydrolysis rates. The porosity is influenced by the total pore volume and available pore volume (Grethlein et al., 1985), which plays a vital role in cellulose accessibility according to eq.1. If the particle size is too large, even for porous particles, the characteristic time for diffusion of enzymes into the particle may become too large and will slow observed hydrolysis rates. To further understand the influence of porosity and particle size, the effect of microporous structures on the diffusion of β-glucosidase was studied by varying the porosity and particle size. By using the model, the effect of porosity on diffusion is shown in Figure 5, assuming that all pores are accessible to the enzyme for diffusion into the biomass particle. The characteristic time for diffusion goes down by a factor of nearly two with increasing porosity from 0.1 – 1.0, which is an expected result due to the fact that as porosity increases, the effective diffusion coefficient of β-glucosidase enzyme increases according to eq. 3.

Based on the results shown in Figure 5, we can conclude that the porosity has a modest effect on the characteristic time for enzyme diffusion of non-adsorbing enzymes. The characteristic time for diffusion of non-adsorbing enzymes will be inversely proportional

15

to D_p/ε according to equation (4) and therefore varies as (2-ε), which over the range 0.1<ε<1, varies by nearly a factor of 2, in agreement with Figure 5. In this study, we assume that all the pores are accessible, but, in reality, all the pores are not readily accessible, which affects the efficiency of enzymatic hydrolysis. For each different value of porosity, the porosity was assumed constant in the numerical solution, but there are studies that imply that the pores increase in size during enzymatic hydrolysis, which will also impact the area of contact between enzymes and cellulose.

Another major determinant of characteristic diffusion time is particle size. The effect of particle radius on characteristic time is shown in Figure 6. The characteristic time is lowest for particle radius $R = 0.0025$ cm (16.65 s) and highest for particle radius of $R = 0.025$ cm (1,665 s); that is, with a 10x increase in particle radius, there is a 100x increase in characteristic time for diffusion. Based on the results of this study, if biomass particle radius were to increase much above 0.25 mm, the characteristic time for diffusion of non-adsorbing enzymes into the particle would increase into many thousands of seconds and ultimately may limit the observed global hydrolysis rate.

In the next section, the effects of biomass particle properties on the characteristic time for diffusion of adsorbing enzymes will be investigated. To increase the surface area for contact, the enhancement of pore accessibility and decrease in particle size is crucial. The pore sizes can be increased by various pretreatment techniques such as chemical, physical pretreatment. The estimation of characteristic time for various porosities and particle sizes is quite helpful in the optimization of enzymatic hydrolysis experiments.
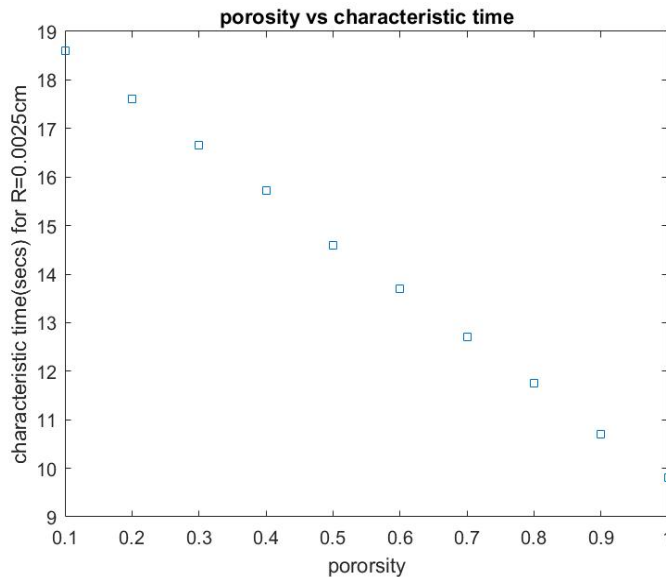
Figure 5. Effect of porosity on the characteristic time of diffusion of β-glucosidase into the Avicel PH-101 biomass particle with $'\varepsilon'$ varying from 0.1 to 1 and all other parameters constant.
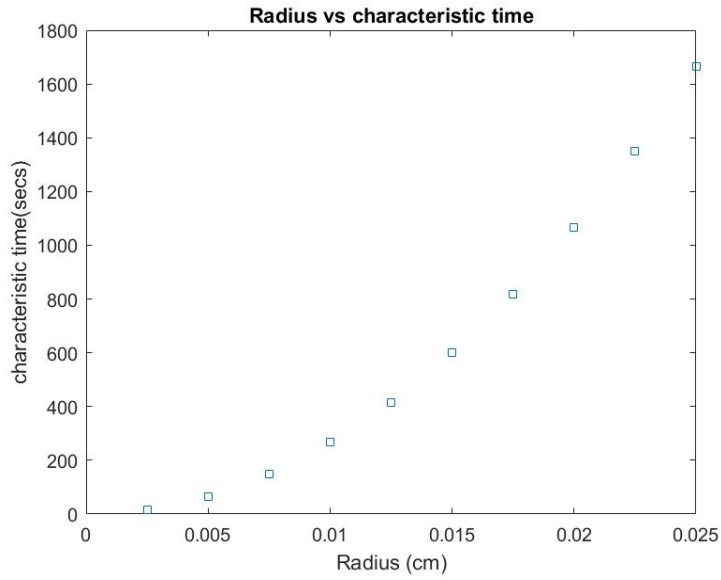
Figure 6. Effect of particle size on the characteristic time of diffusion of β-glucosidase into Avicel PH-101 biomass particle with $'R'$ varying from 0.0025 cm to 0.025 cm and all other parameters constant.

4.2 Effects of microporous structure on transient diffusion of adsorbing hydrolytic enzymes into biomass

The process of enzymatic hydrolysis (EH) involves a complex set of mechanistic steps, firstly, diffusion of adsorbing and non-adsorbing hydrolytic enzymes into the biomass particles followed by adsorption of hydrolytic enzymes onto the adsorption sites, and finally, the enzyme-catalyzed reaction occurs (Zhang et al., 2021). In section 4.1, we have studied the diffusion of non-adsorbing enzymes into biomass particles. In this section, we study the diffusion and adsorption of hydrolytic enzymes such as Endoglucanase (EG) and Cellobiohydrolase (CBH). It is important to understand the relative rates of diffusion and adsorption compared to enzymatic hydrolysis reactions in order to optimize the parameters of the system for minimum process residence time and to maximize yields of sugars. The characteristic time for diffusion of adsorbing enzymes and the influence of porosity and particle size of biomass particles will be investigated in this section.

The mechanistic model for transient diffusion of adsorbing hydrolytic enzymes into lignocellulosic biomass particles is formulated using Fick's law of diffusion and Langmuir adsorption isotherm. The lignocellulosic biomass particles are assumed to be cylindrical in this model since cylindrical geometry resembles the closest to real-life biomass particles. In this model, we consider that diffusion and adsorption occur only in the radial direction, considering that the aspect ratio of the particles is large (particle length to radius). Diffusion at the ends of the cylinder is neglected since the cylinder is exceedingly long. The transient diffusion and adsorption mechanism is described by a partial differential equation (PDE). In this model, the PDE is dependent upon the porosity and, the ratio of available pore volume and total pore volume, and adsorption parameters such as maximum adsorption capacity and affinity constants. The model parameters are mostly experimental values sourced from various literature, but, when necessary, parameters were estimated using appropriate equations. The maximum adsorption capacity of the biomass particle was set to zero and validated against the non-adsorbing diffusion model, which was validated against in analytical solution in section 4.1. Then the characteristic times for different biomass types predicted using the model were compared to literature to ensure the efficiency and accuracy of the model.

4.2.1 Model development

The physiochemical properties such as porosity and solid density are estimated using eq's. 1 and 2 specified in section 4.1. The enzyme effective diffusion coefficient is calculated using eq.3, specified in section 4.1. The solid density does not account for the pore spaces; hence, to further incorporate the internal pore volume, we use apparent density, which is estimated using Eq. 8 of section 4.2 adapted from Zhang et al., (2016).

$$\rho_a = \frac{\rho_s}{1 + V_P \rho_s}, \tag{8}$$

where V_p is the total pore volume, ρ_s is the solid density. In this study, the Langmuir adsorption isotherm adapted from Zhang et al., (2016) is used to model the adsorption of enzymes due to its capability to fit a diverse range of data and its simplicity. The Langmuir adsorption isotherm is given by:

$$q = f(CE) = \frac{q_m K_a CE}{1 + K_a CE},$$ (9)

where q is the equilibrium amount of solid-phase bound enzyme inside the particle pores, q_m is the maximum solid-phase bound capacity, K_a is the affinity constant, and CE is the enzyme concentration inside the pores of the particle. The mass balance equation of the adsorbing enzyme with internal pore diffusion inside the cylindrical particles adapted from Zhang et al., (2016) is given by:

$$\epsilon \frac{\partial CE}{\partial t} + \rho_a \frac{\partial q}{\partial t} = \varphi \frac{1}{r} \frac{\partial}{\partial r}\left(r D_{P_{CE}} \frac{\partial CE}{\partial r}\right) + \frac{1}{r} \frac{\partial}{\partial r}\left(r \rho_a D_{S_{CE}} \frac{\partial q}{\partial r}\right),$$ (10)

where CE is the enzyme concentration inside the pores of the particle, φ is the ratio of accessible pore volume to the enzyme (V_{PA}) to the total pore volume (V_P), $D_{P_{CE}}$ is the effective diffusion coefficient of adsorbing enzyme, $D_{S_{CE}}$ is the surface diffusion coefficient of the enzyme (Eqn. 4), and ϵ is the porosity of the biomass particle. In this study, we assume that pore diffusion is dominant, and that surface diffusion has no significant effect on the characteristic time of diffusion of hydrolytic adsorbing enzymes since enzymes diffuse into the pores and immediately get adsorbed, and after which they hydrolyze the cellulose. Which results in the mass balance equation:

$$\epsilon \frac{\partial CE}{\partial t} + \rho_a \frac{\partial q}{\partial t} = \varphi \frac{1}{r} \frac{\partial}{\partial r}\left(r D_{P_{CE}} \frac{\partial CE}{\partial r}\right),$$ (11)

The model can be further simplified by differentiating eq. 9 w.r.t CE, which yields:

$$dq = f'(CE)dCE,$$ (12)

where, $f'(CE) = \frac{q_m K_a}{(1+K_a CE)^2}$. $f'(CE)$ is the differential of the Langmuir isotherm with respect to the concentration of enzyme in the pore fluid. In this model, instantaneous adsorption equilibrium is assumed for modeling the effects of adsorption on the diffusion characteristic time. Now substituting eq.12 into eq.11 gives:

$$\left(\epsilon + \frac{\rho_a [q_m]_{CE} K_a}{(1 + K_a CE)^2}\right) \frac{\partial [CE]}{\partial t} = \varphi \frac{1}{r} \frac{\partial}{\partial r}\left(r D_{P_{CE}} \frac{\partial [CE]}{\partial r}\right),$$ (13)

4.2.2 Boundary conditions

The initial condition for the model is given by:

At $t = 0 \; \forall \; 0 \leq r \leq R$

$$CE = 0 \tag{14}$$

Boundary conditions for the model are given by:

$t > 0$

At $r = 0$

$$\frac{\partial CE}{\partial r} = 0 \tag{15}$$

At r= R

$$CE = [C_L]_{CE} \tag{16}$$

4.2.3 Material properties and list of parameters

The biomass used in this model is Avicel-PH 101. A mixture of Cellobiohydrolase (CBH) and Endoglucanase (EG), referred to as adsorbing enzymes, is modeled in this study. The model is validated by comparing the characteristic time of diffusion of adsorbing enzymes found from various literature with the characteristic time found using the model. The required parameters are listed in Table 2.

Table 2. List of parameters and their values used in the model.

Parameter	Description	Units	Value and Source					
Biomass	-		Acid Pretreated Wheat Straw [N]	Alkali Pretreated Wheat Straw [N]	Avicel PH-101 [J]	Hydrothermal Bagasse [J]	Organosolv Bagasse [J]	8 min DAP,0 hr EH 160 °C [O]
Particle shape	-		Cylinder [D]	Cylinder [D]	Cylinder [D]	Cylinder [D]	Cylinder [D]	Cylinder [D]
Particle size		cm	0.04[N][I]	0.04[N][I]	0.005[J][H]	<0.05[J][I]	<0.05[J][I]	0.06[O][I]
ρ_a	Apparent density	g/cm^3	1.186[F]	1.11[F]	1.064[F]	1.04[F]	1.06[F]	0.88[F]
ρ_s	Solid density	g/cm^3	1.693[A]	1.592[A]	1.52[A]	1.49[A]	1.513[A]	1.49[A]
M_c	Mass percentage of cellulose	%	52.7[N]	65.0[N]	100[J]	61.07[J]	86.91[J]	58.5[O]
M_h	Mass percentage of hemicellulose	%	12.1[N]	25.3[N]	0[J]	2.10[J]	6.63[J]	13.5[O]
M_l	Mass percentage of lignin	%	20.5[N]	3.6[N]	0[J]	31.97[J]	4.42[J]	28[O]
M_o	Mass percentage of other compositions	%	4.7[N]	3.1[N]	0[J]	6.44[J]	3.74[J]	0[O]
ρ_c	Cellulose density	g/cm^3	1.52[K]	1.52[K]	1.52[K]	1.52[K]	1.52[K]	1.52[K]
ρ_h	Hemicellulose density	g/cm^3	1.56[K]	1.56[K]	1.56[K]	1.56[K]	1.56[K]	1.56[K]
ρ_l	Lignin density	g/cm^3	1.39[K]	1.39[K]	1.39[K]	1.39[K]	1.39[K]	1.39[K]

ρ_o	Density of other compositions	g/cm^3	2.50[K]	2.50[K]	2.50[K]	2.50[K]	2.50[K]	2.50[K]
K_a	Affinity constant	ml/mg	22.50[N]	4.33[N]	4.46[J]	1.28[J]	2.68[J]	-
q_m	Maximum adsorption capacity	mg/g substrate	9.65[N]	31.89[N]	17.41[J]	36.93[J]	29.40[J]	-
V_{pa}	Pore volume accessible to the enzyme	cm^3/g	-	-	-	-	-	-
φ	Pore volume accessible to the enzyme/total pore volume	-	1[D]	1[D]	1[D]	1[D]	1[D]	1[D]
$D_{P_{CE}}$	Pore diffusion coefficient of adsorbing enzymes	cm^2/sec	1×10$^{-7[C]}$	1×10$^{-7[C]}$	1×10$^{-7[C]}$	1×10$^{-7[C]}$	1×10$^{-7[C]}$	1.48 × 10$^{-7[C]}$
Isotherm	-	-	Langmuir [N]	Langmuir [N]	Langmuir [J]	Langmuir [J]	Langmuir [J]	Langmuir [O]
R	Radius of the particle	cm	<0.02 [N]	<0.02 [N]	0.0025[J]	<0.025[J]	<0.025[J]	0.03[O]
ϵ	porosity	-	0.3 [B]	0.3[B]	0.3[B]	0.3[B]	0.3[D]	0.406[D]
V_p	Pore volume	cm^3/g	0.252[D]	0.269[D]	0.282[L]	0.287[D]	0.283[D]	0.46[D]
$C_{L_{CE}}$	Concentration of adsorbing enzymes in the bulk solution	mg /ml	1[D]	1[D]	1[D]	1[D]	1[D]	1[D]
D_w	Diffusion coefficient of	cm^2/sec	5.67 × 10^{-7} [M] [E]	5.67 × 10^{-7} [M] [E]	5.67 × 10$^{-7[M] [E]}$	5.67 × 10^{-7} [M] [E]	5.67 × 10$^{-7[M] [E]}$	5.67 × 10^{-7} [M] [E]

	enzymes in pure water							
CE	Concentration of adsorbing enzymes inside the biomass particle	mg/ml	-	-	-	-	-	-
t	Enzyme diffusion time	sec	-	-	-	-	-	-
r	Radial position inside the particle	cm	-	-	-	-	-	-
τ	Characteristic time for maximum adsorption	min	-	-	-	-	-	-

A- calculated using eq.2, B- calculated using eq.1, C- calculated using eq.3, D- Assumption, E- D_w ranges from 10^{-6} to 10^{-7} cm^2/sec and assumption, F- calculated using eq. 8, G- Mean particle size of a particle size distribution, H – All particles are of the same size, I- Maximum particle size from a particle size distribution, J - Machado et al.,(2015), K- Zhang et al., (2016), L- Tantasucharit.,(1995), M- Yohana et al., (2020), N- Qi et al.,(2011), O- Ankathi et al., (2019)

4.2.4 Method of solution

The transient diffusion model for adsorbing enzymes is numerically solved using eq. 13, boundary conditions, and data from Table 2. The characteristic time (i.e., the time needed for the enzyme concentration inside the particle at $r = 0$ to reach 99% of the enzyme concentration in the bulk solution) is calculated using a custom-written program in MATLAB (MathWorks, Natick, MA, USA). The numerical solution is validated by comparing the characteristic times estimated using the model with characteristic times found in the literature for experimental adsorption data. The effect of porosity, pore size, maximum adsorption capacity, and affinity constant on the characteristic time for diffusion into a cylindrical Avicel particle is estimated by varying the porosity from 0.1 to 1 with intervals of 0.1, varying the pore size from 0.0025 cm to 0.025 cm with intervals of 0.0025 cm, varying maximum adsorption capacity from 0 to 100 mg/ g substrate with intervals of 20 mg/g substrate and varying the affinity constant from 0 to 20 ml/mg with intervals of 4 ml/mg respectively.

4.2.5 Results and discussion

The concentration of adsorbing enzymes at different radial positions inside the cylindrical biomass particle was found by numerically solving eq. 13 using a parabolic partial differential equation solver (i.e., PDEPE function) available in MATLAB and using the model parameters listed in Table 2. The graph in Figure 7 shows the concentration of adsorbing enzymes vs. time (sec) at different radial positions inside the biomass particle. Compared to the concentration profiles for non-adsorbing enzymes shown in Figure 3, the time required for penetration of the enzyme into the particle is much longer for adsorbing enzymes than for non-adsorbing enzymes. For example, for the non-absorbing enzyme in Figure 3, the time required for the enzyme to become detectable at $r=0$ is 1 sec. In contrast, for adsorbing enzyme in Figure 7, the time is approximately 150 sec. This effect is entirely due to the adsorption process.
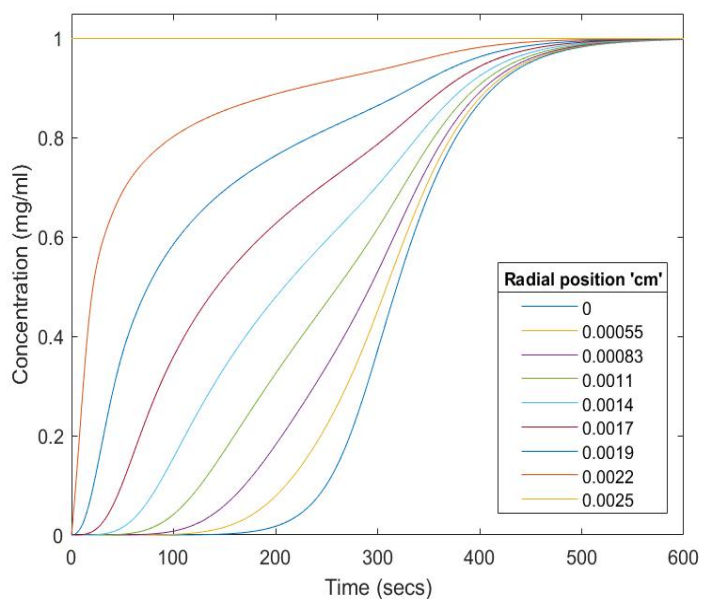
Figure 7. Concentration of Adsorbing enzymes at different radial positions inside the cylindrical Avicel PH-101 biomass particle with q_m=17.41 mg/g substrate, K_a= 4.46 ml/mg, and other constant parameters listed in Table 2.

The characteristic time $'\tau'_{numerical}$ for adsorbing enzymes to diffuse into cylindrical Avicel PH-101 biomass particle was found to be around 8.8 mins. The concentration profile agrees with the specified initial and boundary conditions. The experimental characteristic times were approximated by observing the peaks of time vs. adsorbed cellulase amount in substrate graphs from various literature; the time when the peak reaches maximum was noted as the characteristic time. The model was validated using the characteristic time for maximum cellulase adsorption $'\tau'_{experimental}$ observed from the experimental data of (Machado et al.,2015) is around 10 mins, which is comparatively close to the predicted characteristic time for the Avicel PH-101 particle, whose particle size is constant for all the particles. The predicted characteristic times $'\tau'_{numerical}$ for various other biomass particles along with their respective $'\tau'_{experimental}$ values are listed in Table 3 for comparison. The $'\tau'_{experimental}$ for Acid PWS and Alkali PWS, according to the literature, was around 90 mins but the $'\tau'_{numerical}$ found were not in agreement when the maximum particle size mentioned in the literature was utilized to run the model. To get a numerical characteristic time for Acid PWS and Alkaline PWS closer to the experimental characteristic time, we might have to use a mean particle size of 0.01 cm. This difference in assumed particle sizes to achieve a similar experimental characteristic time is due to the difference in their maximum adsorption capacities shown in Table 3. Similarly, for HB and OB, we might need to assume a mean particle size of 0.01 cm for both the biomass particles; we are assuming a similar mean particle size for both biomass particles because the difference in adsorption capacities is not huge. We also need to note that the particle sizes of Acid PWS,

25

Alkali PWS, HB, and OB were maximum particle sizes that can pass through the screening. A key observation was that when reducing the modeled particle size compared to the experimental value for those from screening, the particles provide a better agreement between the model and the experimental characteristic times.

Table 3. Comparison of characteristic time found using the model with characteristic times from literature for different lignocellulosic biomass.

Biomass	Radius of Particle $'R'$ (cm)	$\tau_{experimental}$ (min)	$\tau_{numerical}$ (min)
Avicel PH-101	**0.0025 [B]**	**~10 [B]**	**8.8**
Acid PWS	<0.02 [D]	~90 [D]	276
	0.01 [A]		70
Alkali PWS	<0.02 [D]	~90 [D]	750
	0.01 [A]		187.8
Hydrothermal Bagasse	<0.025 [B]	~210 [B]	1280
	0.01 [A]		200
Organosolv Bagasse	<0.025 [B]	~180 [B]	1067
	0.01 [A]		170

A- The average particle size predicted using the model, B- Machado et al.,(2015), C- Zhang et al., (2016), D- Qi et al.,(2011).

Researchers like Siqueira et al., (2017) have emphasized the influence of substrate characteristics on the ability of adsorption and diffusion of enzymes into biomass particles. To further understand the influence of microporous structures on the diffusion of adsorbing enzymes, the porosity and particle size of the cylindrical Avicel PH-101 biomass particle was varied. The effect of adsorption characteristics on the diffusion of adsorbing enzymes was studied by varying the maximum adsorption capacity and affinity constant of Avicel biomass particles. Using the model, the effect of porosity on diffusion is shown in Figure 8, assuming that all pores are accessible to the enzyme for diffusion into the biomass particle. The characteristic time for diffusion goes down with increasing porosity, which is an expected result. As porosity increases, it increases the effective diffusion coefficient of adsorbing enzyme according to eq. 3. It is interesting to note that the decrease in characteristic time with increasing porosity is greater for adsorbing enzymes compared to non-adsorbing enzymes.
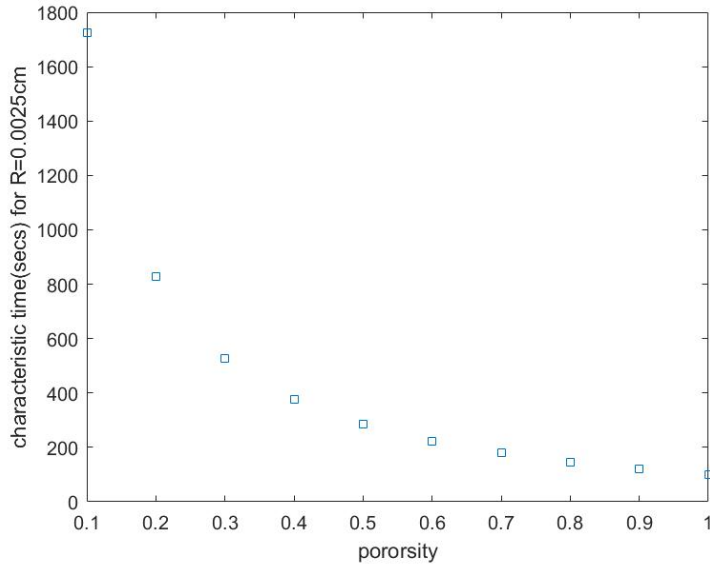
Figure 8. Effect of porosity on the characteristic time of diffusion of Adsorbing enzymes into an Avicel PH-101 biomass particle with $'\varepsilon'$ varying from 0.1 to 1 and all other parameters as constant.

Based on the results shown in Figure 8, we can conclude that the porosity significantly affects the characteristic time for adsorbing enzyme diffusion. In this section, similar to section 4.1, we assume that all the pores are accessible, but, in reality, all the pores are not readily accessible, which affects the efficiency of enzymatic hydrolysis. For each different porosity value, the porosity was assumed constant in the numerical solution, but some studies imply that the pores increase in size during enzymatic hydrolysis, which will also impact the area of contact between enzymes and cellulose. We observed an exponential trend in Figure 8 for adsorbing enzymes contrary to a linear trend in Figure 5 for β-glucosidase enzyme. This change in trend is due to coupling of adsorption isotherm with porosity in eq. 13.

For adsorbing enzymes, the adsorption term is much greater than ε, and over the range of $0.1 < \varepsilon < 1$, the term on the left-hand side of equation 13 involving the Langmuir isotherm is nearly constant. For this case, the characteristic time will vary with changing ε as $(2 - \varepsilon)/\varepsilon$, which is a factor of 19 over the range of $0.1 < \varepsilon < 1$, in close agreement with Figure 8. However, there are limitations to this analysis of characteristic time for adsorbing enzymes. The limitation of the study of the effect of porosity on characteristic time is that the apparent density $'\rho_a'$ and $'q_m'$ were kept constant throughout the study of the effect of changing ε, but in theory, these two parameters should vary with porosity. But due to the lack of data on how these two parameters vary with changing porosity, they were kept constant. With sufficient information, the model could capture the interplay between these parameters and their effect on the characteristic time of diffusion. When the porosity increases, apparent density should decrease based on equations (1) and (8), and maximum

adsorption capacity (q_m) should increase up to a finite maximum value determined by the number of adsorption sites per unit area on the cellulose surface. However, these counteracting trends in ρ_a and q_m with increasing ε are not predictable at this time but must rely on experimental measurements to fully understand them. Therefore in this analysis of characteristic time variation with ε, adsorption parameters were kept constant.

The other major factor influencing the characteristic time of diffusion is particle size. The effect of particle radius on the characteristic time of diffusion of adsorbing enzyme is shown in Figure 9. The characteristic time is lowest for particle radius $R = 0.0025$ cm (526.12 s) and highest for particle radius of $R = 0.025$ cm (52,613 s), that is, with a 10x increase in particle radius, there is a 100x increase in characteristic time for diffusion which is similar to the trend observed for β-glucosidase enzyme. Based on the above observation, to reduce the processing time for enzymatic hydrolysis, the particle diameter must be lowered to a smaller size range, and the biomass must be pretreated to increase the porosity.
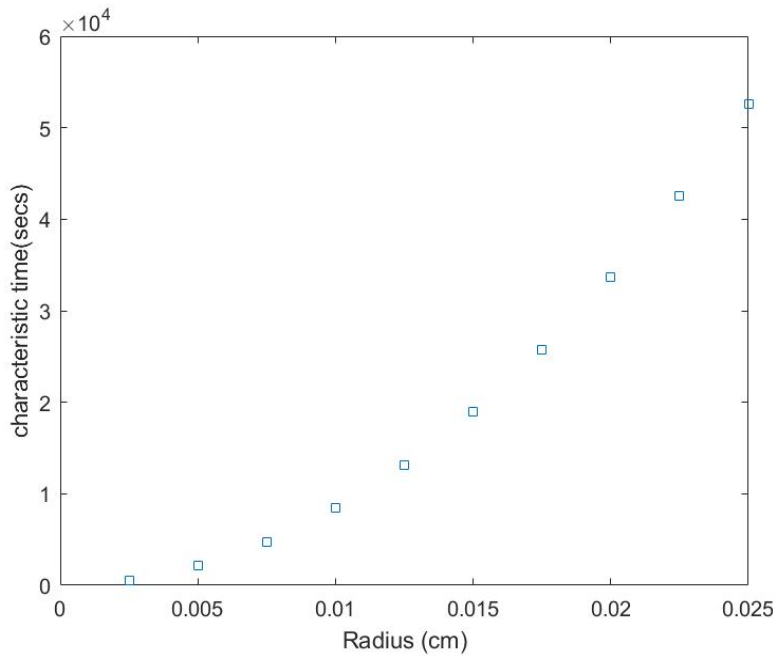
Figure 9. Effect of particle size on the characteristic time of diffusion of adsorbing enzymes into an Avicel PH-101 biomass particle with $'R'$ varying from 0 to 0.025 and all other parameters as constant.

To further understand the effect of substrate characteristics on the diffusion of enzymes, the maximum adsorption capacity of the substrate was varied, and the effect of maximum adsorption capacity on the diffusion of adsorbing enzymes is shown in Figure 10. A linear trend between characteristic time and maximum adsorption capacity was observed. The lowest characteristic time (16.67 s) was observed at ($q_m = 0$ mg/g substrate) and highest characteristic time (2925 s) was observed at ($q_m = 100$ mg/g substrate). This shows that maximum adsorption capacity significantly affects the diffusion of enzymes into a biomass

particle. The Langmuir or affinity constant 'K_a' indicates the extent of interaction between adsorbate and the surface. To understand the effect of affinity constant (extent of interaction between adsorbate and the surface) on the diffusion of enzymes, the $'K_a'$ value was varied from 0 to 10 mg/ml for Avicel PH-101 biomass particle. The graph in Figure 11 depicts the dependence of diffusion of enzymes on affinity constant. When the value of $'k_a'$ was zero, the characteristic time of diffusion was 16.67 secs, which means there was no effect of adsorption on the diffusion of enzymes. As we increased the affinity constant gradually, the characteristic time also increased to a maximum of 547.4 secs for $'k_a' = 3$ ml/mg. After reaching the highest characteristic time, the influence of affinity constant on characteristic time of diffusion of enzymes gradually started decreasing.
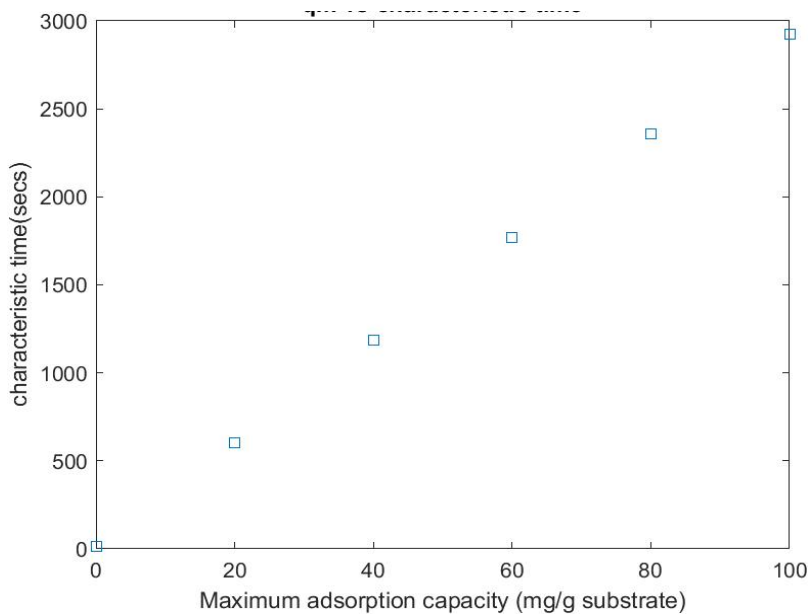
Figure 10. Effect of maximum adsorption capacity on the characteristic time of diffusion of adsorbing enzymes into an Avicel PH-101 biomass particle with $'q_m'$ varying from 0 to 100 and all other parameters as constant.
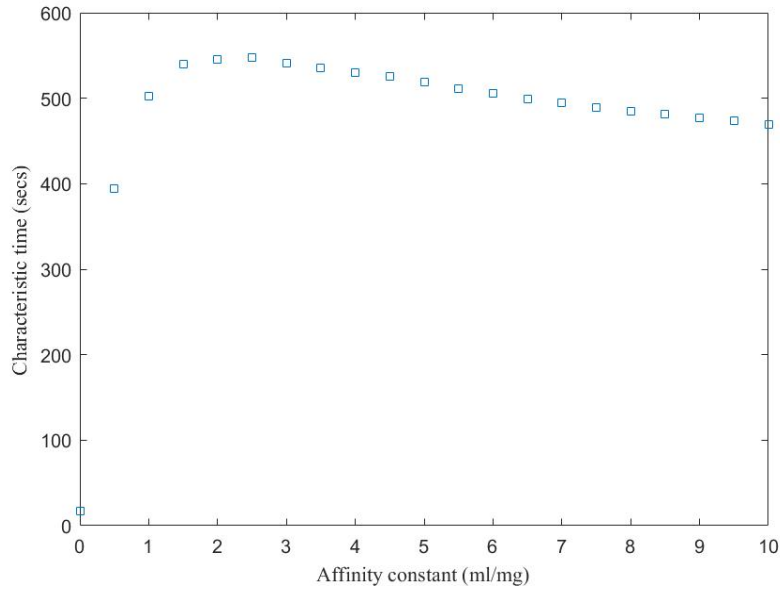
Figure 11. Effect of Affinity constant on the characteristic time of diffusion for adsorbing enzymes into Avicel PH-101 biomass particle with $'K_a'$ varying from 0 to 10 ml/mg and all other parameters as constant.

The model predicted an 18x decrease in characteristic time of diffusion of enzymes when the porosity was varied from 0.1 to 1, a 100x increase in characteristic time of diffusion when the particle size was increased by 10 times the typical particle size of Avicel PH-101, a 180x increase in characteristic time of diffusion when the maximum adsorption capacity was increased over an expected range of values from the literature for Avicel PH-101, and a 50x increase in characteristic time when the affinity constant was increased over an expected range of values from literature according to Figure 8, Figure 9, Figure 10, and Figure 11 respectively. These predictions may not hold true in all cases since the range of values may differ in every scenario. However, for the range of values modeled in this study, we can infer based on the predictions that the maximum adsorption capacity has the strongest effect on the characteristic time of diffusion followed by particle size followed by affinity constant followed by porosity ($q_m > R > K_a > \varepsilon$).

4.3 Modeling the effect of aspect ratio on transient diffusion of hydrolytic enzymes into Avicel PH-101 biomass using *COMSOL® 5.3*

The importance of research into sustainable biofuels and optimization of enzymatic hydrolysis process has been thoroughly emphasized in the previous sections. Since we already know that the enzymatic hydrolysis process involves diffusion of enzymes into pores of the biomass particles and adsorbing to the surface, which enables a hydrolysis reaction to occur. We have studied the effects of microporous structures on the diffusion of hydrolytic enzymes in sections 4.1 and 4.2. The enzymatic hydrolysis model in those sections only considered radial diffusion of enzymes under the assumption that the biomass particle is sufficiently long to justify neglecting particle end effects. In this section, we studied the effect of the aspect ratio of the biomass particle on the diffusion of non-adsorbing enzymes by modeling a cylindrical system in *COMSOL® 5.3*. We expect to show that as the aspect ratio increases, the characteristic times obtained using the 2D COMSOL model will approach and agree with the 1D MATLAB model.

4.3.1 Model development

The biomass particle is modeled as an unsteady isothermal state cylindrical system with axial symmetry and origin at the center of the cylindrical half-section, as shown in Figure 12. A 2D axisymmetric model was developed to predict the diffusion only in the r- direction and the z-direction because of symmetry in the angular direction (θ). Diffusion occurs through three surfaces ($r = R$, $z = L/2$, and $z = -L/2$) of the cylinder. The concentration of enzyme will vary with time, with r, and with z.:

Concentration: $B = B(r, z, t)$
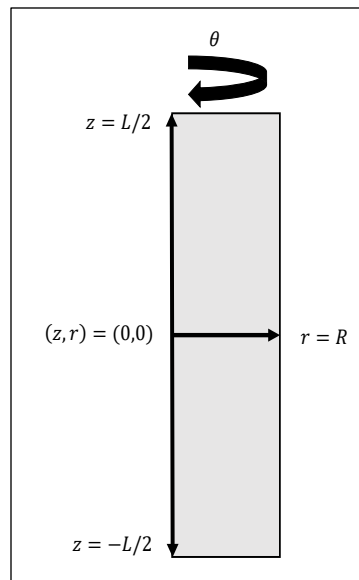
Figure 12. System geometry

31

This model utilizes the equation of continuity or the diffusion equation to account for the mass transfer of enzymes into the pores of the biomass particle, which is given by:

$$\frac{\partial B}{\partial t} = \frac{1}{r}\frac{\partial}{\partial r}\left(r D_p \frac{\partial B}{\partial r}\right) + \frac{1}{r}\frac{\partial}{\partial \theta}\left(D_p \frac{\partial B}{\partial \theta}\right) + \frac{\partial}{\partial z}\left(D_p \frac{\partial B}{\partial z}\right),$$

(17)

where 'B' is the concentration of hydrolytic enzymes inside the biomass particle, 'r' is the radial position, D_p' is the effective diffusion coefficient of hydrolytic enzymes calculated using eq. 3, and assuming that the effective diffusion coefficient is the same in all coordinate directions. This is justified because the biomass particles modeled in this study are produced by the random chaotic breakdown of wood chips in a hammer mill, due to which it is difficult to predict the alignment of fibers or other structures such as lumen for all the particles based on which we decided to assume that the diffusion coefficient is same in all directions. The diffusion equation can be simplified further due to symmetry in θ-direction into:

$$\frac{\partial B}{\partial t} = \frac{1}{r}\frac{\partial}{\partial r}\left(r D_p \frac{\partial B}{\partial r}\right) + \frac{\partial}{\partial z}\left(D_p \frac{\partial B}{\partial z}\right),$$

(28)

The diffusion equation can be further modified to account for porosity and pore volume based on Zhang et al., (2016) into:

$$\epsilon \frac{\partial B}{\partial t} = \varphi \frac{1}{r}\frac{\partial}{\partial r}\left(r D_p \frac{\partial B}{\partial r}\right) + \varphi \frac{\partial}{\partial z}\left(D_p \frac{\partial B}{\partial z}\right),$$

(19)

Where $'\varepsilon'$ is the porosity of the biomass particle calculated using eq. 1, φ is the ratio of accessible pore volume to the enzyme (V_{PA}) to the total pore volume (V_P). The enzymes were assumed to have no restrictions on diffusion.

4.3.1.1 Boundary conditions

The initial and boundary conditions used in the simulation are listed in Table 4.

Table 4. Initial and boundary conditions are used in the 2D model.

	Boundary	Concentration
I.C.	$\forall\, 0 \leq r \leq R, \forall\, -\frac{L}{2} \leq z \leq \frac{L}{2}$	$B = 0$
B.C. 1	$@r = 0$	$\frac{\partial B}{\partial r} = 0$
B.C. 2	$@r = R$	$B = C_{L_B}$
B.C. 3	$@z = 0$	$\frac{\partial B}{\partial z} = 0$
B.C. 4	$@z = -\frac{L}{2}, @z = \frac{L}{2}$	$B = C_{L_B}$

4.3.1.2 COMSOL® 5.3 Multiphysics model description

The diffusion of hydrolytic enzymes has been modeled using the porous media flow module available in COMSOL® 5.3. The physics, study, special dimension, and biomass material required for the model are as follows.

Physics: Chemical species transport → Transport of diluted species in porous media.

Study: Time-dependent.

Space dimension: 2-D axisymmetric.

Biomass material: (Manually defined)

The biomass material (Avicel PH-101) had to be manually defined in *COMSOL® 5.3* as it was unavailable.

4.3.2 Material properties and list of parameters

Due to the availability of biomass property data, Avicel PH-101 with no adsorption capacity was used in this model, and a mixture of adsorbing and non-adsorbing (β-gluconase) enzymes were also used. The data needed for the model are listed in Table 5.

Table 5. Material properties and list of parameters used in the 2D COMSOL model.

Parameter	Description	Units	Value	Source
Biomass	-	-	Avicel PH101	[H]
Particle shape	-	-	Cylinder	[K]
Particle size (D)	Diameter of particle	cm	0.005	[H]
ρ_s	Solid density	g/cm^3	1.52	[A]
M_c	Mass percentage of cellulose	%	100	[H]
M_h	Mass percentage of hemicellulose	%	0	[H]
M_l	Mass percentage of lignin	%	0	[H]
M_o	Mass percentage of other compositions	%	0	[H]
ρ_c	Cellulose density	g/cm^3	1.52	[I]

ρ_h	Hemicellulose density	g/cm^3	1.56	[I]
ρ_l	Lignin density	g/cm^3	1.39	[I]
ρ_o	Density of other compositions	g/cm^3	2.50	[I]
V_{PA}	Pore volume accessible to the enzyme	cm^3/g	0.282	[D]
φ	Pore volume accessible to the enzyme/total pore volume	-	1	[D]
D_p	Pore diffusion coefficient of enzyme	cm^2/sec	1×10^{-7}	[A]
ϵ	Porosity	-	0.3	[B]
V_P	Total pore volume	cm^3/g	0.282	[J]
B	Concentration of enzyme mixture inside the biomass in the pore fluid	mol/m^3	-	-
C_{L_B}	Concentration of enzyme mixture in the bulk solution	mol/m^3	0.014706	[D][G]
D_w	Diffusion coefficient of enzymes in pure water	cm^2/sec	5.67×10^{-7}	[K][E]
t	Enzyme diffusion time	sec	-	-
τ	Characteristic time	sec	-	-
r	Radial position inside the particle	cm	-	-
R	Radius of the particle	cm	0.0025	[H]
L/D	Aspect ratio	-	-	-
K_a	Affinity constant	m^3/mol	0	[D]
q_m	Maximum solid phase bound capacity	mol/kg substrate	0	[D]
L	Length of the particle	cm	-	-

A- calculated using eq.2, B- calculated using eq.1, C- calculated using eq.3, D-
Assumption, E- D_w ranges from 10^{-6} to 10^{-7} cm^2/sec and assumption, F- calculated using
eq.8, G- Converted to moles using the molecular weight of Trichoderma Reesei (68 kDa)

where 1 kDa = 1000g/mol, H- Machado et al.,(2015), I- Zhang et al., (2016), J-Tantasucharit.,(1995), K-Yohana et al. (2020).

The characteristic time is defined as the time needed for the enzyme concentration inside the particle at ($r, z = 0, 0$) to reach 99% of the enzyme concentration in the bulk solution (C_{L_B}). All the pores of the biomass particle are assumed to be accessible to the diffusing enzymes. The aspect ratios evaluated in this model are (***L/D*** = 1, 2, and 4). The characteristic times obtained for different aspect ratios using COMSOL were compared to those obtained for non-adsorbing enzymes using the 1D MATLAB model.

4.3.3 Results and discussion

The COMSOL model was used to develop the concentration profile shown in Figure 13 for the diffusion of hydrolytic enzymes into the Avicel PH-101 biomass particle with an aspect ratio of L= 4D. The concentration profile at the initial condition is shown in Figure 13(a), and the simulation was run until the system reached the characteristic diffusion time, which is defined as the center (i.e., $r=0$, $z=0$) of the biomass particle reaching 99% of the total enzyme bulk concentration. The concentration gradient inside the particle is dark blue at initial conditions since diffusion of enzymes has not started. The edge of the particle is colored dark red, the high concentration of enzymes at the boundary. As the simulation starts, enzymes begin to diffuse into the particle, and the concentration of enzymes increases steadily towards the center of the cylinder. The simulation characteristic time is at 15.508 seconds since the center of the biomass particle has reached 99% of the total enzyme bulk concentration, as shown in Figure 13(b). The concentration gradient scale placed on the right-hand side of the figures is adjusted based on the concentration of enzymes at steady-state; the dark blue color on the scale now represents 99% of the bulk concentration.
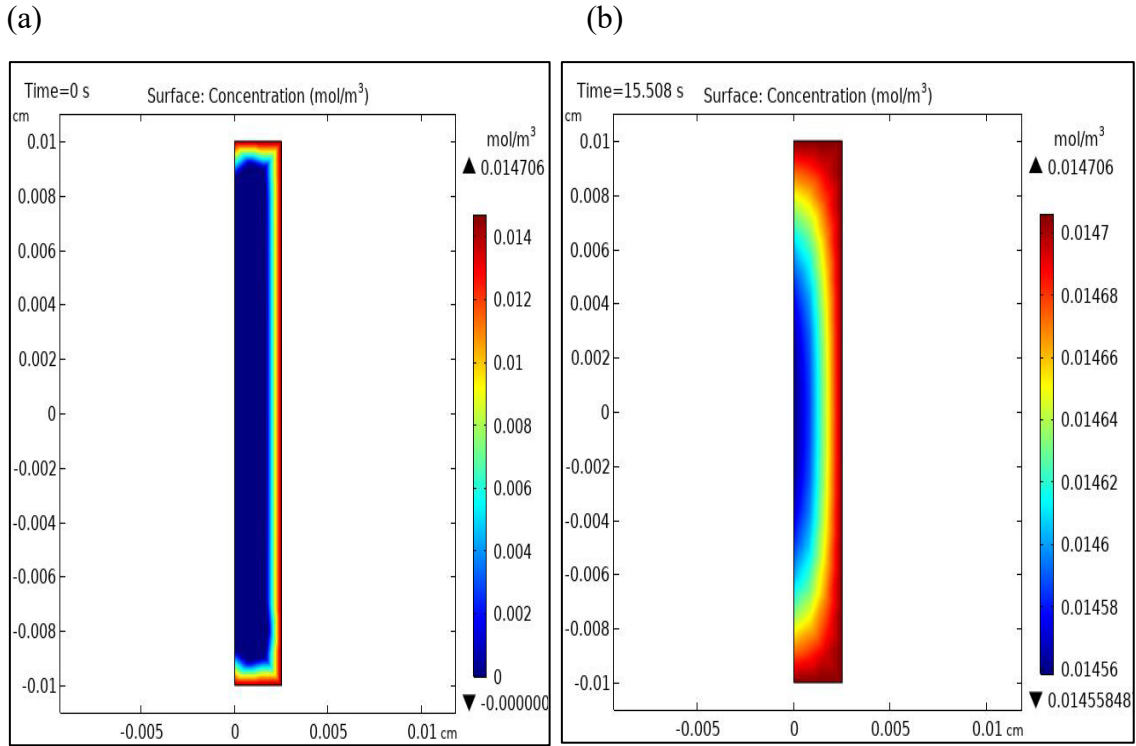
Figure 13. Concentration profile of non-adsorbing enzyme inside the Avicel PH-101 biomass particle with aspect ratio (L/D = 4) at (a) t=0 secs and (b) t = τ secs.

The main objective of this COMSOL model was to observe the effect of aspect ratio on enzyme diffusion characteristic times. To achieve this goal, the aspect ratio was gradually increased from L=D to L=2D, then to L= 4D. When the length of the biomass particle was equal to the diameter of the particle, we observed that the characteristic time was the lowest at 11.49 secs, as shown in Figure 14(a). Then length was increased by two times the diameter, the characteristic time was 14.767 secs, as shown in Figure 14(b). Finally, the length of the particle was increased to four times that of the diameter of the particle, and the characteristic time was predicted to be 15.508 secs, which compared to the characteristic time found using the 1D model numerical solution in section 4.1 of chapter 4 was the closest. This comparison suggests that the effect of aspect ratio on the diffusion of hydrolytic enzymes is not significant, and the characteristic time estimated for Avicel PH-101 in section 4.1, which is 16.65 secs, is closest to the characteristic time estimated using COMSOL was 15.508 secs when Avicel PH-101 particle had an aspect ratio of L=4D. The effect of aspect ratio on diffusion is demonstrated using the graph in Figure 15. The rate of diffusion was highest for aspect ratio L = D and lowest for L = 4D. The aspect ratio, which can be assumed as the closest to a realistic particle based on the observation, is L = 4D.
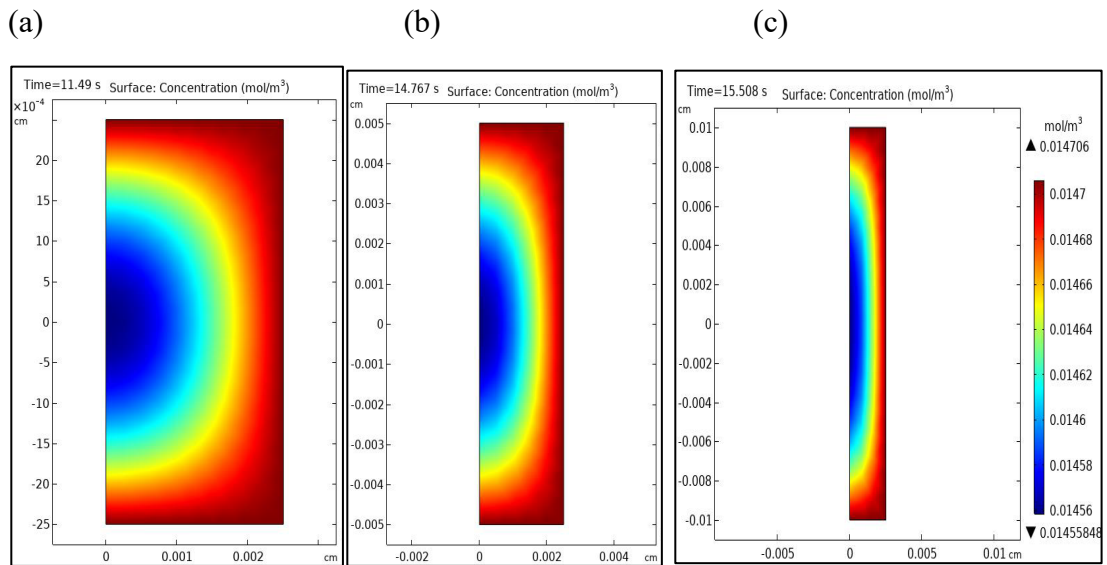
Figure 14. Concentration profiles of non-adsorbing enzymes inside the Avicel PH-101 biomass particle at t = τ with aspect ratio (a) L/D=1, (b) L/D = 2, (c) L/D = 4.
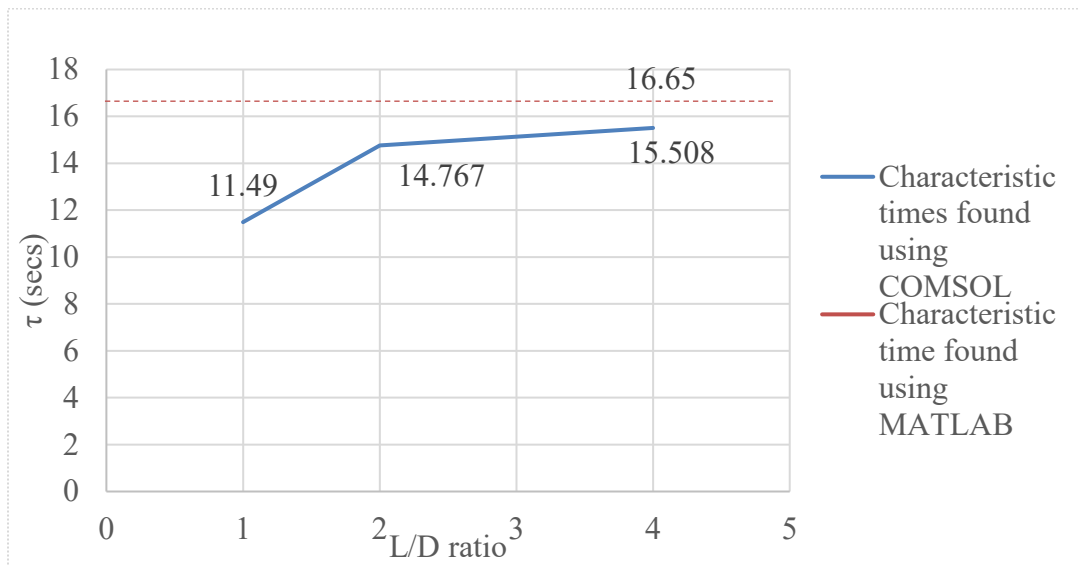
Figure 15. Effect of aspect ratio on the characteristic time for diffusion of hydrolytic enzymes into an Avicel PH-101 biomass particle, the dashed line represents the characteristic time for non-adsorbing enzyme diffusion found using Eq. 13 (MATLAB).

4.4 Effects of microporous structure on glucose yield from the enzymatic conversion of biomass

The last step of EH is the conversion of cellulose into cellobiose and glucose by enzyme-catalyzed reactions at the particle pore surface. In the previous sections 4.1 and 4.2, we modeled the diffusion and adsorption of enzymes, respectively. In this section, we develop a kinetic model for sugar production coupled with the enzyme diffusion and adsorption model developed in the earlier sections to account for relative rates of diffusion, adsorption, and enzymatic hydrolysis at different radial positions inside the particle. To maximize the sugar yield, it is essential to understand the influence of diffusion and adsorption of enzymes, particle porosity, and particle size.

The kinetic model developed in this section for the bulk change in glucose concentrations is adapted from Kadam et al., (2004) and modified by coupling it with the particle scale hydrolytic enzyme diffusion and adsorption model. The particle scale transient diffusion and adsorption model described using partial differential equations (PDE's) earlier in this thesis is converted into ordinary differential equations (ODE's) using the numerical method of lines by Scheiesser et al.,(1991). The change in hydrolytic enzyme concentrations in the bulk solution (the flask liquid between the biomass particles) are calculated using mass balance equations governed by the film mass transfer coefficients surrounding each biomass particle, the total area covered by the biomass particles, the concentration gradient of the enzymes, and the bulk volume of particles. The kinetics of cellobiose, glucose, and cellulose are modeled using the cellulose to cellobiose, cellulose to glucose, and cellobiose to glucose rate equations, governed by kinetic rate constants and Langmuir adsorption isotherm. The model is validated by comparing the model results with data from the literature.

4.4.1 Model development

The first step in the model development is the conversion of particle-scale PDEs to ODEs for the non-adsorbing and adsorbing enzymes given by equations 4 and 13 from sections 4.1 and 4.2, respectively, using the numerical method of lines. In this model, we divided the cylindrical biomass particle from the origin $'r = 0'$ to $'r = R'$ into 'N' equal radial sections, each represented by 'n', and $'N + 1'$ radial nodes represented by 'i' as shown in Figure 16.
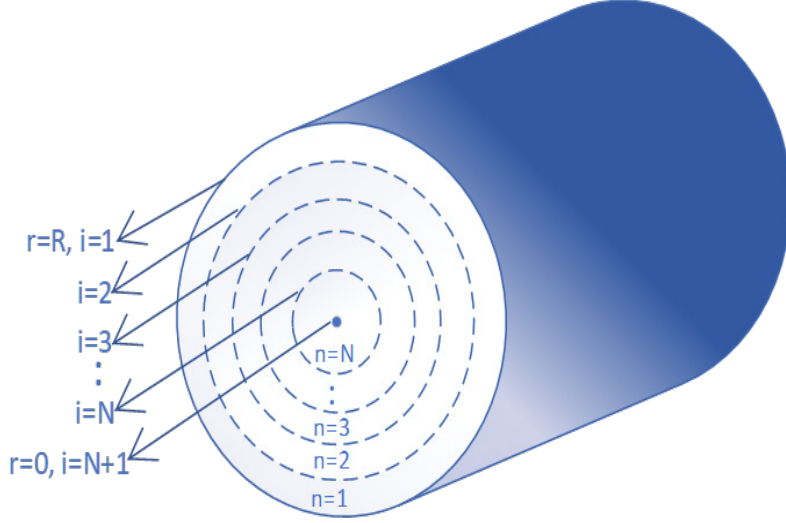
Figure 16. Cross-section of a cylindrical biomass particle used in the model.

Starting with the non-adsorbing enzyme, we convert eq.4 using a second-order central difference formula for the second derivative to give:

$$\frac{dBG(i)}{dt} = \frac{\varphi D_p}{\epsilon} \left[\frac{BG(i+1) - 2BG(i) + BG(i-1)}{\Delta r^2} \right.$$
$$\left. + \frac{1}{R - (i-1)\Delta r} \left(\frac{BG(i+1) - BG(i-1)}{2\Delta r} \right) \right], \qquad (20)$$

where, $i = 2,3,4, \ldots, N$, $BG(i)$ is the concentration of non-adsorbing enzyme (β-glucosidase) φ is the ratio of pore volume accessible to the enzyme to the total pore volume, D_p is the effective diffusion coefficient of the non-adsorbing enzyme, ε is porosity, and BG is the volume average pore enzyme concentration at different radial positions, Δr is the ratio of the radius of the particle and number of sections which is given by:

$$\Delta r = \frac{R}{N}, \qquad (21)$$

The initial condition for the non-adsorbing enzyme is:

$$BG(0) = 0 \ \forall \ 0 \leq r \leq R , \qquad (22)$$

The no flux boundary condition for the non-adsorbing enzyme at $r = 0$ represented by eq. 6 can be rewritten using second-order backward finite difference formula for first-order derivative (Cutlip and Shacham.,2008) as :

$$\left. \frac{\partial BG(i = N+1)}{\partial r} \right|_{r=0} = \frac{3BG(N+1) - 4BG(N) + BG(N-1)}{2\Delta r} = 0, \qquad (23)$$

Eq. 23 can be solved for $BG(N+1)$ to yield:

$$BG(N+1)|_{r=0} = \frac{4BG(N) - BG(N-1)}{3},\tag{24}$$

The flux boundary condition for the non-adsorbing enzyme at $r = R$ is given by:

$$D_p \left.\frac{\partial BG}{\partial r}\right|_{r=R} = -k(C_{BG} - BG|_{r=R}),\tag{25}$$

where k represents the external-film mass transfer coefficient, D_p is the effective diffusion coefficient of the non-adsorbing enzyme, C_{BG} is the concentration of non-adsorbing enzyme in the bulk solution. The transient boundary condition at $r = R$ represented by eq. 25 can be rewritten using second-order forward finite difference formula for first-order derivative (Cutlip and Shacham.,2008) as:

$$\left.\frac{\partial BG(i=1)}{\partial r}\right|_{r=R} = \frac{-3BG(1) + 4BG(2) - BG(3)}{2\Delta r} = -\frac{k}{D_p}(C_{BG} - BG(1)|_{r=R}),\tag{26}$$

Eq. 26 can be solved for $BG(1)$ to yield:

$$BG(1)|_{r=R} = \frac{4BG(2) - BG(3) + \left(\frac{2k\Delta r}{D_p}\right)C_{BG}}{3 + \frac{2k\Delta r}{D_p}},\tag{27}$$

The change in concentration of BG enzyme in the bulk solution is given by the mass balance equation:

$$V\frac{dC_{BG}}{dt} = -kA(C_{BG} - BG(1)|_{r=R}),\tag{28}$$

where V is the initial volume of the fluid inside the flask, A is the total outer surface area of the biomass particles inside the flask given by:

$$A = n_{particle}\pi DL\tag{29}$$

where D is the diameter of the biomass particle and L is the length of the biomass particle, $n_{particle}$ is the total number of particles inside the flask given by:

$$n_{particle} = \frac{W_{biomass}}{W_{particle}},\tag{30}$$

where, $W_{biomass}$ is the dry weight of biomass particles inside the flask, $W_{particle}$ is the weight of each particle inside the flask given by:

$$W_{particle} = V_{particle} \times \rho_{bulk},\tag{31}$$

where, $V_{particle}$ is the volume of the particle and ρ_{bulk} is the bulk density of the biomass particles given by eq. 32 and eq. 33 respectively:

$$V_{particle} = \pi R^2 L, \tag{32}$$

$$\rho_{bulk} = (1 - \varepsilon)\rho_s, \tag{33}$$

where, ρ_s is the solid density of the biomass particle.

The next step is to model the diffusion of adsorbing enzyme into the biomass particle, for which we convert eq. 13 using a central difference formula for the second derivative to:

$$
\begin{aligned}
\frac{dCE(i)}{dt} &= \frac{\varphi D_{P_{CE}}}{\left(\epsilon + \frac{\rho_a q_m K_a}{(1 + K_a CE(i))^2}\right)} \left[\frac{CE(i+1) - 2CE(i) + CE(i-1)}{\Delta r^2}\right. \\
&\quad + \left.\frac{1}{R - (i-1)\Delta r}\left(\frac{CE(i+1) - CE(i-1)}{\Delta r}\right)\right]
\end{aligned}
\tag{34}
$$

where $CE(i)$ is the concentration of adsorbing enzyme at different radial positions, $D_{p_{CE}}$ is the effective diffusion coefficient of adsorbing enzyme, ρ_a is apparent density calculated using eq. 8, q_m is maximum adsorption capacity of the substrate, k_a is the affinity constant.

The initial condition for the adsorbing enzyme is:

$$CE(0) = 0 \ \forall \ 0 \leq r \leq R \ , \tag{35}$$

The no flux boundary condition for the adsorbing enzyme at $r = 0$ represented by eq. 6 can be rewritten using second-order backward finite difference formula for first-order derivative (Cutlip and Shacham.,2008) as :

$$\left.\frac{\partial CE(i = N + 1)}{\partial r}\right|_{r=0} = \frac{3CE(N+1) - 4CE(N) + CE(N-1)}{2\Delta r} = 0, \tag{36}$$

Eq. 36 can be solved for $CE(N + 1)$ to yield:

$$CE(N+1)|_{r=0} = \frac{4CE(N) - CE(N-1)}{3}, \tag{37}$$

The flux boundary condition for the adsorbing enzyme at $r = R$ is given by:

$$\left.D_{p_{CE}}\frac{\partial CE}{\partial r}\right|_{r=R} = -k(C_{CE} - CE|_{r=R}), \tag{38}$$

where k represents the external-film mass transfer coefficient, $D_{p_{CE}}$ is the effective diffusion coefficient of adsorbing enzyme, C_{CE} is the concentration of adsorbing enzyme in the bulk solution. The transient boundary condition at $r = R$ represented by eq. 38 can be rewritten using second-order forward finite difference formula for first-order derivative (Cutlip and Shacham.,2008) as:

$$\left.\frac{\partial CE(i=1)}{\partial r}\right|_{r=R} = \frac{-3CE(1) + 4CE(2) - CE(3)}{2\Delta r} = -\frac{k}{D_{p_{CE}}}(C_{CE} - CE(1)|_{r=R}), \quad (39)$$

Eq. 39 can be solved for $CE(1)$ to yield:

$$CE(1)|_{r=R} = \frac{4CE(2) - CE(3) + \left(\frac{2k\Delta r}{D_{p_{CE}}}\right)C_{CE}}{3 + \frac{2k\Delta r}{D_{p_{CE}}}}, \quad (40)$$

The change in concentration of CE enzyme in the bulk solution is given by the mass balance equation:

$$V\frac{dC_{CE}}{dt} = -kA(C_{CE} - CE(1)|_{r=R}), \quad (41)$$

The cellulose, cellobiose, and glucose kinetics in the bulk solutions are modeled using the mathematical model proposed by Kadam et al., (2004). The three pathways, conversion of cellulose to cellobiose (p_1), conversion of cellulose to glucose (p_2), conversion of cellobiose to glucose (p_3) are illustrated in Figure 17. A number of assumptions were made to model the hydrolysis of cellulose; the adsorption of enzymes follows Langmuir isotherm given by eq. 9 with first-order reactions occurring at the cellulose surface, all the particles inside the flask are identical and lumped together in terms of exposure to enzymes, enzyme activity is constant throughout the reaction, the adsorbing enzyme is responsible for reaction pathways p_1 and p_2, the non-adsorbing enzyme is responsible for the reaction pathway p_3, the intermediate and final products do not inhibit the reactions in this model. The production of xylose glucose through hemicellulose reaction has not been considered in this model. In addition, because the diffusion of monomer sugars is much faster than enzymes, this model does not consider any diffusion mass transfer resistance for the enzyme hydrolysis kinetics. As rapidly as the enzymes produce sugars, these immediately diffuse into the bulk solution.
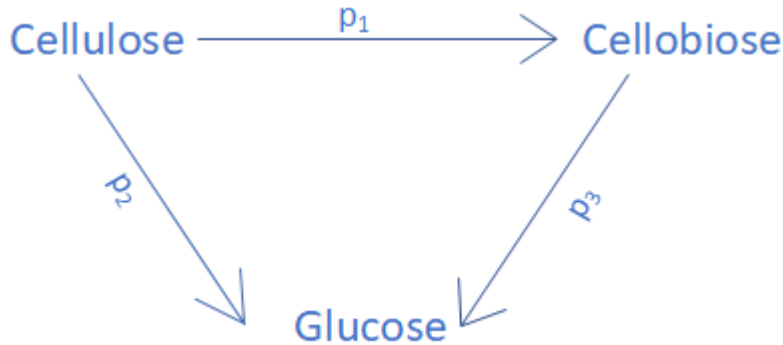
Figure 17. Reaction pathways used for modeling enzymatic hydrolysis of cellulose adapted and modified from Kadam et al., (2004).

The cellulose to cellobiose reaction pathway is given by:

$$r_1 = k_{1r}CE_B(n)R_sC(n), \tag{42}$$

The cellulose to glucose reaction pathway is given by:

$$r_2 = k_{2r}CE_B(n)R_sC(n), \tag{43}$$

The cellobiose to glucose reaction pathway is given by:

$$r_3 = \frac{k_{3r}BG(n)CB(n)}{k_{3M} + CB(n)}, \tag{44}$$

where, $n = 1,2,3,4,....,N$, $C(n)$ is the cellulose concentration at different sections inside the biomass particle, C k_{1r}, k_{2r}, and k_{3r} are kinetic rate parameters, k_{3M} is the affinity parameter. The bound enzyme concentration at different sections $CE_B(n)$ based on Langmuir adsorption, isotherm is given by:

$$CE_B(n) = \frac{q_m k_a \left(\frac{CE(i+1) + CE(i)}{2}\right)C(n)}{1 + k_a \left(\frac{CE(i+1) + CE(i)}{2}\right)}, \tag{45}$$

where, $i = n = 1, 2, 3,........,N$, $CE(i+1)$ and $CE(i)$ is the volume average pore fluid concentration of free adsorbing enzyme at different radial node locations, q_m and k_a are the adsorption parameters. The concentration of BG enzyme location at different radial sections is given by:

$$BG(n) = \frac{BG(i+1) + BG(i)}{2}, \tag{46}$$

Where $BG(i+1)$ and $BG(i)$ are the concentrations of non-adsorbing enzymes at different radial node locations. The Substrate reactivity is given by:

$$R_s = \alpha \frac{C(n)}{C_0(n)} \tag{47}$$

The cellulose mass balance at each section is given by:

$$\frac{dC(n)}{dt} = -p_1 - p_2 \tag{48}$$

The initial cellulose concentration at each section is given by:

$$C_0(n) = C_0 \frac{A(n)}{A_T} \tag{49}$$

where, C_0 is the initial concentration of cellulose in the bulk solution inside the flask, $A(n)$ is the cross-sectional area of each section of the particle given by:

$$A(n) = \pi(R_n^2 - R_{(n+1)}^2) \tag{50}$$

where, R_n is the radius of the particle at the different radial position given by:

$$R_n = R - (n-1)\Delta r \tag{51}$$

Where R is the radius of the particle, the total cross-sectional area of the particle is given by:

$$A_T = \pi R^2 \tag{52}$$

The bulk cellulose mass balance is given by:

$$C = \sum C(n) \tag{53}$$

The cellobiose mass balance reflected at the bulk flask scale for each particle section is given by:

$$\frac{dCB(n)}{dt} = 1.056p_1 - p_3 \tag{54}$$

where 1.056 is the water of hydration parameter for cellulose to cellobiose conversion. It is calculated using $\frac{342.3}{2 \times 162.14}$ Where 342.3 is the molar mass of cellobiose, and 162.14 is the molar mass of cellulose. The initial concentration of cellobiose is:

$$CB_0(n) = 0 \tag{55}$$

The bulk cellobiose mass balance is given by:

$$CB = \sum CB(n) \tag{56}$$

The glucose mass balance reflected at the bulk flask scale for each section is given by:

$$\frac{dG(n)}{dt} = 1.1116p_2 + 1.053p_3 \tag{57}$$

where 1.111 and 1.053 are the water of hydration parameters for cellulose to glucose conversion and cellobiose to glucose conversion, respectively. It is calculated using $\frac{180.16}{162.14}$ and $\frac{180.18 \times 2}{342.3}$, respectively. Where 342.3 is the molar mass of cellobiose, 180.16 is the molar mass of glucose, and 162.14 is the molar mass of cellulose. The initial concentration of glucose is:

$$CB_0(n) = 0 \tag{58}$$

The bulk cellobiose mass balance is given by:

$$G = \sum G(n) \tag{59}$$

4.4.2 Material properties and list of parameters

The biomass used in this model are Avicel-PH101 and dilute acid pretreated (DAP) poplar. The diffusion of non-adsorbing enzymes, diffusion and adsorption of adsorbing enzymes, cellulose kinetics, cellobiose kinetics, and glucose kinetics were modeled in this study. The model is validated by comparing the predicted glucose concentrations with experimental glucose kinetic data from different literature sources for Avicel PH-101 and DAP poplar. The required parameters are listed in Table 6.

Table 6. Material and parameter data used in the model.

Parameter	Description	Units	Value and Source			
Biomass	-		Avicel PH-101 [U]	8 min DAP poplar[Y]	15 min DAP poplar[Y]	21 min DAP poplar[Y]
Particle shape	-	-	Cylinder [D]	Cylinder [D]	Cylinder [D]	Cylinder [D]
D	Diameter of the biomass particle	cm	$0.005^{[U][H]}$	$0.06^{[Y][I]}$	$0.06^{[Y][I]}$	$0.06^{[Y][I]}$
ρ_a	Apparent density	g/cm^3	$1.064^{[F]}$	$0.88^{[F]}$	$0.296^{[F]}$	$0.272^{[F]}$
ρ_s	Solid density	g/cm^3	$1.52^{[A]}$	$1.49^{[A]}$	$1.49^{[A]}$	$1.49^{[A]}$
M_c	Mass percentage of cellulose	%	$100^{[U]}$	$58.5^{[Y]}$	$62.3^{[Y]}$	$62.6^{[Y]}$
M_h	Mass percentage of hemicellulose	%	$0^{[U]}$	$13.5^{[Y]}$	$8.2^{[Y]}$	$7.4^{[Y]}$
M_l	Mass percentage of lignin	%	$0^{[U]}$	$28^{[Y]}$	$29.5^{[Y]}$	$29.9^{[Y]}$

M_o	Mass percentage of other compositions	%	0[U]	0[Y]	0[Y]	0[Y]
ρ_c	Cellulose density	g/cm^3	1.52[V]	1.52[V]	1.52[V]	1.52[V]
ρ_h	Hemicellulose density	g/cm^3	1.56[V]	1.56[V]	1.56[V]	1.56[V]
ρ_l	Lignin density	g/cm^3	1.39[V]	1.39[V]	1.39[V]	1.39[V]
ρ_o	Density of other compositions	g/cm^3	2.50[V]	2.50[V]	2.50[V]	2.50[V]
q_m	Maximum adsorption capacity	mg/g biomass	0.0325[Z]	7.12[A1]	12.24[A1]	17.56[A1]
K_a	Affinity constant	ml/mg	1.238[Z]	1 [D]	1 [D]	1 [D]
V_{pa}	Pore volume accessible to the enzyme	cm^3/g	0.282[D]	0.565[Y]	3.2[Y]	3.25[Y]
φ	Pore volume accessible to the enzyme/total pore volume	-	1[D]	0.85[Y]	0.92[Y]	0.93[Y]
$D_{p_{BG}}$	Pore diffusion coefficient of non-adsorbing enzymes	cm^2/sec	$1\times10^{-7[C]}$	$1.8 \times 10^{-7[C]}$	$4 \times 10^{-7[C]}$	$4.1 \times 10^{-7[C]}$

$D_{P_{CE}}$	Pore diffusion coefficient of adsorbing enzymes	cm^2 /sec	$1\times10^{-7[C]}$	$1.8 \times 10^{-7[C]}$	$4 \times 10^{-7[C]}$	$4.1 \times 10^{-7[C]}$
Isotherm	-	-	Langmuir [Z]	Langmuir [A1]	Langmuir [A1]	Langmuir [A1]
R	Radius of the particle	cm	$0.0025^{[U]}$	$0.03^{[Y]}$	$0.03^{[Y]}$	$0.03^{[Y]}$
ϵ	porosity	-	$0.3^{[B]}$	$0.49^{[B]}$	$0.835^{[B]}$	$0.84^{[B]}$
V_p	Pore volume	cm^3/g	$0.282^{[W]}$	$0.665^{[Y]}$	$3.45^{[Y]}$	$3.5^{[Y]}$
Δr	Ratio of radius of the particle and number of sections	cm	$0.000125^{[J]}$	$0.0015^{[J]}$	$0.0015^{[J]}$	$0.0015^{[J]}$
D_w	Diffusion coefficient of enzymes in pure water	cm^2 /sec	$5.67 \times 10^{-7[X][E]}$	$5.67 \times 10^{-7 [X]} [E]$	$5.67 \times 10^{-7 [X]} [E]$	$5.67 \times 10^{-7 [X][E]}$
t	Enzyme diffusion time	sec	-	-	-	-
i	Node number	-	$2,3,4,..,N$	$2,3,4,..,N$	$2,3,4,..,N$	$2,3,4,...,N$
$BG(i)$	Non-adsorbing enzyme concentration at different radial positions	mg /ml	-	-	-	-

C_{BG}	Concentration of non-adsorbing enzymes in the bulk solution	mg/ml	-	-	-	-
$CE(i)$	Adsorbing enzyme concentration at different radial positions	mg/ml	-	-	-	-
C_{CE}	Concentration of adsorbing enzymes in the bulk solution	mg/ml	-	-	-	-
N	Number of sections	-	20[D]	20[D]	20[D]	20[D]
k	External-film mass transfer coefficient	cm/sec	0.0004[D]	0.02[D]	0.02[D]	0.02[D]
V	Initial volume of the fluid inside the flask	ml	10[D]	10[Y]	10[Y]	10[Y]
A	Total outer surface area of the biomass particles inside the flask	cm^2	112.8[K]	40.812[K]	40.812[K]	40.812[K]

L	Length of the biomass particle	cm	$0.02^{[L]}$	$0.24^{[L]}$	$0.24^{[L]}$	$0.24^{[L]}$
$n_{particle}$	Number of particles inside the flask	-	$361533^{[M]}$	$902.14^{[M]}$	$902.14^{[M]}$	$902.14^{[M]}$
$W_{biomass}$	Dry weight of biomass particles inside the flask	mg	$150^{[D]}$	$150^{[Y]}$	$150^{[Y]}$	$150^{[Y]}$
$W_{particle}$	Weight of each particle inside the flask	mg	$4.149 \times 10^{-4[N]}$	$0.16^{[N]}$	$0.16^{[N]}$	$0.16^{[N]}$
$V_{particle}$	Volume of the particle	cm^3	$3.9 \times 10^{-7[O]}$	$6.78 \times 10^{-4[O]}$	$6.78 \times 10^{-4[O]}$	$6.78 \times 10^{-4[O]}$
$'\rho'_{bulk}$	bulk density of the biomass particles	g/cm^3	$1.064^{[P]}$	$0.885^{[P]}$	$0.245^{[P]}$	$0.245^{[P]}$
n	Section number	-	$1,2,3,.,N$	$1,2,3,..,N$	$1,2,3,..,N$	$1,2,3,..,N$
$C(n)$	Cellulose concentration at different sections	mg/ml	-	-	-	-
$'CE_B(n)'$	bound enzyme concentration at different sections	mg/ml	-	-	-	-

R_s	Substrate reactivity	-	-	-	-	-
α	Dimensionless constant for substrate reactivity	-	$1^{[Z][D]}$	$1^{[D]}$	$1^{[D]}$	$1^{[D]}$
C_0	Initial concentration of cellulose in the bulk solution inside the flask	mg/ml	$100^{[D]}$	$8.775^{[Y]}$	$9.345^{[Y]}$	$9.39^{[Y]}$
C_{BG_0}	Initial concentration of BG in the bulk solution inside the flask	mg/ml	$0.59^{[Z]}$	$0.1107^{[R]}$	$0.1107^{[R]}$	$0.1107^{[R]}$
C_{CE_0}	Initial concentration of CE in the bulk solution inside the flask	mg/ml	$1.58^{[Z]}$	$0.3075^{[R]}$	$0.3075^{[R]}$	$0.3075^{[R]}$
$A(n)$	Cross-sectional area of each section of the particle	cm^2	-	-	-	-
R_n	Radius of the particle at different radial position	cm	-	-	-	-

A_T	Total cross-sectional area of the particle	cm^2	1.9×10^{-5} [S]	2.83×10^{-3} [T]	2.82×10^{-3} [T]	2.83×10^{-3} [T]
k_{1r}	kinetic rate parameter	ml/mg /sec	6.6×10^{-5} [T]	4×10^{-6} [T]	6.6×10^{-6} [T]	5.5×10^{-6} [T]
k_{2r}	kinetic rate parameter	ml/mg /sec	8.2×10^{-5} [T]	1.5×10^{-6} [T]	5×10^{-7} [T]	9×10^{-7} [T]
k_{3r}	kinetic rate parameter	1/sec	2.1×10^{-4} [T]	1.1 [T]	0.092 [T]	0.14 [T]
k_{3M}	kinetic rate parameter	mg/ml	3.174[T]	24[T]	24[T]	24[T]
$CB(n)$	Cellobiose concentration at different sections	mg/ml	-	-	-	-
$G(n)$	Glucose concentration at different sections	mg/ml	-	-	-	-
C	Bulk cellulose concentration	mg/ml	-	-	-	-
CB	Bulk cellobiose concentration	mg/ml	-	-	-	-
G	Bulk Glucose concentration	mg/ml	-	-	-	-

A- calculated using eq.2, B- calculated using eq.1, C- calculated using eq.3, D-Assumption, E- D_w ranges from 10^{-6} to 10^{-7} cm^2/sec and assumption, F- calculated using eq. 8, G- Mean particle size of a particle size distribution, H – All particles are of the same size, I- Lowest particle size from a particle size distribution (28 mesh, Tyler), J- calculated using eq. 21, K-calculated using eq.29, L- aspect ratio L=4D, M- calculated using eq. 30, N- calculated using eq.31, O-calculated by eq.32, P- calculated using eq.33, Q-calculated using eq.46; R1- (BG enzyme loading: 13.5 μL for 0.15 g of dry biomass in each flask),(CE enzyme loading: 37.5 μL for 0.15 g of dry biomass in each flask), the protein concentration of Accelerase 1500 and Accelerase BG enzyme is 82 mg/ml; S- calculated using 51, T-Parameters obtained by regression of data obtained from this model, U- Based on solids loading from Ankathi et al., (2019), U- Machado et al.,(2015), V- Zhang et al., (2016), W-Tantasucharit.,(1995), X-Yohana et al., (2020), Y- Ankathi et al., (2019), Z- Tsai et al., (2014), A1- Min et al., (2011).

4.4.3 Method of solution

The multi-scale diffusion and reaction model is numerically solved using eq. 42 through eq. 59, boundary conditions and data from Table 6 for Avicel Ph-101 and 8 min,15 min, and 21 min DAP poplar. The concentrations of non-adsorbing and adsorbing enzymes at different radial locations at the particle level and in the bulk solution and concentrations of cellulose, cellobiose, and glucose for both biomass materials were predicted using a custom-written code in Polymath. The numerical solution is validated by comparing the predicted glucose concentrations with the experimental kinetic data found in the literature. The effect of particle size on glucose yields from enzymatic hydrolysis of 15 min DAP poplar was predicted for a range of particle sizes starting from 0.006 cm to 0.6 cm. The effect of porosity and pore volume on the glucose yield for 8 min DAP poplar were modeled for nine different cases in a scenario analysis; φ= 0.8, ϵ= 0.40, φ= 0.8, ϵ= 0.49, φ= 0.8, ϵ= 0.58; φ= 0.85, ϵ= 0.40; φ= 0.85, ϵ= 0.49; φ= 0.85, ϵ= 0.58; φ= 0.9, ϵ= 0.40; φ= 0.9, ϵ= 0.49; φ= 0.9, ϵ= 0.58 keeping all other parameters constant.

4.4.4 Results and Discussion

The concentration of BG enzyme at different radial positions of the particle and in the bulk solution was found by numerically solving ordinary differential eq. 42 through 58 using Polymath and Avicel PH-101 data from Table 6. The graph in Figure 18. BG enzyme concentration in the bulk solution and at different radial positions for Avicel PH-101 shows the concentration of BG enzymes at different radial positions inside the Avicel PH-101 biomass particle and the concentration of BG enzymes in the bulk solution vs. time (secs). Compared to the concentration profiles for BG enzymes with constant boundary conditions shown in Figure 2, the time required for enzymes to completely penetrate biomass particle despite all the parameters of the biomass particle being the same is longer due to change in bulk concentration of BG enzymes over time. For example, for the non-adsorbing enzyme with constant boundary condition, the diffusion time for the enzymes to reach steady-state was around 16.65 secs, but in the case of BG enzyme diffusion with a flux boundary condition, the diffusion time of enzymes to reach steady state is around 120 secs. The

concentration of BG enzymes in the bulk solution (CBG) decreases with time since the enzymes start diffusing into the biomass particle with time. The governing equation Eq.20 used to develop this graph is validated in chapter 4.1 by comparing the characteristic time of diffusion obtained numerically with the characteristic time obtained analytically.
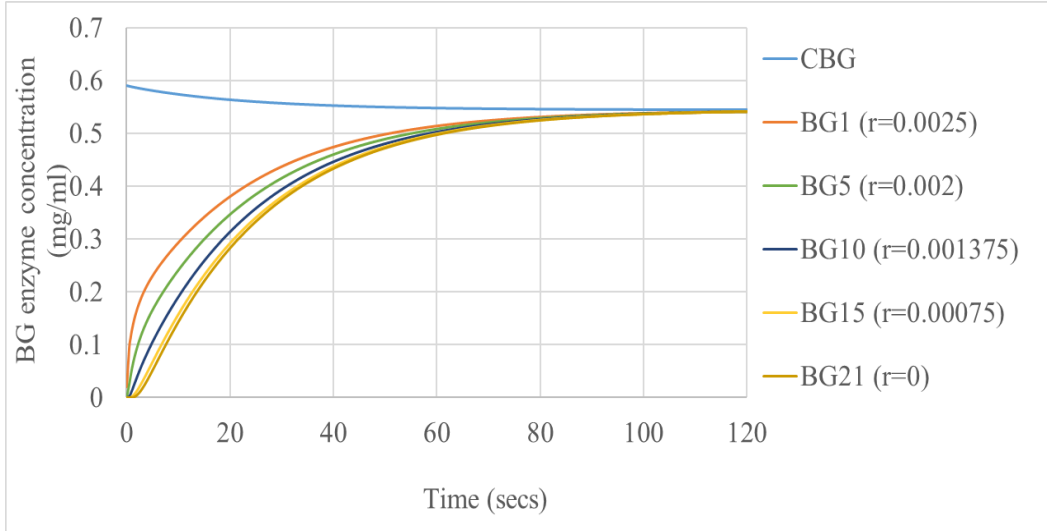
Figure 18. BG enzyme concentration in the bulk solution and at different radial positions for Avicel PH-101

The concentration of adsorbing enzymes at different radial positions inside the cylindrical biomass particle and in the bulk solution vs. time (secs) is shown in Figure 19. Compared to the concentration profiles of adsorbing enzyme shown in Figure 7, the time required for penetration of the enzyme into the particles is lower in Figure 19; for example, the time to reach steady-state in Figure 7 is 528 secs and in Figure 19 is 160 secs, despite it is Avicel PH-101 is due to change in adsorption parameters, the maximum adsorption capacity $'q'_m$ used in chapter 4.2 was 17.41 mg/g substrate and the maximum adsorption capacity used to generate the concentration profiles in this chapter was 0.03257 mg/g substrate measured by Tsai et al., (2014). This shows that the adsorption kinetics have a strong dependence on maximum adsorption capacity. The concentration of adsorbing enzyme in the bulk solution in Figure 19 drops from 1.59 mg/ml to 1.42 mg/ml, which is a more significant drop compared to the drop in BG enzyme concentration in bulk is due to the effect of adsorption. The governing equation eq.34 used to generate this graph was validated by comparing the characteristic obtained using the numerical solution with adsorption kinetics from literature.
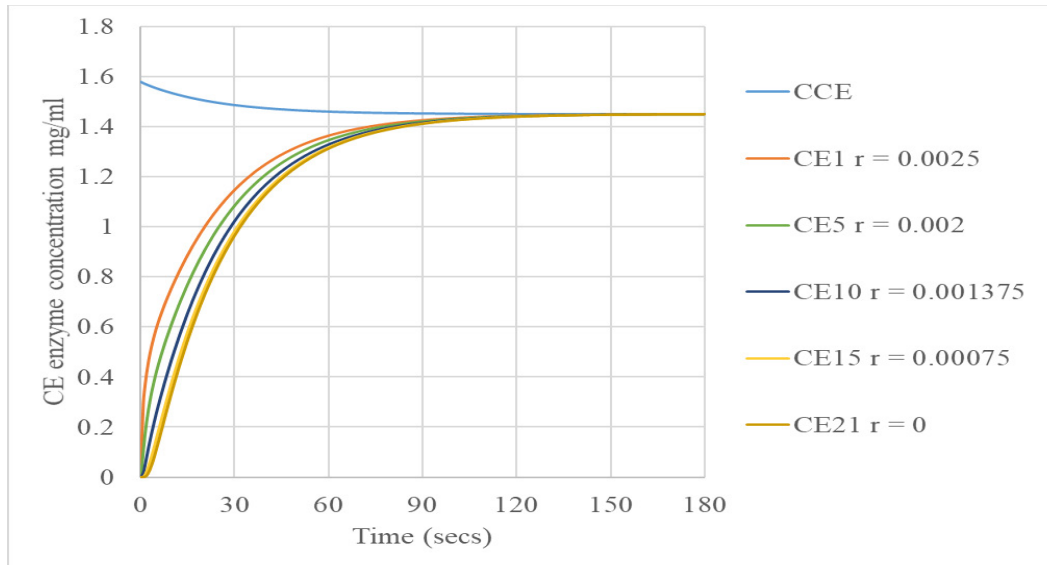
Figure 19. CE enzyme concentration in the bulk solution and at different radial positions for Avicel PH-101 with q_m=0.0325 mg/g biomass , K_a= 1.238 ml/mg (Table 6) .

Avicel: The cellulose, cellobiose, and glucose concentration profiles at different radial positions vs. enzymatic hydrolysis time for Avicel PH-101 biomass particles are shown in Figure 20, Figure 21, and Figure 22, respectively. As shown in Figure 20(A), the cellulose concentration at the outer radius $r = R$ drops the highest compared to cellulose concentrations at other radial positions, and the cellulose concentration closer to $r = 0$ does not drop due to extremely low cellulose concentration and low surface area for enzyme attack compared to the surface area available for enzymatic activity at the outer radius. After 48 hours of enzymatic hydrolysis, the cellulose concentration does not reach zero at any of the radial positions; this shows there is some more cellulose that can be converted to glucose with longer enzymatic hydrolysis times. In Figure 20(B), the normalized cellulose concentrations versus time are shown, indicating that the changes in cellulose relative to initial concentration are the greatest near the particle surface, where cellulose concentrations are the highest. The cellobiose concentration spiked with EH time and simultaneously decreased since BG enzymes consume the cellobiose to produce glucose. The cellobiose concentration profile shows a greater production rate and cellobiose consumption rate as we got closer to the outer radius since more cellulose is accessible to enzymes attack. The glucose concentration steadily increases with EH time at all radial positions with the highest glucose production at $r = R$ as expected due to high cellulose and CE enzyme activity and high cellobiose and BG enzyme interaction compared to other radial positions. The bulk concentration profiles of cellulose, cellobiose and glucose vs. EH time are shown in Figure 23. The cellulose concentration goes down with EH time as it is converted to cellobiose and glucose. The cellobiose concentration goes up during the early hours of EH, and as time progresses, the cellobiose concentration goes down as it is converted to glucose. The model was validated by comparing the predicted glucose kinetic data with the experimental kinetic data of glucose obtained from

54

model 1 strategy 1 with 100mg/ml Avicel solids loading and Celluclast enzyme loading of 15.9mg/ g substrate, N188 enzyme loading 5.9 mg/g substrate of Tsai et al., (2014), the validation is shown in the graph of Figure 24.
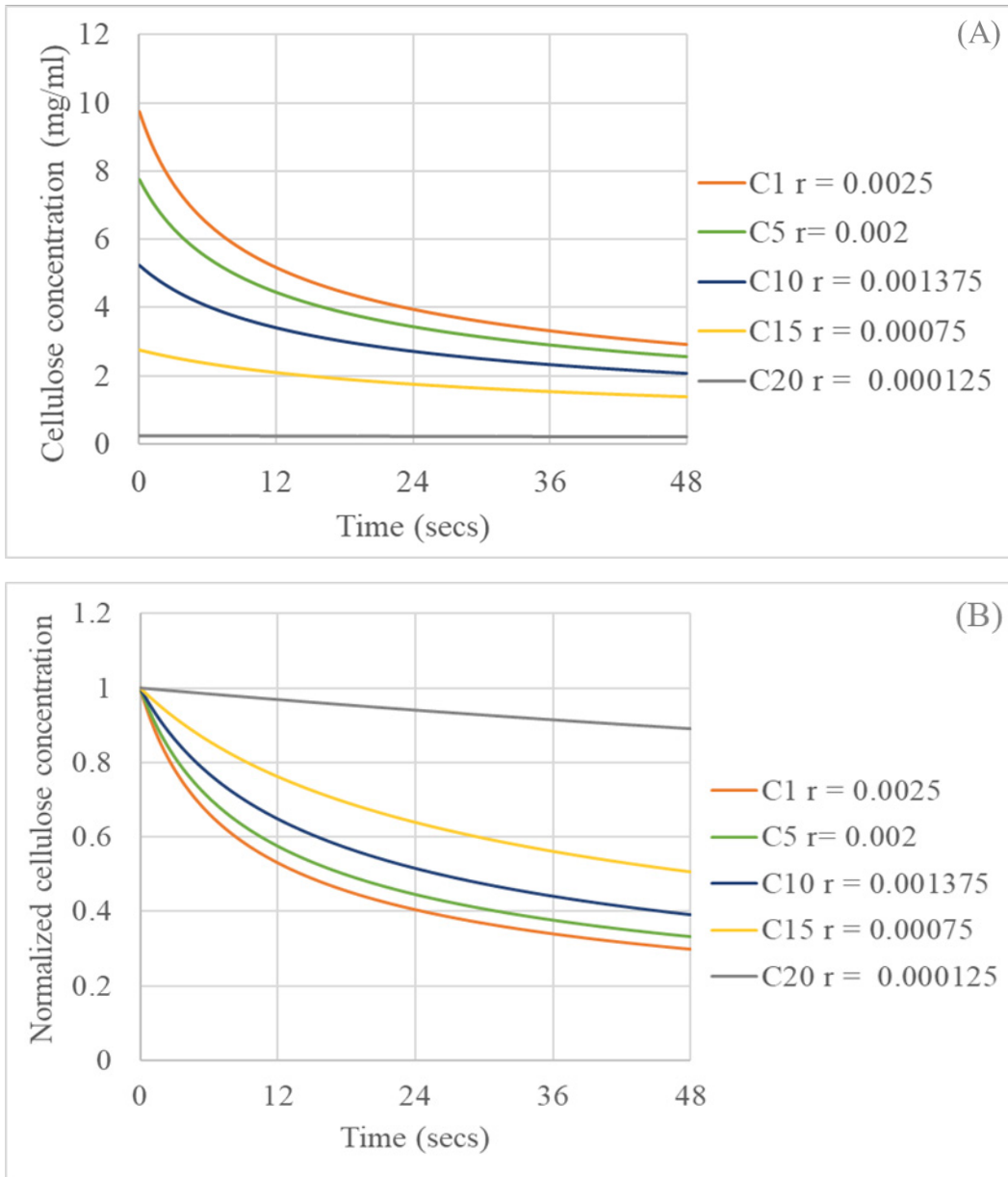
Figure 20. (A) Cellulose concentration, and (B) Normalized cellulose concentration at different radial positions for Avicel PH-101. Normalization means dividing the cellulose concentration at each radial position by its initial value.
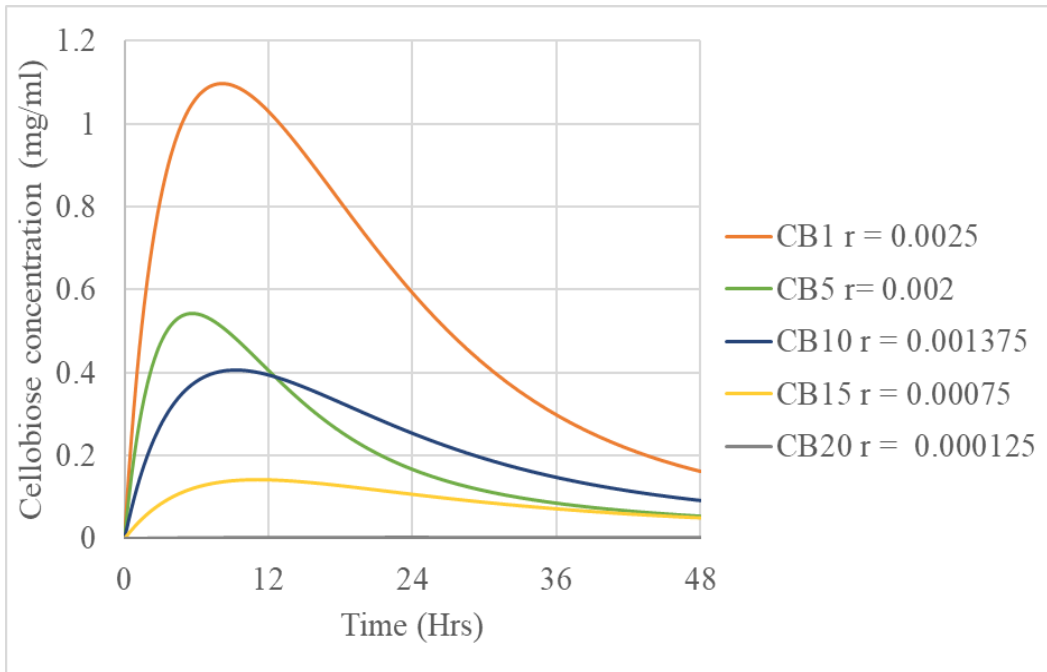
Figure 21. Bulk cellobiose concentrations from different radial positions for Avicel PH-101.
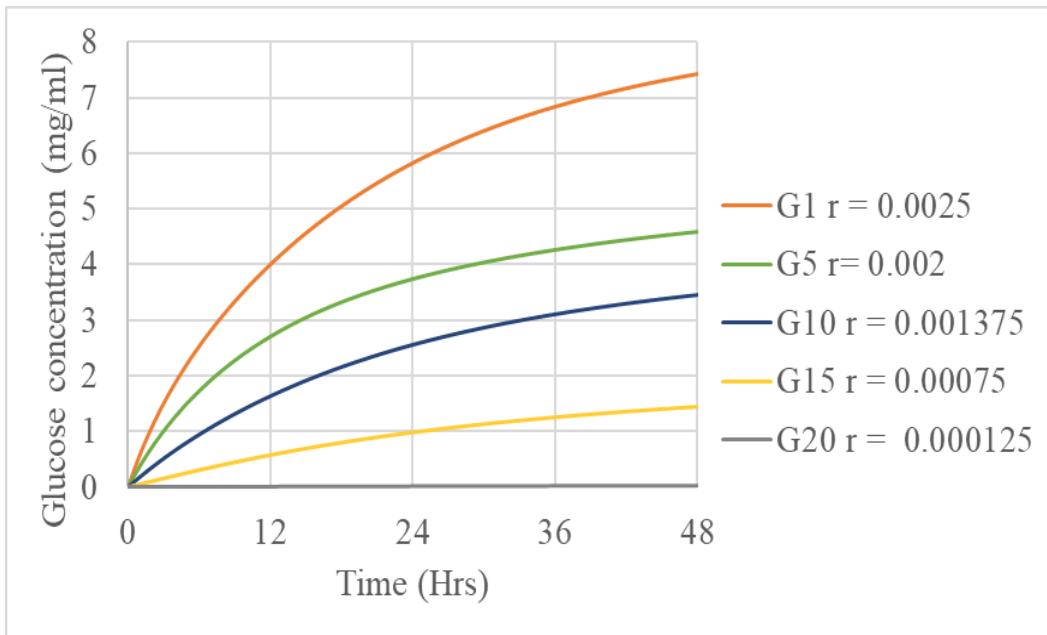
Figure 22. Bulk glucose concentrations from different radial positions for Avicel PH-101
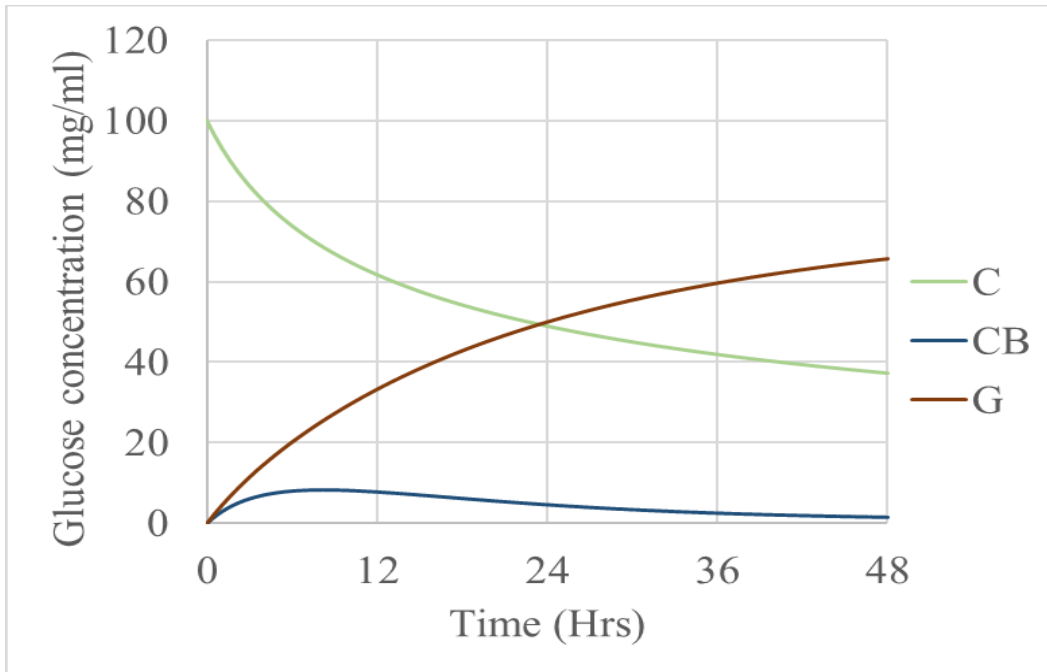
Figure 23. Bulk cellulose, cellobiose, and glucose concentration in the bulk solution inside the flask for Avicel PH-101 particle.
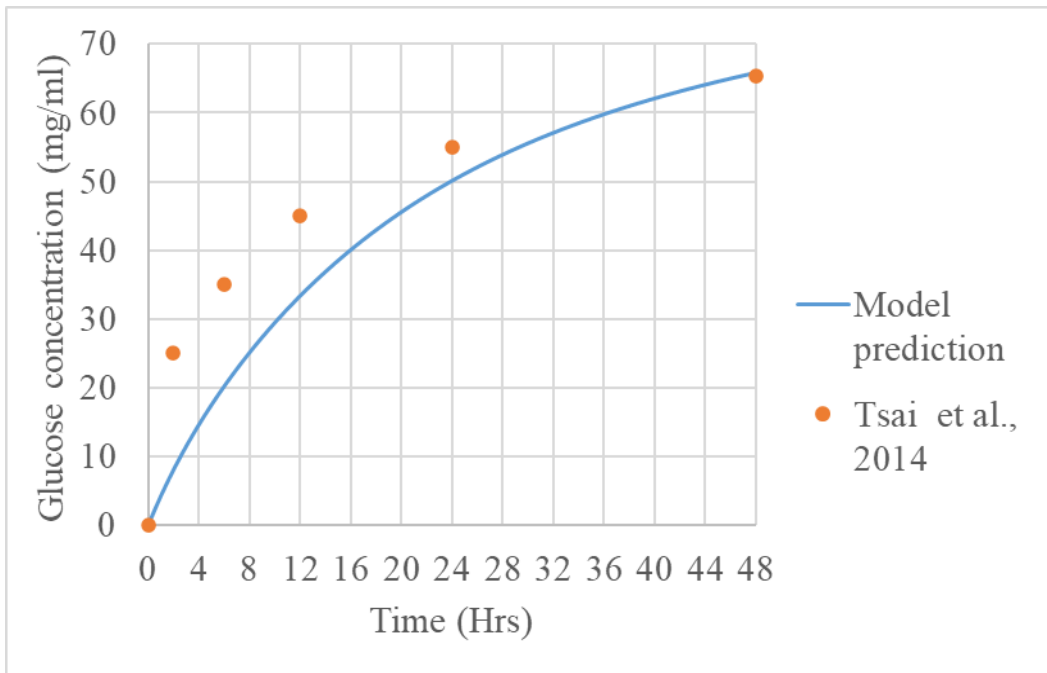
Figure 24. Comparison of glucose yield with the experimental hydrolysis kinetic data from Tsai et al., 2014.

DAP Poplar: The concentration profile of BG enzyme at different radial positions of the particle and in the bulk solution was predicted by numerically solving the ordinary

differential eq. 42 through 59 using polymath and 15 min DAP poplar data from Table 6. The graph in Figure 25 shows the concentration of BG enzymes at different radial positions inside the 15 min DAP pretreated biomass particle and in the bulk solution vs. time (secs). Compared to the concentration profiles for BG enzymes for Avicel PH-101 shown in Figure 18, the time required to diffuse completely into the biomass particle is significantly longer. For example, the diffusion time for enzymes into Avicel particles is 120 secs, whereas the diffusion time for enzymes into DAP poplar is 4800 secs. The difference between these two diffusion times is due to the large particle size difference. The Avicel PH-101 has a particle diameter of 50 microns, whereas the DAP poplar has a particle diameter of 600 microns. The concentration of BG enzyme in the bulk solution goes down as expected even in the case of 15 min DAP poplar.
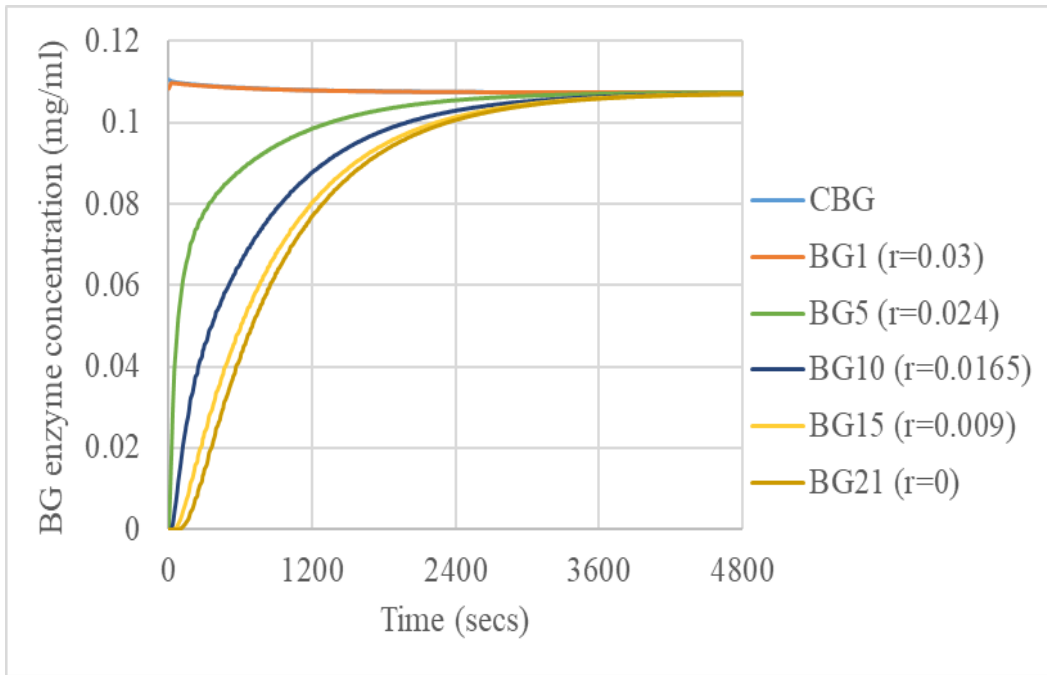
Figure 25. BG enzyme concentration in the bulk solution and at different radial positions for 15 min DAP poplar.

The concentration of adsorbing enzymes at different radial positions inside the cylindrical biomass particle and the bulk solution vs. time (secs) is shown in Figure 26. When compared to CE enzyme concentration profiles of CE enzyme shown in Figure 19, we observed that the rates of diffusion and adsorption were extremely slow for 15 min DAP poplar compared to Avicel PH-101. The CE enzyme takes around 160 secs to reach steady state in Avicel PH-101 (CT = 120 sec), whereas the CE enzyme reaches steady state at around 4.5 hours in 15 min DAP poplar. The major factors for this phenomenon are particle size and maximum adsorption capacity. The particle size of Avicel PH-101 is 50 microns, and the DAP poplar has a particle size of 600 microns. The maximum adsorption capacity of Avicel PH-101 is around 0.03257 mg/g substrate. In contrast, the 15 min DAP poplar

has an adsorption capacity of 12.24 mg/g substrate; the maximum adsorption capacity for 15 min DAP polar was calculated from the percentage of enzyme adsorption vs. pretreatment severity graph provided by Min et al., (2011).
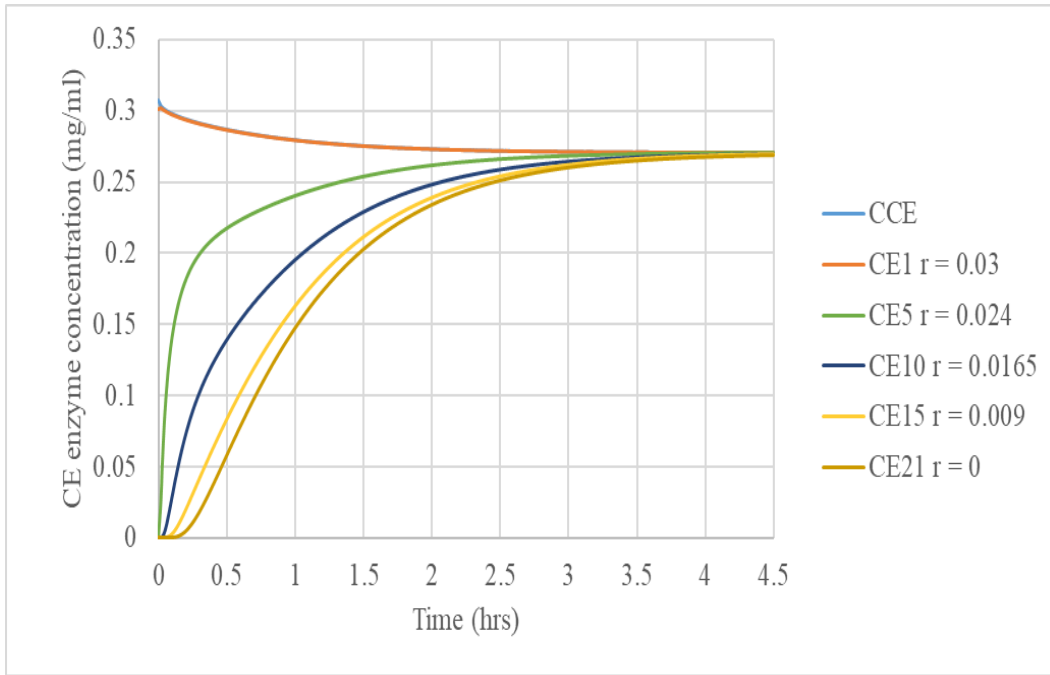
Figure 26. CE enzyme concentration in the bulk solution and at different radial positions for 15 min DAP poplar. The CCE and CE1 curves are coincidental on this graph.

The cellulose, cellobiose, and glucose concentration profiles at different radial positions vs. EH time (Hrs.) for 15 min DAP poplar biomass particle are shown in Figure 27, Figure 28, and Figure 29, respectively. Similar to the cellulose concentration profile of Avicel, the cellulose concentration at the outer radius $r = R$ drops faster compared to cellulose concentrations at other radial positions, due to high cellulose accessibility and high enzyme activity at the outer radial sections compared to the inner radial sections and a similar trend to Avicel Ph-101 for normalized cellulose concentration was observed 15 min DAP poplar normalized cellulose concentration shown in Figure 27(B). The kinetic parameters were found by fitting the glucose and cellobiose yields predicted by the model to the experimental glucose and cellobiose EH data found from literature; the kinetic parameters obtained from our model were of the correct order starting with $k_{3r} > k_{1r} > k_{2r}$ based on the data from literature review (Tsai et al., 2014). The cellulose at radial positions closer to the origin did not go down after 24 hours of EH due to low initial cellulose concentrations and low enzyme activity closer to the origin; with longer enzymatic hydrolysis times, the unconverted cellulose can be converted to cellobiose and glucose. In the case of cellobiose, the concentrations of cellobiose went up initially, but with increasing, EH time cellobiose concentration went down as we saw for Avicel PH-101 after 24 hours of enzymatic hydrolysis. The cellobiose concentrations were an order of

magnitude lower compared to the glucose concentrations at the outer radial sections and two orders of magnitude lower closer at inner radial sections closer to the origin. The rate of cellobiose production by the CE enzymes was lower than the rate of cellobiose consumption by BG enzymes. The glucose concentration, as expected, goes up with EH time at all radial positions for DAP poplar. The bulk concentration profiles of cellulose, cellobiose, and glucose vs. EH time for DAP poplar are shown in Figure 30. The bulk cellulose concentration went down as it was converted to cellobiose and glucose. The cellobiose concentration in the bulk solution went up initially but immediately went down due to the high conversion rate of cellobiose to glucose. The glucose in the bulk solution went up with EH time.
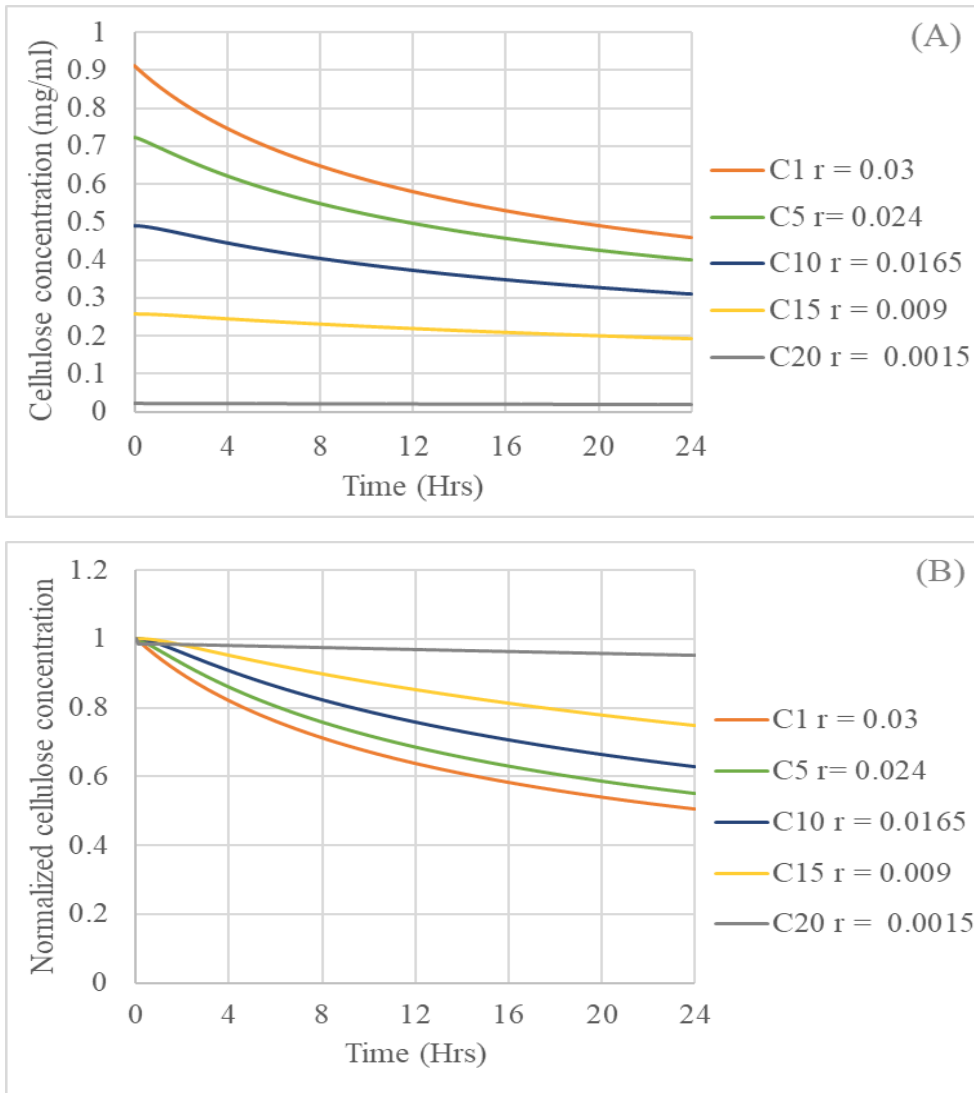
Figure 27. (A) Cellulose concentration, and (B) Normalized cellulose concentration at different radial positions for 15 min DAP poplar.
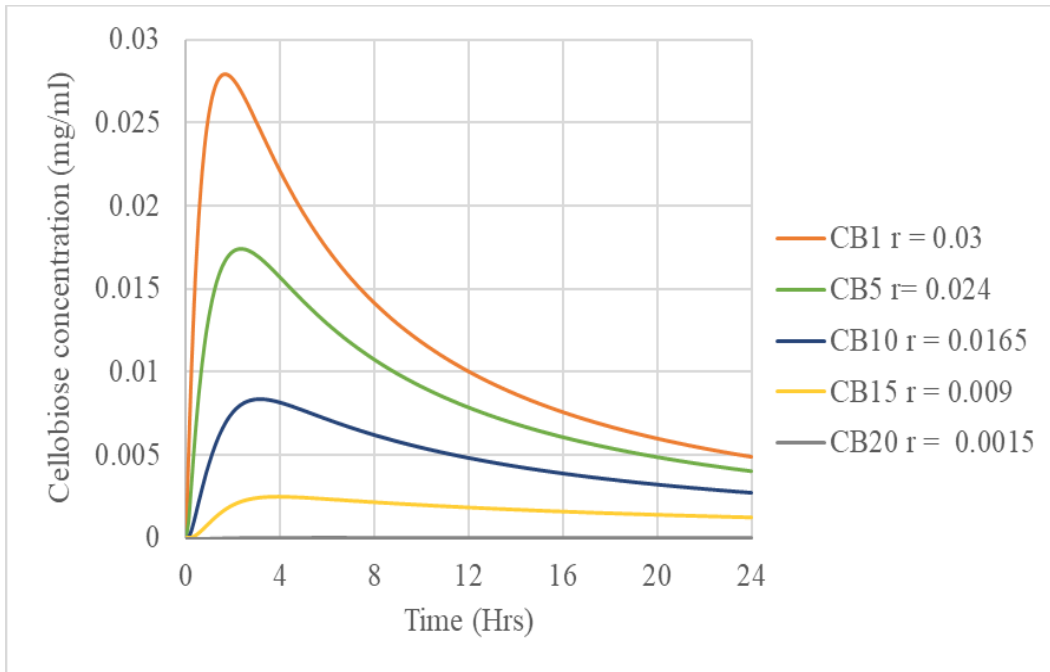
Figure 28. Bulk cellobiose concentrations from different radial positions for 15 min DAP poplar.
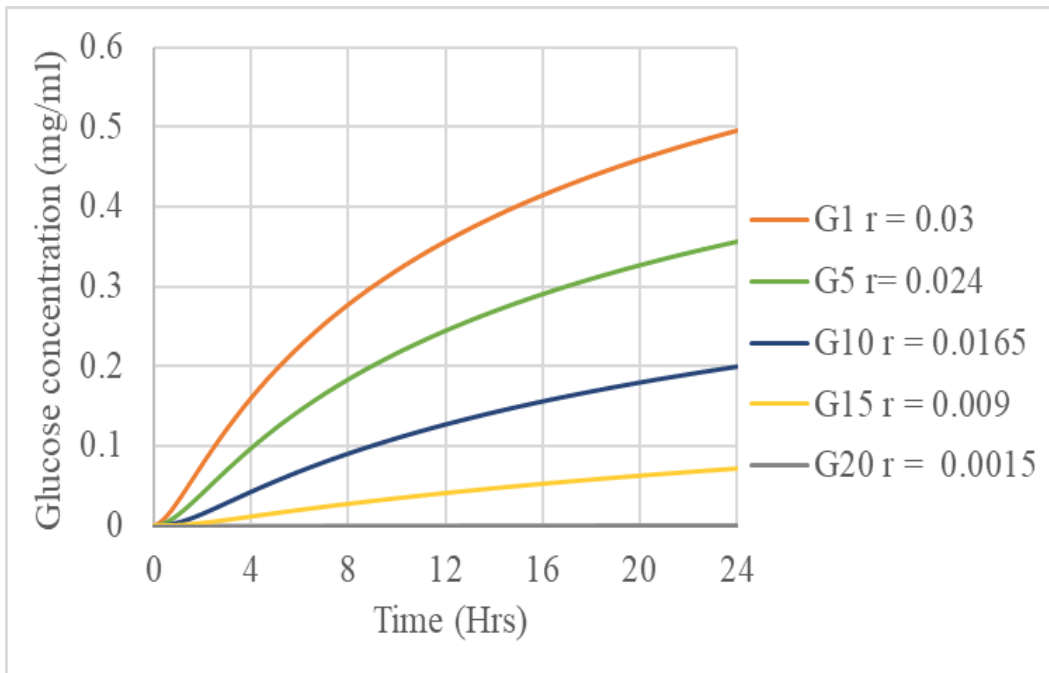
Figure 29. Bulk glucose concentration from different radial positions for 15 min DAP poplar.
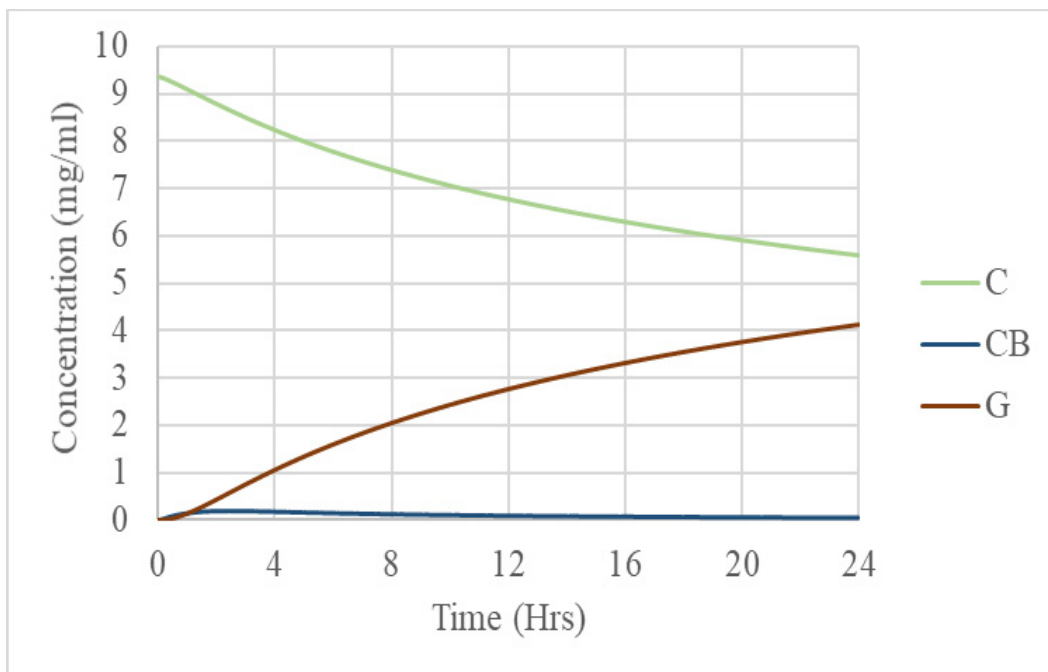
Figure 30. Cellulose, Cellobiose, and Glucose concentration in the bulk solution inside the flask for 15 min DAP pretreated poplar.
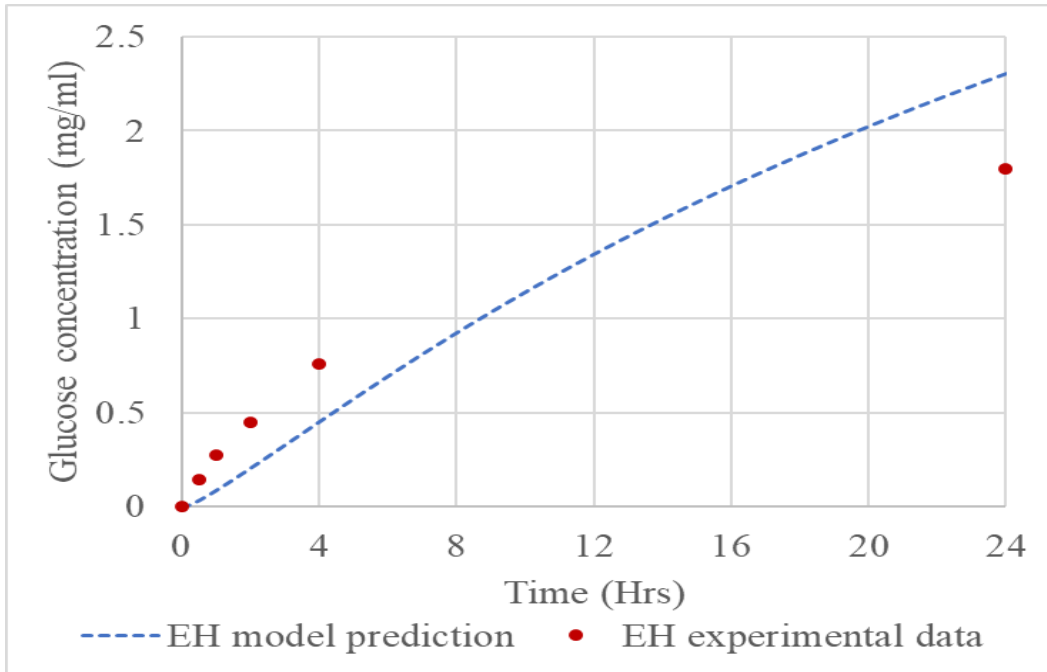
Figure 31. Comparison of glucose yield with experimental hydrolysis data of 8 min DAP pretreated poplar from Ankathi et al., 2019.
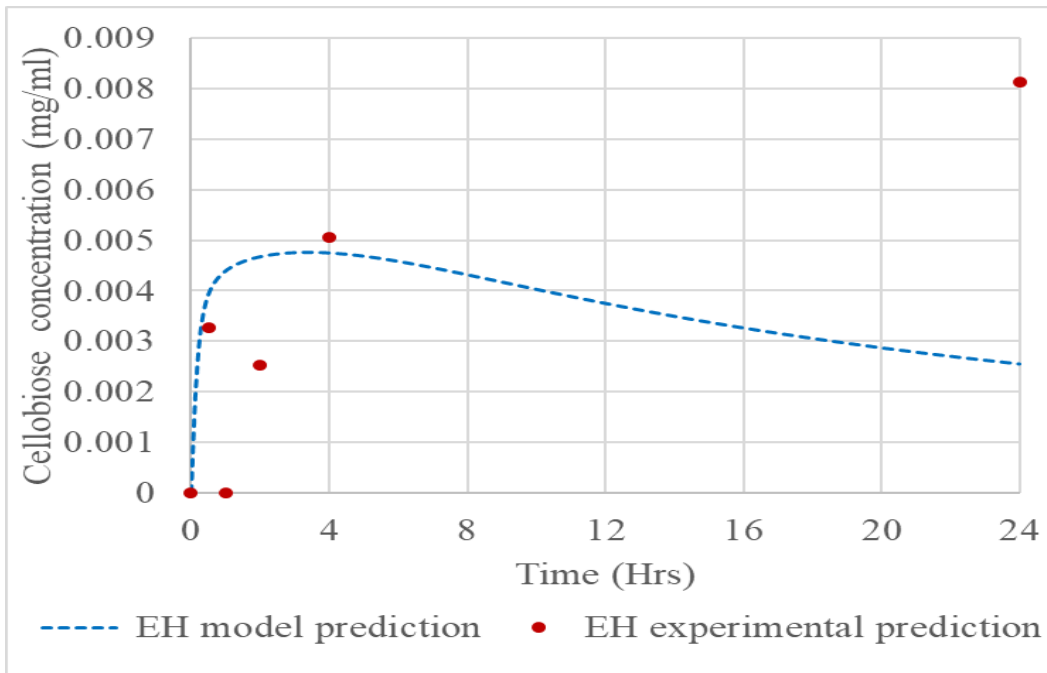
Figure 32. Comparison of cellobiose yield with experimental hydrolysis data of 8 min DAP pretreated poplar from Ankathi et al., 2019.
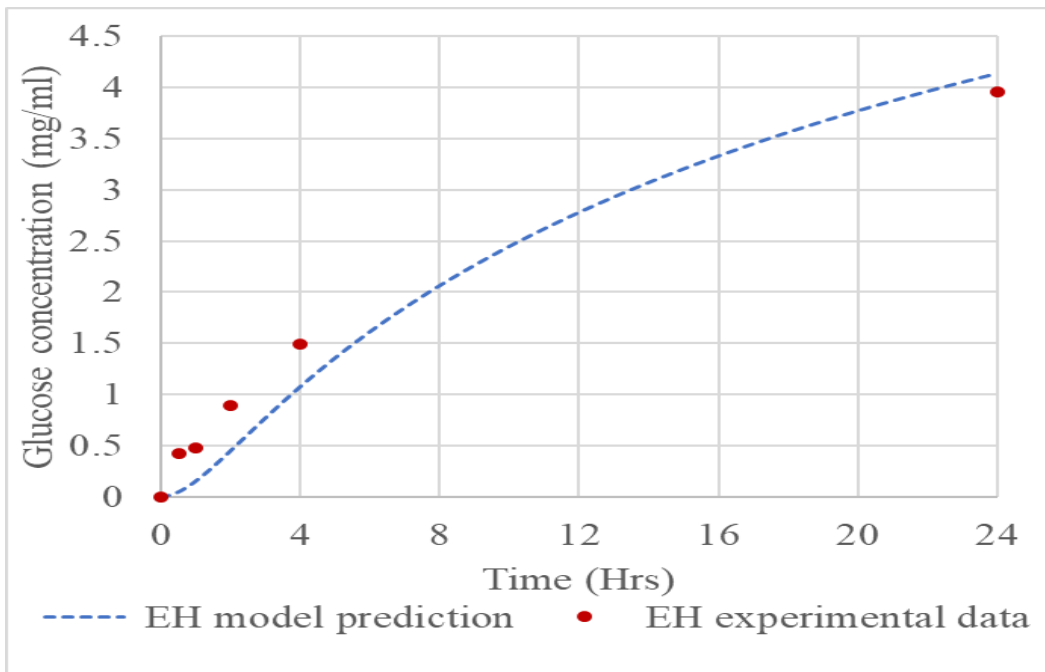
Figure 33. Comparison of glucose yield with experimental hydrolysis data of 15 min DAP pretreated poplar from Ankathi et al., 2019.
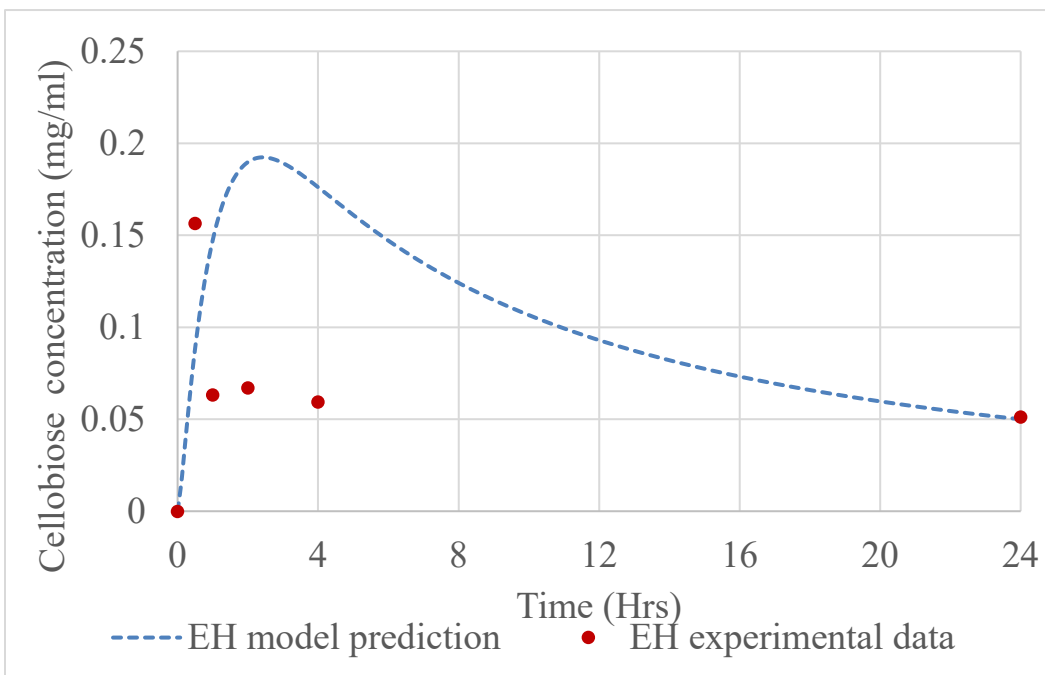
Figure 34. Comparison of cellobiose yield with experimental hydrolysis data of 15 min DAP pretreated poplar from Ankathi et al., 2019.
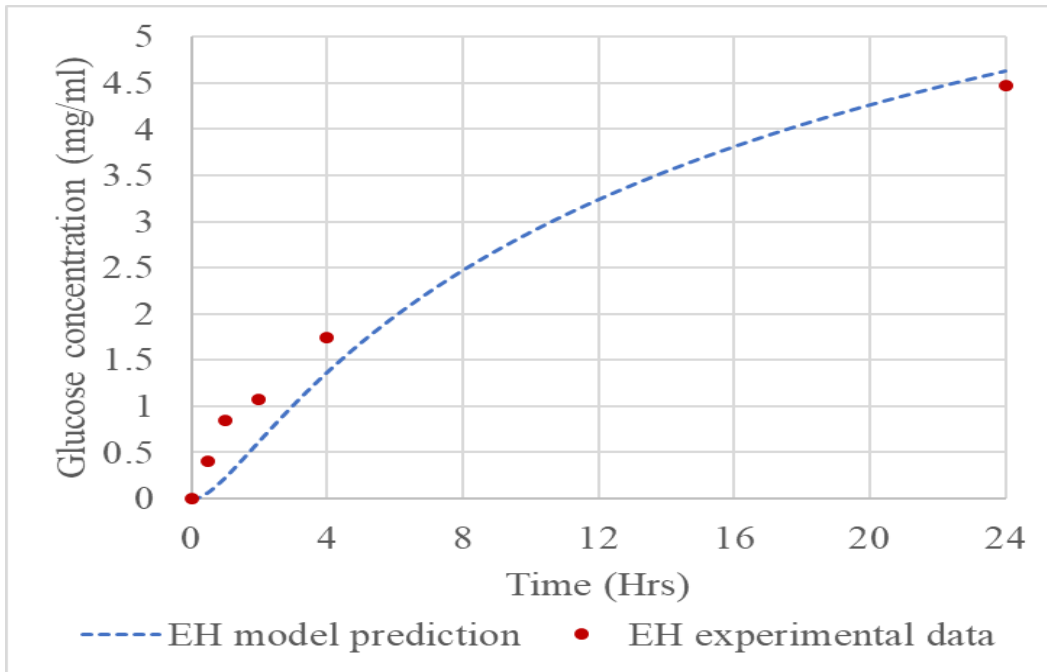
Figure 35. Comparison of glucose yield with experimental hydrolysis data of 21 min DAP pretreated poplar from Ankathi et al., 2019.
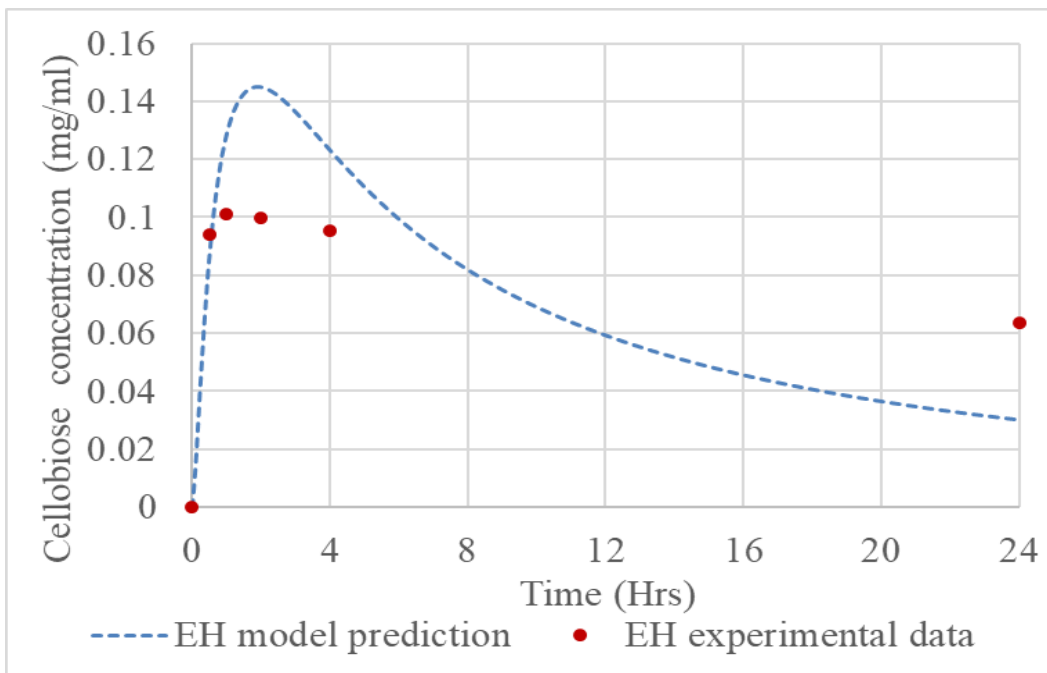
Figure 36. Comparison of cellobiose yield with experimental hydrolysis data of 21 min DAP pretreated poplar from Ankathi et al., 2019.

65

The model was validated by comparing the predicted glucose kinetic data and cellobiose kinetic data with the experimental kinetic data of glucose and cellobiose obtained from Ankathi et al., (2019) shown in Figure 31, Figure 32 for 8 min DAP poplar, Figure 33, Figure 34 for 15 min DAP poplar and Figure 35, Figure 36 respectively. The model predictions for glucose were an excellent fit to the experimental EH data found from Ankathi et al., (2019) for all pretreatment times; the cellobiose model predictions showed the right trend for all pretreatment times, and due to the low concentrations of experimental cellobiose data, which fall in the detection limit of the measuring instrument and due to this inaccuracy of the experimental data the model predictions were not a perfect fit to experimental cellobiose concentration data from Ankathi et al., (2019) but overall the fit was good. The glucose model predictions for different pretreatment times are shown in Figure 37. The glucose yield was highest for the highest 21 min DAP poplar, followed by 15 min DAP poplar, and the lowest was for 8 min pretreatment time. The difference in glucose yields was due to adsorption parameters, cellulose accessibility, porosity, pore volumes, and initial cellulose concentrations.
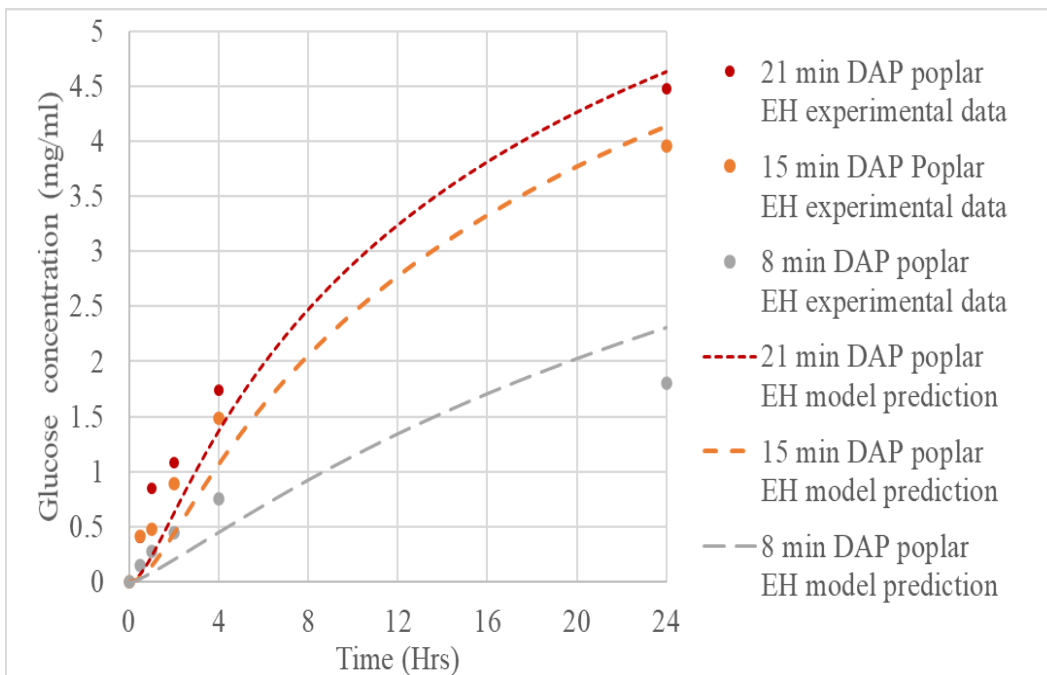
Figure 37. Comparison of experimental and model-predicted glucose yields from different pretreatment times.

Scenario analysis:

Effect of particle size: The model was applied to a range of particle sizes starting from 0.006 cm (Typical particle size of Avicel PH-101) to 0.6 cm (10x greater than the typical particle size of DAP poplar biomass) to study the effect of particle size and enzyme

diffusion on glucose yield. The model predictions are shown in the graph of Figure 38. The glucose predictions for R=0.03 cm(Base case-15 min DAP poplar), R=0.015cm, and R=0.003 cm were closely grouped, suggesting that the particle size and enzyme diffusion were not key-rate limiting steps for particle sizes smaller than 0.06 cm (diameter) similar to the results found by (Luterbacher. J. S. et al., 2012). Contrary to this, for particle radii larger than R=0.03 cm, the glucose production went down significantly, suggesting that the particle size and enzyme diffusion influence was strong on glucose production for particle diameter greater than $D = 0.06$ cm (diameter). Based on these results, it is recommended to use biomass particles of diameter closer to 0.06 cm to ensure maximum conversion.
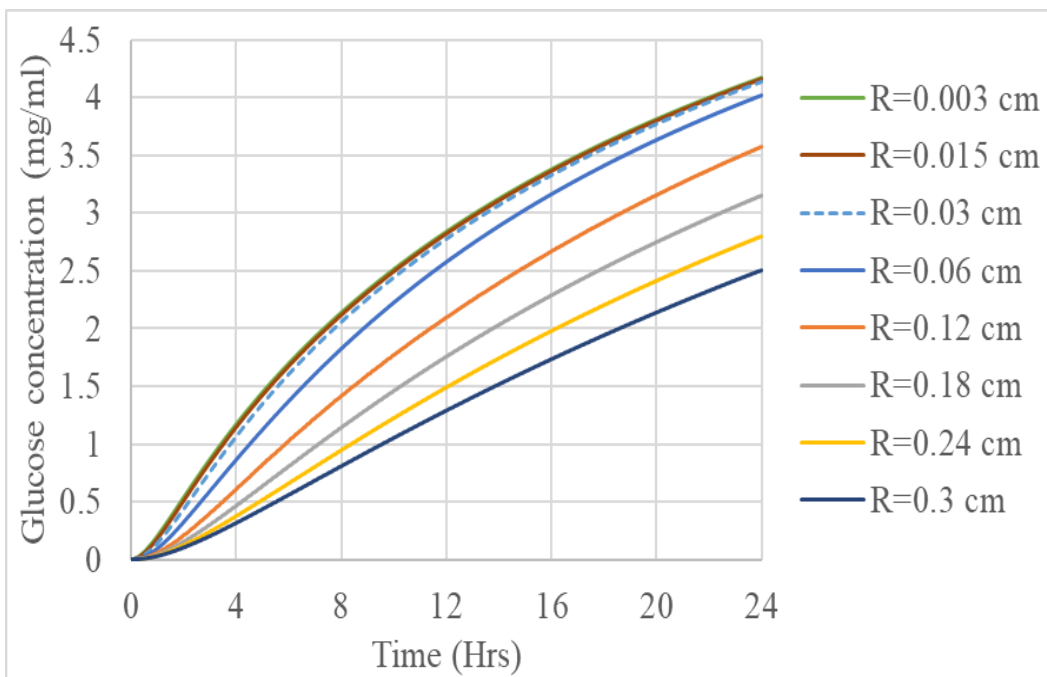
Figure 38. Comparison of glucose yields predicted by the model for different particle radius 'R' for 15 min DAP poplar.

Effect of changing φ and ε: The effect of the ratio of pore volume and total pore volume and porosity was predicted by varying the ratio of pore volume and total pore volume from 0.8 to 0.9, and porosity was varied from 0.40 to 0.59 for 8 min DAP poplar; we did not observe a significant change in accessibility factor and porosity for EH of 15 min and 21 min DAP polar. Based on the NMR cryoporometry results for different pretreatment times from Ankathi et al., (2019), we observed that the inaccessible pore volume always remained the same, but the total pore volume changed with increasing EH time for 8 min DAP poplar EH, the accessibility factor φ varied from 0.8 to 0.9, the available pore volume was calculated by subtracting the total pore volume with inaccessible pore volume and then dividing the available pore volume with the total pore volume from the graphs of figure 7

67

of Ankathi et al., (2019), the porosity initially is at 0.4 and increases to 0.58 as the EH progresses, porosity is calculated using Eq. 1 based on the total pore volumes from figure 7 of Ankathi et al., (2019). Based on the simulation, the comparison of glucose kinetics for different φ and ϵ are shown in Figure 39. According to the results, glucose kinetics for different φ and ϵ are all closely grouped, and no significant effect was found in the glucose yields for different φ and ϵ. Based on the simulated results, we can conclude that the glucose yield does not vary significantly with accessibility factor and porosity, at least for the range of φ and ϵ modelled in this study. This may not hold for scenarios where there is a tremendous change in accessibility factor such as 0.1 to 1 and porosity such as 0.1 to 1, compared to accessibility factor varying from 0.8 to 0.9 and porosity varying from 0.4 to 0.58 in this model.
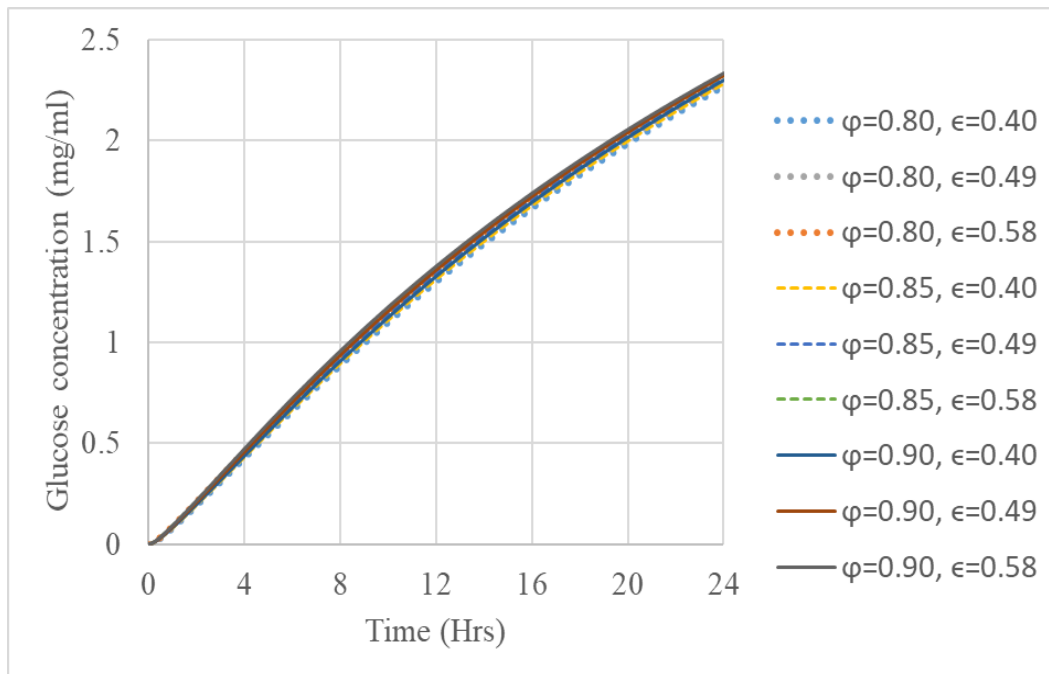
Figure 39. Comparison of bulk glucose concentrations from EH of 8 min DAP poplar for different φ and ϵ.

5 Conclusions

The hydrolytic enzyme diffusion and adsorption model provides a fundamental understanding of the effect parameters such as the particle size, porosity, maximum adsorption capacity on the characteristic's times of diffusion and adsorption. The results demonstrated that the particle size and characteristic time of diffusion had a strong correlation, the characteristic time of diffusion for non-adsorbing enzymes varied from 0 to 1650 secs for an Avicel PH-101 biomass particle radius range of 0.0025 cm to 0.025 cm. The porosity also showed an effect on the characteristic time of diffusion for non-adsorbing enzyme but not as strong as the particle radius, the characteristic time of diffusion for an Avicel PH-101 biomass particle of radius 0.0025 cm went from 18.5 secs to 9.8 secs when the porosity was varied from 0.1 to 0.9. The characteristic time of diffusion for adsorbing enzymes also showed a strong relationship with particle radius, a 10x increase in particle radius; there is a 100x increase in characteristic time of diffusion. The maximum adsorption capacity had a significant effect on the characteristic time of diffusion of adsorbing enzymes, The lowest characteristic time (16.67 s) was observed at (q_m= 0 mg/g substrate), and the highest characteristic time (2925 s) was observed at (q_m= 100 mg/g substrate). These results provide valuable insights on choosing the correct biomass pretreatment and enzyme behavior.

The multi-scale reaction kinetic model for the enzymatic hydrolysis developed by incorporating particle scale diffusion and adsorption model with a bulk liquid reaction model successfully predicted the change in bulk enzyme concentrations and glucose production kinetics of Avicel PH-101 and 15 min DAP poplar. The enzyme diffusion time incorporating the change in bulk enzyme concentration for the non-adsorbing enzyme (BG) was estimated to be 120 secs for Avicel PH -101and 4800 secs for DAP poplar. The difference in diffusion times for non-adsorbing enzymes shows the effect of particle size on diffusion times. The diffusion time was estimated to be 160 secs for Avicel PH-101 and 4.5 hrs for adsorbing enzymes. The results of the research demonstrated the effects of particle size and adsorption capacity on the adsorption kinetics. The cellulose, cellobiose, and glucose reaction model at the bulk liquid scale was coupled with particle scale enzymes. It demonstrated the effects of microporous structures on enzymatic yields of Avicel PH-101 and DAP poplar. The sensitivity analysis, conducted by varying the porosity and accessible pore volume to total pore volume ratio, demonstrated the effect of change in particle features on glucose yields. According to the results, we can conclude that the glucose yield does not vary significantly with accessibility factor and porosity, at least for the range of φ and ϵ modeled in this study. The multiscale model was also applied to particles of various sizes. Based on the results, it is recommended to use biomass particles of sizes closer to 0.06 cm to improve the enzymatic conversion yields. The multi-scale model for enzymatic hydrolysis of lignocellulosic biomass provides a better and more complete fundamental understanding of the complex enzymatic hydrolysis processes and

the relative significance of characteristics parameters that affect the hydrolysis rates and sugar yields.

6 Future work

The model can be further improved by incorporating other factors such as particle shapes, reaction temperature, pH, enzyme loading, different enzyme cocktails, inhibition by cellobiose on glucose production, inhibition by glucose-on-glucose production, degree of polymerization, cellulose crystallinity, and enzymatic hydrolysis time whose effect on EH efficiency are good areas for further investigation. Another area of improvement of this model is to incorporate the change in adsorption capacity and apparent density with change porosity during the study of the effect of porosity on characteristic time of diffusion, and this is possible by generating experimental data which can be used to estimate the range of adsorption capacities and apparent density for a range of values of porosities. Another improvement is the use of particle size distribution data instead of constant particle size is also an area that can be further improved. The kinetic model used in this study is a semi-mechanistic model, and the rate equations for cellulose show a strong dependence on cellulose concentration. To improve the kinetic model, a more mechanistic approach that can account for rates at different radial sections of the biomass particle more accurately can be reconsidered. The comparison of glucose yields from enzymatic hydrolysis of different pretreated biomass and prolonged EH times is yet to be investigated. Incorporating all these factors into the model and using a range of experimental results to optimize the model will help in deepening the understanding of enzymatic hydrolysis and aid in enzymatic hydrolysis design.

7 Bibliography

Adoption of the Paris Agreement.
https://unfccc.int/resource/docs/2015/cop21/eng/l09r01.pdf (United Nations, 2015).

Ankathi, S. K., Zhou, W., Webber, J. B., Patil, R., Chaudhari, U., & Shonnard, D. (2019). Synergistic Effects between Hydrolysis Time and Microporous Structure in Poplar. *ACS Sustainable Chemistry & Engineering*, *7*(15), 12920–12929. https://doi.org/10.1021/acssuschemeng.9b01926

Arantes, V., & Saddler, J. N. (2011). Cellulose accessibility limits the effectiveness of minimum cellulase loading on the efficient hydrolysis of pretreated lignocellulosic substrates. *Biotechnology for Biofuels*, *4*(1), 3. https://doi.org/10.1186/1754-6834-4-3

Bhagia, S., Dhir, R., Kumar, R., & Wyman, C. E. (2018). Deactivation of cellulase at the air-liquid interface is the main cause of incomplete cellulose conversion at low enzyme loadings. *Scientific Reports*, *8*(1). https://doi.org/10.1038/s41598-018-19848-3

Biofuel basics. Energy.gov. (n.d.). Retrieved November 4, 2021, from https://www.energy.gov/eere/bioenergy/biofuel-basics.

Carrillo, F., Lis, M. J., Colom, X., López-Mesas, M., & Valldeperas, J. (2005). Effect of alkali pretreatment on cellulase hydrolysis of wheat straw: Kinetic Study. *Process Biochemistry*, *40*(10), 3360–3364. https://doi.org/10.1016/j.procbio.2005.03.003

Cellulase from Trichoderma reesei aqueous solution, ≥700 units/g: Sigma-Aldrich. aqueous solution, ≥700 units/g | 9012-54-8. (n.d.). https://www.sigmaaldrich.com/US/en/product/sigma/c2730.

Chen, L., Zhang, H., Li, J., Lu, M., Guo, X., & Han, L. (2015). A novel diffusion–biphasic hydrolysis coupled kinetic model for Dilute Sulfuric Acid Pretreatment of corn stover. *Bioresource Technology*, *177*, 8–16. https://doi.org/10.1016/j.biortech.2014.11.060

Cho, E. J., Trinh, L. T., Song, Y., Lee, Y. G., & Bae, H.-J. (2020). Bioconversion of biomass waste into high value chemicals. *Bioresource Technology*, *298*, 122386. https://doi.org/10.1016/j.biortech.2019.122386

Crank, J. (1956). *The mathematics of diffusion*. Clarendon.

Cutlip, M. B., & Shacham, M. (2008). *Problem solving in chemical and biochemical engineering with polymath, Excel, and Matlab*. Prentice Hall.

Fierro, V., Torné-Fernández, V., Montané, D., & Celzard, A. (2008). Adsorption of phenol onto activated carbons having different textural and surface properties. *Microporous and Mesoporous Materials*, *111*(1-3), 276–284. https://doi.org/10.1016/j.micromeso.2007.08.002

Gao, D., Chundawat, S. P., Sethi, A., Balan, V., Gnanakaran, S., & Dale, B. E. (2013). Increased enzyme binding to substrate is not necessary for more efficient cellulose hydrolysis. *Proceedings of the National Academy of Sciences*, *110*(27), 10922–10927. https://doi.org/10.1073/pnas.1213426110

Grethlein, H. E. (1985). The Effect of Pore Size Distribution on the Rate of Enzymatic Hydrolysis of Cellulosic Substrates. *Bio/Technology*, *3*(2), 155–160. https://doi.org/10.1038/nbt0285-155

IEA (2013), Medium-Term Renewable Energy Market Report 2013, IEA, Paris https://www.iea.org/reports/medium-term-renewable-energy-market-report-2013

Ji, G., Xiao, W., Gao, C., Cao, Y., Zhang, Y., & Han, L. (2018). Mechanical fragmentation of wheat and rice straw at different scales: Energy requirement in relation to microstructure properties and enzymatic hydrolysis. *Energy Conversion and Management*, *171*, 38–47. https://doi.org/10.1016/j.enconman.2018.05.087

Kadam, K. L., Rydholm, E. C., & McMillan, J. D. (2004). Development and validation of a kinetic model for enzymatic saccharification of lignocellulosic biomass. *Biotechnology Progress*, *20*(3), 698–705. https://doi.org/10.1021/bp034316x

Kumar, P., Barrett, D. M., Delwiche, M. J., & Stroeve, P. (2009). Methods for pretreatment of lignocellulosic biomass for efficient hydrolysis and biofuel production. *Industrial & Engineering Chemistry Research*, *48*(8), 3713–3729. https://doi.org/10.1021/ie801542g

Kumar, R., & Wyman, C. E. (2009). Access of cellulase to cellulose and lignin for Poplar Solids produced by leading Pretreatment Technologies. *Biotechnology Progress*, *25*(3), 807–819. https://doi.org/10.1002/btpr.153

Levine, S. E., Fox, J. M., Blanch, H. W., & Clark, D. S. (2010). A mechanistic model of the enzymatic hydrolysis of cellulose. *Biotechnology and Bioengineering*, *107*(1), 37–51. https://doi.org/10.1002/bit.22789

Li, C., Yoshimoto, M., Tsukuda, N., Fukunaga, K., & Nakao, K. (2004). A kinetic study on enzymatic hydrolysis of a variety of pulps for its enhancement with continuous ultrasonic irradiation. *Biochemical Engineering Journal*, *19*(2), 155–164. https://doi.org/10.1016/j.bej.2003.12.010

Liu, Y., Nie, Y., Lu, X., Zhang, X., He, H., Pan, F., Zhou, L., Liu, X., Ji, X., & Zhang, S. (2019). Cascade utilization of lignocellulosic biomass to high-value products. *Green Chemistry*, *21*(13), 3499–3535. https://doi.org/10.1039/c9gc00473d

Luterbacher, J. S., Parlange, J.-Y., & Walker, L. P. (2012). A pore-hindered diffusion and reaction model can help explain the importance of pore size distribution in enzymatic hydrolysis of biomass. *Biotechnology and Bioengineering*, *110*(1), 127–136. https://doi.org/10.1002/bit.24614

Machado, D. L., Moreira Neto, J., da Cruz Pradella, J. G., Bonomi, A., Rabelo, S. C., & da Costa, A. C. (2015). Adsorption characteristics of cellulase and β-glucosidase on Avicel, pretreated sugarcane bagasse, and lignin. *Biotechnology and Applied Biochemistry*, *62*(5), 681–689. https://doi.org/10.1002/bab.1307

Min, B.-C., Koo, B.-W., Gwak, K.-S., Yeo, H.-M., Choi, J.-W., & Choi, I.-G. (2011). Effects of dilute acid pretreatment on enzyme adsorption and surface morphology of Liriodendron tulipifera. *Journal of the Korean Wood Science and Technology*, *39*(2), 187–195. https://doi.org/10.5658/wood.2011.39.2.187

O'Dwyer, J. P., Zhu, L., Granda, C. B., & Holtzapple, M. T. (2007). Enzymatic hydrolysis of lime-pretreated corn stover and investigation of the HCH-1 model: Inhibition pattern, degree of inhibition, validity of simplified HCH-1 model. *Bioresource Technology*, *98*(16), 2969–2977. https://doi.org/10.1016/j.biortech.2006.10.014

OECD/FAO (2021), *OECD-FAO Agricultural Outlook 2021-2030*, OECD Publishing, Paris, https://doi.org/10.1787/19428846-en.

Pakarinen, A., Haven, M. Ø., Djajadi, D. T., Várnai, A., Puranen, T., & Viikari, L. (2014). Cellulases without carbohydrate-binding modules in high consistency ethanol production process. *Biotechnology for Biofuels*, *7*(1). https://doi.org/10.1186/1754-6834-7-27

Perera, F. (2017). Pollution from fossil-fuel combustion is the leading environmental threat to Global Pediatric Health and Equity: Solutions Exist. *International Journal of Environmental Research and Public Health*, *15*(1), 16. https://doi.org/10.3390/ijerph15010016

Qi, B., Chen, X., Su, Y., & Wan, Y. (2011). Enzyme adsorption and recycling during hydrolysis of wheat straw lignocellulose. *Bioresource Technology*, *102*(3), 2881–2889. https://doi.org/10.1016/j.biortech.2010.10.092

Rohrbach, J. C., & Luterbacher, J. S. (2021). Investigating the effects of substrate morphology and experimental conditions on the enzymatic hydrolysis of lignocellulosic biomass through modeling. *Biotechnology for Biofuels*, *14*(1). https://doi.org/10.1186/s13068-021-01920-2

Sasmal, S., & Mohanty, K. (2017). Pretreatment of lignocellulosic biomass toward biofuel production. *Biofuel and Biorefinery Technologies*, 203–221. https://doi.org/10.1007/978-3-319-67678-4_9

Schiesser, W.E. (1991) The Numerical Method of Lines: Integration of Partial Differential Equations. Academic Press, San Diego.

Siqueira, G., Arantes, V., Saddler, J. N., Ferraz, A., & Milagres, A. M. (2017). Limitation of cellulose accessibility and unproductive binding of cellulases by pretreated sugarcane bagasse lignin. *Biotechnology for Biofuels*, *10*(1). https://doi.org/10.1186/s13068-017-0860-7

Sousa Jr., R., Carvalho, M. L., Giordano, R. L., & Giordano, R. C. (2011). Recent trends in the modeling of cellulose hydrolysis. *Brazilian Journal of Chemical Engineering*, *28*(4), 545–564. https://doi.org/10.1590/s0104-66322011000400001

Tantasucharit, U., (1995). *Porosity, surface area and enzymatic saccharification of microcrystalline cellulose*. [online] ScholarsArchive@OSU. Available at: https://ir.library.oregonstate.edu/concern/graduate_thesis_or_dissertations/g445ch62v [Accessed 5 February 2021].

Tsai, C.-T., Morales-Rodriguez, R., Sin, G., & Meyer, A. S. (2014). A dynamic model for cellulosic biomass hydrolysis: A comprehensive analysis and validation of hydrolysis and product inhibition mechanisms. *Applied Biochemistry and Biotechnology*, *172*(6), 2815–2837. https://doi.org/10.1007/s12010-013-0717-x

Várnai, A., Siika-aho, M., & Viikari, L. (2013). Carbohydrate-binding modules (cbms) revisited: Reduced amount of water counterbalances the need for cbms. *Biotechnology for Biofuels*, *6*(1). https://doi.org/10.1186/1754-6834-6-30

Wang, L.-S., Zhang, Y.-Z., Yang, H., & Gao, P.-J. (2004). Quantitative estimate of the effect of cellulase components during degradation of cotton fibers. *Carbohydrate Research*, *339*(4), 819–824. https://doi.org/10.1016/j.carres.2004.01.004

Whitaker, S. (1999). The method of volume averaging. *Theory and Applications of Transport in Porous Media*. https://doi.org/10.1007/978-94-017-3389-2

Yi Zheng, Zhongli Pan, Ruihong Zhang, & Bryan M Jenkins. (2009). Kinetic modeling for enzymatic hydrolysis of pretreated creeping wild ryegrass. *2009 Reno, Nevada, June 21 - June 24, 2009*. https://doi.org/10.13031/2013.26928

Yohana Chaerunisaa, A., Sriwidodo, S., & Abdassah, M. (2020). Microcrystalline Cellulose as Pharmaceutical Excipient. *Pharmaceutical Formulation Design - Recent Practices*. https://doi.org/10.5772/intechopen.88092

Zhang, H., Chen, L., Li, J., Lu, M., & Han, L. (2017). Quantitative characterization of enzyme adsorption and hydrolytic performance for ultrafine grinding pretreated corn stover. *Bioresource Technology*, *234*, 23–32. https://doi.org/10.1016/j.biortech.2017.03.013

 Zhang, H., Chen, L., Lu, M., Li, J., & Han, L. (2016). A novel film–pore–surface diffusion model to explain the enhanced enzyme adsorption of corn stover pretreated by ultrafine grinding. *Biotechnology for Biofuels*, *9*(1). https://doi.org/10.1186/s13068-016-0602-2

Zhang, H., Han, L., & Dong, H. (2021). An Insight to pretreatment, enzyme adsorption and enzymatic hydrolysis of lignocellulosic biomass: Experimental and modeling studies. *Renewable and Sustainable Energy Reviews*, *140*, 110758. https://doi.org/10.1016/j.rser.2021.110758

Zhang, Y., & Hess, H. (2019). Enhanced Diffusion of Catalytically Active Enzymes. *ACS Central Science*, *5*(6), 939–948. https://doi.org/10.1021/acscentsci.9b00228

Zhang, Y.-H. P., & Lynd, L. R. (2004). Toward an aggregated understanding of enzymatic hydrolysis of cellulose: Noncomplexed cellulase systems. *Biotechnology and Bioengineering*, *88*(7), 797–824. https://doi.org/10.1002/bit.20282

Zhao, X., Zhang, L., & Liu, D. (2012). Biomass recalcitrance. Part I: the chemical compositions and physical structures affecting the enzymatic hydrolysis of lignocellulose. *Biofuels, Bioproducts and Biorefining*, *6*(4), 465–482. https://doi.org/10.1002/bbb.1331

Appendix

The custom-written codes in MATLAB to predict the characteristic time of diffusion and concentrations at different radial positions for non-adsorbing enzymes and adsorbing enzymes are in Appendix A.1 and A.2, respectively. The polymath code for the multiscale model is in Appendix A.2.

A.1   MATLAB code for non-adsorbing enzymes

```matlab
function BGenzyme
global varepsilon DP CL DW
global varphi
varepsilon=1; %porosity
DW=5.67*10^-7;
DP=DW*(varepsilon/(2-varepsilon));    %cm^2/s

CL=1; %mg/mL
varphi=1; %ratio of accessible/total pore volume
tend=20;%sec
R=0.0025;%cm
m = 1;

x = linspace(0,R,10);

t = linspace(0,tend,1000);
assignin('base','t',t)
assignin('base','x',x)
sol=pdepe(m,@BGpdepde,@BGpdepdeic,@BGpdepdebc,x,t);

m=sol(:,1).';
row=find(abs(m-(0.99*CL))< 0.0001);
row1=row(1);
tau=t(row1);

assignin('base','row',row)
assignin('base','tau',tau)

concentration = sol(:,:,1);

assignin('base','C',concentration)

figure, plot(x,concentration(end,:))
title(strcat('Solution at t = ', num2str(tau)))
xlabel('Radial position r')
ylabel('concentration (mg/ml)')
```

```matlab
ylabel('concentation (mg/ml)')
%Plot concentration vs. time
figure, plot(t,concentration(:,1))
title('concentration (mg/ml) at radial position r=0 (cm)')
xlabel('Time (s)')
ylabel('concentration of enzyme (mg/ml)')
figure, plot(t,concentration)
shg


% ------------------------------------------------------------
-----
function [c,f,s] = BGpdepde(x,t,u,dudx)
global varepsilon DP varphi
c = varepsilon/varphi;
f = DP*dudx;
s = 0;
% ------------------------------------------------------------
-----
function u0 = BGpdepdeic(x)
u0 = 0;
% ------------------------------------------------------------
-----
function [pl,ql,pr,qr] = BGpdepdebc(rl,ul,xr,ur,t)
global CL
pl = 0;
ql = 0;
pr = ur-CL;
```

A.2   MATLAB code for Adsorbing enzymes

```matlab
function Econcentration
global varepsilon DP CL DW
global varphi
global rho qm ka
R=0.0025;% cm
varepsilon=1; %porosity
rho=1.69;% cm3/g
ka=11.5;% ml/mg
qm=0;% mg/g
DW=5.67*10^-7;
DP=DW*(varepsilon/(2-varepsilon));   %cm^2/s whittaker
relation
CL=1; %mg/mL
varphi=1; %ratio of accessible/total pore volume
```

```matlab
tend=20;%sec

m = 1;

x = linspace(0,R,10);

t = linspace(0,tend,1000);
assignin('base','t',t)
assignin('base','x',x)
sol=pdepe(m,@Econcentrationpdepde,@Econcentrationpdepdeic,@
Econcentrationpdepdebc,x,t);


C=sol(:,1).';
row=find(abs(C-(0.99*CL))< 0.0001);
row1=row(1);
tau=t(row1);
assignin('base','C',C)

E = sol(:,:,1);
assignin('base','E',E)

assignin('base','row',row)
assignin('base','tau',tau)

figure, plot(x,E(end,:))
title(strcat('concentration at t = ', num2str(tend)))
xlabel('Radial position r')
ylabel('concentation (mg/ml)')

%Plot concentration vs. time
figure, plot(t,E(:,1))
title('concentration of enzyme at r=0')
xlabel('Time (s)')
ylabel('concentration (mg/ml)')
figure, plot(t,E)
shg


% ------------------------------------------------------------
-----
function [c,f,s] = Econcentrationpdepde(x,t,E,dEdx)
global varepsilon DP varphi rho qm ka
c = (varepsilon+((rho*qm*ka)/(1+(ka.*E))^2))/varphi;
f = DP*dEdx;
s = 0;
```

```
% --------------------------------------------------------------
-----
function u0 = Econcentrationpdepdeic(x)
u0 = 0;
% --------------------------------------------------------------
-----
function [pl,ql,pr,qr] =
Econcentrationpdepdebc(rl,ul,xr,ur,t)
global CL
pl = 0;
ql = 0;
pr = ur-CL;
qr = 0;
```

A.3   Multiscale model Polymath code

d(CBG)/ d(t)= -(k*A/V)*(CBG-BG1)

CBG(0)=0.1107 # BG concentration

BG1=(4*BG2-BG3+((2*k*deltar)/DPBG)*CBG)/(3+((2*k*deltar)/DPBG))

d(BG2) / d(t) = ((phi*DPBG)/epsilon)*(((BG3-2*BG2+BG1)/deltar^2)+(1/(R-1*deltar))*(BG3-BG1)/2*deltar)

BG2(0) =0

d(BG3) / d(t) = ((phi*DPBG)/epsilon)*(((BG4-2*BG3+BG2)/deltar^2)+(1/(R-2*deltar))*(BG4-BG2)/2*deltar)

BG3(0) = 0

d(BG4) / d(t) = ((phi*DPBG)/epsilon)*(((BG5-2*BG4+BG3)/deltar^2)+(1/(R-3*deltar))*(BG5-BG3)/2*deltar)

BG4(0) = 0

d(BG5) / d(t) = ((phi*DPBG)/epsilon)*(((BG6-2*BG5+BG4)/deltar^2)+(1/(R-4*deltar))*(BG6-BG4)/2*deltar)

BG5(0) = 0

d(BG6) / d(t) = ((phi*DPBG)/epsilon)*(((BG7-2*BG6+BG5)/deltar^2)+(1/(R-5*deltar))*(BG7-BG5)/2*deltar)

BG6(0) = 0

d(BG7) / d(t) = ((phi*DPBG)/epsilon)*(((BG8-2*BG7+BG6)/deltar^2)+(1/(R-6*deltar))*(BG8-BG6)/2*deltar)

BG7(0) = 0

d(BG8) / d(t) = ((phi*DPBG)/epsilon)*(((BG9-2*BG8+BG7)/deltar^2)+(1/(R-7*deltar))*(BG9-BG7)/2*deltar)

BG8(0) = 0

d(BG9) / d(t) =((phi*DPBG)/epsilon)*(((BG10-2*BG9+BG8)/deltar^2)+(1/(R-8*deltar))*(BG10-BG8)/2*deltar)

BG9(0) = 0

d(BG10) / d(t) = ((phi*DPBG)/epsilon)*(((BG11-2*BG10+BG9)/deltar^2)+(1/(R-9*deltar))*(BG11-BG9)/2*deltar)

BG10(0) = 0

d(BG11) / d(t) = ((phi*DPBG)/epsilon)*(((BG12-2*BG11+BG10)/deltar^2)+(1/(R-10*deltar))*(BG12-BG10)/2*deltar)

BG11(0) = 0

d(BG12) / d(t) = ((phi*DPBG)/epsilon)*(((BG13-2*BG12+BG11)/deltar^2)+(1/(R-11*deltar))*(BG13-BG11)/2*deltar)

BG12(0) = 0

d(BG13) / d(t) = ((phi*DPBG)/epsilon)*(((BG14-2*BG13+BG12)/deltar^2)+(1/(R-12*deltar))*(BG14-BG12)/2*deltar)

BG13(0) = 0

d(BG14) / d(t) = ((phi*DPBG)/epsilon)*(((BG15-2*BG14+BG13)/deltar^2)+(1/(R-13*deltar))*(BG15-BG13)/2*deltar)

BG14(0) = 0

d(BG15) / d(t) = ((phi*DPBG)/epsilon)*(((BG16-2*BG15+BG14)/deltar^2)+(1/(R-14*deltar))*(BG16-BG14)/2*deltar)

BG15(0) = 0

d(BG16) / d(t) = ((phi*DPBG)/epsilon)*(((BG17-2*BG16+BG15)/deltar^2)+(1/(R-15*deltar))*(BG17-BG15)/2*deltar)

BG16(0) = 0

d(BG17) / d(t) = ((phi*DPBG)/epsilon)*(((BG18-2*BG17+BG16)/deltar^2)+(1/(R-16*deltar))*(BG18-BG16)/2*deltar)

BG17(0) = 0

d(BG18) / d(t) = ((phi*DPBG)/epsilon)*(((BG19-2*BG18+BG17)/deltar^2)+(1/(R-17*deltar))*(BG19-BG17)/2*deltar)

BG18(0) = 0

d(BG19) / d(t) = ((phi*DPBG)/epsilon)*(((BG20-2*BG19+BG18)/deltar^2)+(1/(R-18*deltar))*(BG20-BG18)/2*deltar)

BG19(0) = 0

d(BG20) / d(t) = ((phi*DPBG)/epsilon)*(((BG21-2*BG20+BG19)/deltar^2)+(1/(R-19*deltar))*(BG21-BG19)/2*deltar)

BG20(0) = 0

BG21=(4*BG20-BG19)/3

d(CCE)/ d(t)= -(k*A/V)*(CCE-CE1)

CCE(0)=0.3075 #Accelerase CE concentration

CE1=(4*CE2-CE3+((2*k*deltar)/DPCE)*CCE)/(3+((2*k*deltar)/DPCE))

d(CE2) / d(t) = ((phi*DPCE)/(epsilon+((rhoa*qm*ka)/(1+(ka*CE2))^2)))*(((CE3-2*CE2+CE1)/deltar^2)+(1/(R-1*deltar))*(CE3-CE1)/2*deltar)

CE2(0) =0

d(CE3) / d(t) = ((phi*DPCE)/(epsilon+((rhoa*qm*ka)/(1+(ka*CE3))^2)))*(((CE4-2*CE3+CE2)/deltar^2)+(1/(R-2*deltar))*(CE4-CE2)/2*deltar)

CE3(0) = 0

d(CE4) / d(t) = ((phi*DPCE)/(epsilon+((rhoa*qm*ka)/(1+(ka*CE4))^2)))*(((CE5-2*CE4+CE3)/deltar^2)+(1/(R-3*deltar))*(CE5-CE3)/2*deltar)

CE4(0) = 0

d(CE5) / d(t) = ((phi*DPCE)/(epsilon+((rhoa*qm*ka)/(1+(ka*CE5))^2)))*(((CE6-2*CE5+CE4)/deltar^2)+(1/(R-4*deltar))*(CE6-CE4)/2*deltar)

CE5(0) = 0

d(CE6) / d(t) = ((phi*DPCE)/(epsilon+((rhoa*qm*ka)/(1+(ka*CE6))^2)))*(((CE7-2*CE6+CE5)/deltar^2)+(1/(R-5*deltar))*(CE7-CE5)/2*deltar)

CE6(0) = 0

d(CE7) / d(t) = ((phi*DPCE)/(epsilon+((rhoa*qm*ka)/(1+(ka*CE7))^2)))*(((CE8-2*CE7+CE6)/deltar^2)+(1/(R-6*deltar))*(CE8-CE6)/2*deltar)

CE7(0) = 0

d(CE8) / d(t) = ((phi*DPCE)/(epsilon+((rhoa*qm*ka)/(1+(ka*CE8))^2)))*(((CE9-2*CE8+CE7)/deltar^2)+(1/(R-7*deltar))*(CE9-CE7)/2*deltar)

CE8(0) = 0

d(CE9) / d(t) = ((phi*DPCE)/(epsilon+((rhoa*qm*ka)/(1+(ka*CE9))^2)))*(((CE10-2*CE9+CE8)/deltar^2)+(1/(R-8*deltar))*(CE10-CE8)/2*deltar)

CE9(0) = 0

d(CE10) / d(t) = ((phi*DPCE)/(epsilon+((rhoa*qm*ka)/(1+(ka*CE10))^2)))*(((CE11-2*CE10+CE9)/deltar^2)+(1/(R-9*deltar))*(CE11-CE9)/2*deltar)

CE10(0) = 0

d(CE11) / d(t) = ((phi*DPCE)/(epsilon+((rhoa*qm*ka)/(1+(ka*CE11))^2)))*(((CE12-2*CE11+CE10)/deltar^2)+(1/(R-10*deltar))*(CE12-CE10)/2*deltar)

CE11(0) = 0

d(CE12) / d(t) = ((phi*DPCE)/(epsilon+((rhoa*qm*ka)/(1+(ka*CE12))^2)))*(((CE13-2*CE12+CE11)/deltar^2)+(1/(R-11*deltar))*(CE13-CE11)/2*deltar)

CE12(0) = 0

d(CE13) / d(t) = ((phi*DPCE)/(epsilon+((rhoa*qm*ka)/(1+(ka*CE13))^2)))*(((CE14-2*CE13+CE12)/deltar^2)+(1/(R-12*deltar))*(CE14-CE12)/2*deltar)

CE13(0) = 0

d(CE14) / d(t) = ((phi*DPCE)/(epsilon+((rhoa*qm*ka)/(1+(ka*CE14))^2)))*(((CE15-2*CE14+CE13)/deltar^2)+(1/(R-13*deltar))*(CE15-CE13)/2*deltar)

CE14(0) = 0

d(CE15) / d(t) = ((phi*DPCE)/(epsilon+((rhoa*qm*ka)/(1+(ka*CE15))^2)))*(((CE16-2*CE15+CE14)/deltar^2)+(1/(R-14*deltar))*(CE16-CE14)/2*deltar)

CE15(0) = 0

d(CE16) / d(t) = ((phi*DPCE)/(epsilon+((rhoa*qm*ka)/(1+(ka*CE16))^2)))*(((CE17-2*CE16+CE15)/deltar^2)+(1/(R-15*deltar))*(CE17-CE15)/2*deltar)

CE16(0) = 0

d(CE17) / d(t) = ((phi*DPCE)/(epsilon+((rhoa*qm*ka)/(1+(ka*CE17))^2)))*(((CE18-2*CE17+CE16)/deltar^2)+(1/(R-16*deltar))*(CE18-CE16)/2*deltar)

CE17(0) = 0

d(CE18) / d(t) = ((phi*DPCE)/(epsilon+((rhoa*qm*ka)/(1+(ka*CE18))^2)))*(((CE19-2*CE18+CE17)/deltar^2)+(1/(R-17*deltar))*(CE19-CE17)/2*deltar)

CE18(0) = 0

d(CE19) / d(t) = ((phi*DPCE)/(epsilon+((rhoa*qm*ka)/(1+(ka*CE19))^2)))*(((CE20-2*CE19+CE18)/deltar^2)+(1/(R-18*deltar))*(CE20-CE18)/2*deltar)

CE19(0) = 0

d(CE20) / d(t) = ((phi*DPCE)/(epsilon+((rhoa*qm*ka)/(1+(ka*CE20))^2)))*(((CE21-2*CE20+CE19)/deltar^2)+(1/(R-19*deltar))*(CE21-CE19)/2*deltar)

CE20(0) = 0

CE21=(4*CE20-CE19)/3

C1(0)=0.911

Co1=0.911

d(C1)/d(t)= -k1r*(qm*ka*(CE2+CE1)/2*C1)/(1+ka*(CE2+CE1)/2)*alpha*C1/Co1*C1-k2r*(qm*ka*(CE2+CE1)/2*C1)/(1+ka*(CE2+CE1)/2)*alpha*C1/Co1*C1

C2(0)=0.864

Co2=0.864

d(C2)/d(t)= -k1r*(qm*ka*(CE3+CE2)/2*C2)/(1+ka*(CE3+CE2)/2)*alpha*C2/Co2*C2-k2r*(qm*ka*(CE3+CE2)/2*C2)/(1+ka*(CE3+CE2)/2)*alpha*C2/Co2*C2

C3(0)=0.818

Co3=0.818

d(C3)/d(t)= -k1r*(qm*ka*(CE4+CE3)/2*C3)/(1+ka*(CE4+CE3)/2)*alpha*C3/Co3*C3-k2r*(qm*ka*(CE4+CE3)/2*C3)/(1+ka*(CE4+CE3)/2)*alpha*C3/Co3*C3

C4(0)=0.771

Co4=0.771

d(C4)/d(t)= -k1r*(qm*ka*(CE5+CE4)/2*C4)/(1+ka*(CE5+CE4)/2)*alpha*C4/Co4*C4-
k2r*(qm*ka*(CE5+CE4)/2*C4)/(1+ka*(CE5+CE4)/2)*alpha*C4/Co4*C4

C5(0)=0.724

Co5=0.724

d(C5)/d(t)= -k1r*(qm*ka*(CE6+CE5)/2*C5)/(1+ka*(CE6+CE5)/2)*alpha*C5/Co5*C5-
k2r*(qm*ka*(CE6+CE5)/2*C5)/(1+ka*(CE6+CE5)/2)*alpha*C5/Co5*C5

C6(0)=0.678

Co6=0.678

d(C6)/d(t)= -k1r*(qm*ka*(CE7+CE6)/2*C6)/(1+ka*(CE7+CE6)/2)*alpha*C6/Co6*C6-
k2r*(qm*ka*(CE7+CE6)/2*C6)/(1+ka*(CE7+CE6)/2)*alpha*C6/Co6*C6

C7(0)=0.631

Co7=0.631

d(C7)/d(t)= -k1r*(qm*ka*(CE8+CE7)/2*C7)/(1+ka*(CE8+CE7)/2)*alpha*C7/Co7*C7-
k2r*(qm*ka*(CE8+CE7)/2*C7)/(1+ka*(CE8+CE7)/2)*alpha*C7/Co7*C7

C8(0)=0.584

Co8=0.584

d(C8)/d(t)= -k1r*(qm*ka*(CE9+CE8)/2*C8)/(1+ka*(CE9+CE8)/2)*alpha*C8/Co8*C8-
k2r*(qm*ka*(CE9+CE8)/2*C8)/(1+ka*(CE9+CE8)/2)*alpha*C8/Co8*C8

C9(0)=0.537

Co9=0.537

d(C9)/d(t)= -
k1r*(qm*ka*(CE10+CE9)/2*C9)/(1+ka*(CE10+CE9)/2)*alpha*C9/Co9*C9-
k2r*(qm*ka*(CE10+CE9)/2*C9)/(1+ka*(CE10+CE9)/2)*alpha*C9/Co9*C9

C10(0)=0.491

Co10=0.491

d(C10)/d(t)= -
k1r*(qm*ka*(CE11+CE10)/2*C10)/(1+ka*(CE11+CE10)/2)*alpha*C10/Co10*C10-
k2r*(qm*ka*(CE11+CE10)/2*C10)/(1+ka*(CE11+CE10)/2)*alpha*C10/Co10*C10

C11(0)=0.444

Co11=0.444

d(C11)/d(t)= -
k1r*(qm*ka*(CE12+CE11)/2*C11)/(1+ka*(CE12+CE11)/2)*alpha*C11/Co11*C11-
k2r*(qm*ka*(CE12+CE11)/2*C11)/(1+ka*(CE12+CE11)/2)*alpha*C11/Co11*C11

C12(0)=0.397

Co12=0.397

d(C12)/d(t)= -
k1r*(qm*ka*(CE13+CE12)/2*C12)/(1+ka*(CE13+CE12)/2)*alpha*C12/Co12*C12-
k2r*(qm*ka*(CE13+CE12)/2*C12)/(1+ka*(CE13+CE12)/2)*alpha*C12/Co12*C12

C13(0)=0.350

Co13=0.350

d(C13)/d(t)= -
k1r*(qm*ka*(CE14+CE13)/2*C13)/(1+ka*(CE14+CE13)/2)*alpha*C13/Co13*C13-
k2r*(qm*ka*(CE14+CE13)/2*C13)/(1+ka*(CE14+CE13)/2)*alpha*C13/Co13*C13

C14(0)=0.304

Co14=0.304

d(C14)/d(t)= -
k1r*(qm*ka*(CE15+CE14)/2*C14)/(1+ka*(CE15+CE14)/2)*alpha*C14/Co14*C14-
k2r*(qm*ka*(CE15+CE14)/2*C14)/(1+ka*(CE15+CE14)/2)*alpha*C14/Co14*C14

C15(0)=0.257

Co15=0.257

d(C15)/d(t)= -
k1r*(qm*ka*(CE16+CE15)/2*C15)/(1+ka*(CE16+CE15)/2)*alpha*C15/Co15*C15-
k2r*(qm*ka*(CE16+CE15)/2*C15)/(1+ka*(CE16+CE15)/2)*alpha*C15/Co15*C15

C16(0)=0.210

Co16=0.210

d(C16)/d(t)= -
k1r*(qm*ka*(CE17+CE16)/2*C16)/(1+ka*(CE17+CE16)/2)*alpha*C16/Co16*C16-
k2r*(qm*ka*(CE17+CE16)/2*C16)/(1+ka*(CE17+CE16)/2)*alpha*C16/Co16*C16

C17(0)=0.164

Co17=0.164

d(C17)/d(t)= -
k1r*(qm*ka*(CE18+CE17)/2*C17)/(1+ka*(CE18+CE17)/2)*alpha*C17/Co17*C17-
k2r*(qm*ka*(CE18+CE17)/2*C17)/(1+ka*(CE18+CE17)/2)*alpha*C17/Co17*C17

C18(0)=0.117

Co18=0.117

d(C18)/d(t)= -
k1r*(qm*ka*(CE19+CE18)/2*C18)/(1+ka*(CE19+CE18)/2)*alpha*C18/Co18*C18-
k2r*(qm*ka*(CE19+CE18)/2*C18)/(1+ka*(CE19+CE18)/2)*alpha*C18/Co18*C18

C19(0)=0.07

Co19=0.07

d(C19)/d(t)= -
k1r*(qm*ka*(CE20+CE19)/2*C19)/(1+ka*(CE20+CE19)/2)*alpha*C19/Co19*C19-
k2r*(qm*ka*(CE20+CE19)/2*C19)/(1+ka*(CE20+CE19)/2)*alpha*C19/Co19*C19

C20(0)=0.023

Co20=0.023

d(C20)/d(t)= -
k1r*(qm*ka*(CE21+CE20)/2*C20)/(1+ka*(CE21+CE20)/2)*alpha*C20/Co20*C20-
k2r*(qm*ka*(CE21+CE20)/2*C20)/(1+ka*(CE21+CE20)/2)*alpha*C20/Co20*C20

C=C1+C2+C3+C4+C5+C6+C7+C8+C9+C10+C11+C12+C13+C14+C15+C16+C17+C1
8+C19+C20

d(CB1) / d(t) =
1.056*k1r*(qm*ka*(CE2+CE1)/2*C1)/(1+ka*(CE2+CE1)/2)*alpha*C1/Co1*C1-
((k3r*((BG2+BG1)/2)*CB1)/(k3M+CB1))

CB1(0) =0

d(CB2) / d(t) =
1.056*k1r*(qm*ka*(CE3+CE2)/2*C2)/(1+ka*(CE3+CE2)/2)*alpha*C2/Co2*C2-
((k3r*((BG3+BG2)/2)*CB2)/(k3M+CB2))

CB2(0) = 0

d(CB3) / d(t) =
1.056*k1r*(qm*ka*(CE4+CE3)/2*C3)/(1+ka*(CE4+CE3)/2)*alpha*C3/Co3*C3-
((k3r*((BG4+BG3)/2)*CB3)/(k3M+CB3))

CB3(0) = 0

d(CB4) / d(t) =
1.056*k1r*(qm*ka*(CE5+CE4)/2*C4)/(1+ka*(CE5+CE4)/2)*alpha*C4/Co4*C4-
((k3r*((BG5+BG4)/2)*CB4)/(k3M+CB4))

CB4(0) = 0

d(CB5) / d(t) =
1.056*k1r*(qm*ka*(CE6+CE5)/2*C5)/(1+ka*(CE6+CE5)/2)*alpha*C5/Co5*C5-
((k3r*((BG6+BG5)/2)*CB5)/(k3M+CB5))

CB5(0) = 0

d(CB6) / d(t) =
1.056*k1r*(qm*ka*(CE7+CE6)/2*C6)/(1+ka*(CE7+CE6)/2)*alpha*C6/Co6*C6-
((k3r*((BG7+BG6)/2)*CB6)/(k3M+CB6))

CB6(0) = 0

d(CB7) / d(t) =
1.056*k1r*(qm*ka*(CE8+CE7)/2*C7)/(1+ka*(CE8+CE7)/2)*alpha*C7/Co7*C7-
((k3r*((BG8+BG7)/2)*CB7)/(k3M+CB7))

CB7(0) = 0

d(CB8) / d(t) =
1.056*k1r*(qm*ka*(CE9+CE8)/2*C8)/(1+ka*(CE9+CE8)/2)*alpha*C8/Co8*C8-
((k3r*((BG9+BG8)/2)*CB8)/(k3M+CB8))

CB8(0) = 0

d(CB9) / d(t) =
1.056*k1r*(qm*ka*(CE10+CE9)/2*C9)/(1+ka*(CE10+CE9)/2)*alpha*C9/Co9*C9-
((k3r*((BG10+BG9)/2)*CB9)/(k3M+CB9))

CB9(0) = 0

d(CB10) / d(t) =
1.056*k1r*(qm*ka*(CE11+CE10)/2*C10)/(1+ka*(CE11+CE10)/2)*alpha*C10/Co10*C
10-((k3r*((BG11+BG10)/2)*CB10)/(k3M+CB10))

CB10(0) = 0

d(CB11) / d(t) =
1.056*k1r*(qm*ka*(CE12+CE11)/2*C11)/(1+ka*(CE12+CE11)/2)*alpha*C11/Co11*C
11-((k3r*((BG12+BG11)/2)*CB11)/(k3M+CB11))

CB11(0) = 0

d(CB12) / d(t) =
1.056*k1r*(qm*ka*(CE13+CE12)/2*C12)/(1+ka*(CE13+CE12)/2)*alpha*C12/Co12*C12-((k3r*((BG13+BG12)/2)*CB12)/(k3M+CB12))

CB12(0) = 0

d(CB13) / d(t) =
1.056*k1r*(qm*ka*(CE14+CE13)/2*C13)/(1+ka*(CE14+CE13)/2)*alpha*C13/Co13*C13-((k3r*((BG14+BG13)/2)*CB13)/(k3M+CB13))

CB13(0) = 0

d(CB14) / d(t) =
1.056*k1r*(qm*ka*(CE15+CE14)/2*C14)/(1+ka*(CE15+CE14)/2)*alpha*C14/Co14*C14-((k3r*((BG15+BG14)/2)*CB14)/(k3M+CB14))

CB14(0) = 0

d(CB15) / d(t) =
1.056*k1r*(qm*ka*(CE16+CE15)/2*C15)/(1+ka*(CE16+CE15)/2)*alpha*C15/Co15*C15-((k3r*((BG16+BG15)/2)*CB15)/(k3M+CB16))

CB15(0) = 0

d(CB16) / d(t) =
1.056*k1r*(qm*ka*(CE17+CE16)/2*C16)/(1+ka*(CE17+CE16)/2)*alpha*C16/Co16*C16-((k3r*((BG17+BG16)/2)*CB16)/(k3M+CB16))

CB16(0) = 0

d(CB17) / d(t) =
1.056*k1r*(qm*ka*(CE18+CE17)/2*C17)/(1+ka*(CE18+CE17)/2)*alpha*C17/Co17*C17-((k3r*((BG18+BG17)/2)*CB17)/(k3M+CB17))

CB17(0) = 0

d(CB18) / d(t) =
1.056*k1r*(qm*ka*(CE19+CE18)/2*C18)/(1+ka*(CE19+CE18)/2)*alpha*C18/Co18*C18-((k3r*((BG19+BG18)/2)*CB18)/(k3M+CB18))

CB18(0) = 0

d(CB19) / d(t) =
1.056*k1r*(qm*ka*(CE20+CE19)/2*C19)/(1+ka*(CE20+CE19)/2)*alpha*C19/Co19*C19-((k3r*((BG20+BG19)/2)*CB19)/(k3M+CB19))

CB19(0) = 0

d(CB20) / d(t) =
1.056*k1r*(qm*ka*(CE21+CE20)/2*C20)/(1+ka*(CE21+CE20)/2)*alpha*C20/Co20*C20-((k3r*((BG21+BG20)/2)*CB20)/(k3M+CB20))

CB20(0) = 0

CB=CB1+CB2+CB3+CB4+CB5+CB6+CB7+CB8+CB9+CB10+CB11+CB12+CB13+CB14+CB15+CB16+CB17+CB18+CB19+CB20

d(G1) / d(t) =
1.111*k2r*(qm*ka*(CE2+CE1)/2*C1)/(1+ka*(CE2+CE1)/2)*alpha*C1/Co1*C1+1.053*((k3r*((BG2+BG1)/2)*CB1)/(k3M+CB1))

G1(0) =0

d(G2) / d(t) =
1.111*k2r*(qm*ka*(CE3+CE2)/2*C2)/(1+ka*(CE3+CE2)/2)*alpha*C2/Co2*C2+1.053*((k3r*((BG3+BG2)/2)*CB2)/(k3M+CB2))

G2(0) = 0

d(G3) / d(t) =
1.111*k2r*(qm*ka*(CE4+CE3)/2*C3)/(1+ka*(CE4+CE3)/2)*alpha*C3/Co3*C3+1.053*((k3r*((BG4+BG3)/2)*CB3)/(k3M+CB3))

G3(0) = 0

d(G4) / d(t) =
1.111*k2r*(qm*ka*(CE5+CE4)/2*C4)/(1+ka*(CE5+CE4)/2)*alpha*C4/Co4*C4+1.053*((k3r*((BG5+BG4)/2)*CB4)/(k3M+CB4))

G4(0) = 0

d(G5) / d(t) =
1.111*k2r*(qm*ka*(CE6+CE5)/2*C5)/(1+ka*(CE6+CE5)/2)*alpha*C5/Co5*C5+1.053*((k3r*((BG6+BG5)/2)*CB5)/(k3M+CB5))

G5(0) = 0

d(G6) / d(t) =
1.111*k2r*(qm*ka*(CE7+CE6)/2*C6)/(1+ka*(CE7+CE6)/2)*alpha*C6/Co6*C6+1.053*((k3r*((BG7+BG6)/2)*CB6)/(k3M+CB6))

G6(0) = 0

d(G7) / d(t) =
1.111*k2r*(qm*ka*(CE8+CE7)/2*C7)/(1+ka*(CE8+CE7)/2)*alpha*C7/Co7*C7+1.053*
((k3r*((BG8+BG7)/2)*CB7)/(k3M+CB7))

G7(0) = 0

d(G8) / d(t) =
1.111*k2r*(qm*ka*(CE9+CE8)/2*C8)/(1+ka*(CE9+CE8)/2)*alpha*C8/Co8*C8+1.053*
((k3r*((BG9+BG8)/2)*CB8)/(k3M+CB8))

G8(0) = 0

d(G9) / d(t) =
1.111*k2r*(qm*ka*(CE10+CE9)/2*C9)/(1+ka*(CE10+CE9)/2)*alpha*C9/Co9*C9+1.05
3*((k3r*((BG10+BG9)/2)*CB9)/(k3M+CB9))

G9(0) = 0

d(G10) / d(t) =
1.111*k2r*(qm*ka*(CE11+CE10)/2*C10)/(1+ka*(CE11+CE10)/2)*alpha*C10/Co10*C
10+1.053*((k3r*((BG11+BG10)/2)*CB10)/(k3M+CB10))

G10(0) = 0

d(G11) / d(t) =
1.111*k2r*(qm*ka*(CE12+CE11)/2*C11)/(1+ka*(CE12+CE11)/2)*alpha*C11/Co11*C
11+1.053*((k3r*((BG12+BG11)/2)*CB11)/(k3M+CB11))

G11(0) = 0

d(G12) / d(t) =
1.111*k2r*(qm*ka*(CE13+CE12)/2*C12)/(1+ka*(CE13+CE12)/2)*alpha*C12/Co12*C
12+1.053*((k3r*((BG13+BG12)/2)*CB12)/(k3M+CB12))

G12(0) = 0

d(G13) / d(t) =
1.111*k2r*(qm*ka*(CE14+CE13)/2*C13)/(1+ka*(CE14+CE13)/2)*alpha*C13/Co13*C
13+1.053*((k3r*((BG14+BG13)/2)*CB13)/(k3M+CB13))

G13(0) = 0

d(G14) / d(t) =
1.111*k2r*(qm*ka*(CE15+CE14)/2*C14)/(1+ka*(CE15+CE14)/2)*alpha*C14/Co14*C
14+1.053*((k3r*((BG15+BG14)/2)*CB14)/(k3M+CB14))

G14(0) = 0

d(G15) / d(t) =
1.111*k2r*(qm*ka*(CE16+CE15)/2*C15)/(1+ka*(CE16+CE15)/2)*alpha*C15/Co15*C15+1.053*((k3r*((BG16+BG15)/2)*CB15)/(k3M+CB15))

G15(0) = 0

d(G16) / d(t) =
1.111*k2r*(qm*ka*(CE17+CE16)/2*C16)/(1+ka*(CE17+CE16)/2)*alpha*C16/Co16*C16+1.053*((k3r*((BG17+BG16)/2)*CB16)/(k3M+CB16))

G16(0) = 0

d(G17) / d(t) =
1.111*k2r*(qm*ka*(CE18+CE17)/2*C17)/(1+ka*(CE18+CE17)/2)*alpha*C17/Co17*C17+1.053*((k3r*((BG18+BG17)/2)*CB17)/(k3M+CB17))

G17(0) = 0

d(G18) / d(t) =
1.111*k2r*(qm*ka*(CE19+CE18)/2*C18)/(1+ka*(CE19+CE18)/2)*alpha*C18/Co18*C18+1.053*((k3r*((BG19+BG18)/2)*CB18)/(k3M+CB18))

G18(0) = 0

d(G19) / d(t) =
1.111*k2r*(qm*ka*(CE20+CE19)/2*C19)/(1+ka*(CE20+CE19)/2)*alpha*C19/Co19*C19+1.053*((k3r*((BG20+BG19)/2)*CB19)/(k3M+CB19))

G19(0) = 0

d(G20) / d(t) =
1.111*k2r*(qm*ka*(CE21+CE20)/2*C20)/(1+ka*(CE21+CE20)/2)*alpha*C20/Co20*C20+1.053*((k3r*((BG21+BG20)/2)*CB20)/(k3M+CB20))

G20(0) = 0

G=G1+G2+G3+G4+G5+G6+G7+G8+G9+G10+G11+G12+G13+G14+G15+G16+G17+G18+G19+G20

k1r=0.0000066

k2r=0.0000005

k3r=0.092

k3M=24

alpha=1

k=0.02

A=11.304

V=10

rhoa=0.296

qm=12.24

ka=1

deltar=R/N

N=20

R=0.03

phi=0.92

epsilon=0.835

DPBG=DW*(epsilon/(2-epsilon))

DPCE=DW*(epsilon/(2-epsilon))

DW=567.e-9

t(0) = 0

t(f) = 86400